Self-sensing and Self-powering Multifunctional Mechanical Metamaterials

by

Kaveh Barri

Undergraduate degree, University of Tabriz, 1998

Master's degree, Sahand University of Technology, 2002

Submitted to the Graduate Faculty of the

Swanson School of Engineering in partial fulfillment

of the requirements for the degree of

Doctor of Philosophy

University of Pittsburgh

2022

UNIVERSITY OF PITTSBURGH

SWANSON SCHOOL OF ENGINEERING

This thesis was presented

by

Kaveh Barri

It was defended on

June 3, 2022

and approved by

Lev Khazanovich, Ph.D. Professor,
Department of Civil and Environmental Engineering

Steven Sachs, Ph.D. Assistant Professor,
Department of Civil and Environmental Engineering

Jun Chen, Ph.D. Assistant Professor,
Department of Electrical and Computer Engineering

Dissertation Director: Amir H. Alavi, Ph.D., Assistant Professor
Department of Civil and Environmental Engineering

Self-sensing and Self-powering Multifunctional Mechanical Metamaterials

Kaveh Barri, PhD

University of Pittsburgh, 2022

There is an unmet need to explore new classes of active, scalable and adaptive multifunctional materials for a broad range of engineering applications. Mechanical metamaterials are one of the major classes of the function-integrated materials. They gain their tailored counterintuitive mechanical properties from their rationally-designed structures rather than inheriting them directly from their chemical composition. Thus far, nearly all of the mainstream studies in the area of mechanical metamaterials have focused on identifying unprecedented mechanical properties via changing the geometrical design of micro/nano-architectures. In this dissertation, a new generation of multifunctional mechanical metamaterials called "meta-tribomaterials" is introduced by combining the fields of mechanical metamaterials and nano energy harvesting. The proposed concept enables creating active architected materials in which active sensing and energy harvesting are new types of material properties, alongside the traditional material properties. Meta-tribomaterials, a.k.a. self-aware composite mechanical metamaterials, are composed of rationally designed micro/nano structures with built-in contact-electrification mechanisms to realize such advanced functionalities. The term self-aware refers to the ability of a meta-tribomaterial system to self-sense and self-monitor its condition using its constituent components and without a need for any external power source. Theoretical and experimental studies are conducted to understand the mechanical and electrical behavior of 2D and 3D meta-tribomaterial systems. The broad application of the proposed concept for designing multiscale artificial materials with novel functionalities is highlighted. Various self-powering and

self-sensing structural systems and medical implants are developed including multifunctional implants with diagnostic functionality, shock absorbers, composite structural beams, and lightweight reinforced concrete systems. The maximum voltage and power output of the created meta-tribomaterial systems reach 9 volts and 600 nW, respectively. Further discussions are provided to pave the way for enhancing the electrical and mechanical performance of the proposed designs using various material option and surface optimization techniques. Finally, a future vision toward creating truly autonomous architected materials is presented via incorporating information processing and data storage functionalities into the fabric of meta-tribomaterials.

Table of Contents

List of Tables

<div align="center">**List of Figures**</div>

Preface

I would like to express my sincere gratitude to my advisor, Dr. Alavi, who always believed in me and helped me to move in the right direction. His expertise and constant support were invaluable. Working on such innovative and exciting research under his supervision was a great experience that pushed me to sharpen my thinking.

I would like to express my deepest appreciation to my Ph.D. committee members: Dr. Lev Khazanovich, Dr. Steven Sachs and, Dr. Jun Chen whose constructive suggestions and guidance during my Ph.D. studies brought my work to a higher level.

I also want to thank all of my friends and colleagues for their kind help and support.

A special thanks to my family for all of the sacrifices that they have made. Words cannot express how grateful I am to my parents and siblings. Not seeing them for more than five years was the most difficult part of this journey.

Finally, I would like to acknowledge my dearest friend, my beloved wife Farzaneh, for her patience and continued support. After a pause of over 20 years in my academic career, I renewed my effort to complete my research. Without her support in both the personal and professional aspects of my life, I could not follow my dreams and have achieved the goals that I set.

1.0 Introduction and Vision

The next generation of materials needs to be adaptive, multifunctional and tunable. This goal can be achieved by metamaterials that enable development of advanced artificial materials with novel functionalities. During the last few years, the emerging concept of structure-dominated mechanical metamaterials has received increasing attention. Mechanical metamaterials gain their tailored unprecedented/counterintuitive mechanical properties from their rationally-designed structures rather than inheriting them directly from their chemical composition (Jiao and Alavi, 2020a, 2020b). Additive manufacturing has been a major driving force in the exploration of mechanical metamaterials since virtually any topology can be obtained to probe the vast design space created by geometric changes in the material structure. However, a substantial portion of the current effort in the arena of mechanical metamaterials has been merely going into exploring new geometrical design of micro/nano-architectures to improve or identify unusual sets of mechanical properties. There is a critical shortage in research needed to engineer new aspects of intelligence into the texture of mechanical metamaterials for multifunctional applications. In this context, the next stage of this technological revolution is development of self-aware mechanical metamaterials that can sense, empower and program themselves. To address this challenge, this dissertation introduces a new class of multifunctional mechanical metamaterials that offers new sensing and energy harvesting functionalities in addition to the enhanced mechanical properties of classical mechanical metamaterials. The vision of this research is to propose a new generation of composite mechanical metamaterials called "meta-tribomaterials", a.k.a. self-aware composite mechanical metamaterials (SCMMs), with complex internal structures toward achieving self-sensing and self-powering functionalities along with the boosted mechanical properties. The proposed research

1

is based on the following hypotheses: (a) finely tailored and seamlessly integrated microstructures composed of topologically different triboelectric materials can form a hybrid mechanical metamaterial system that can both harvest the energy from the mechanical excitations and measure various levels of the forces applied to its structure; and (b) a composite mechanical metamaterial composed of different materials that are organized in a periodic manner will boost the mechanical properties. This study demonstrates the feasibility of the proposed meta-tribomaterial concept for creating a metamaterial structure with energy harvesting capabilities. The grand vision for the proposed research study is shown in Figure 1. In this vision, architecture tailoring of triboelectric materials via additive manufacturing forms a new class of multifunctional mechanical metamaterials for a broad range of applications. Deformation mode of the fabricated microstructures should be engineered through a unique design so that contact electrification will occur between the two surfaces as the meta-tribomaterial structure undergoes periodic deformations due to mechanical excitations. The meta-tribomaterial contacting/sliding surfaces will act as conductive and dielectric layers similar to a triboelectric nanogenerator as shown in Figure 1a. Due to the contact electrification, the conductive and dielectric layers will accumulate positive and negative charges, respectively. As the meta-tribomaterial structure is unloaded, the transferred charge will remain on the dielectric surface. This will form a static electric field and a potential difference between the conductive layers. By increasing the loading amplitude, more conductive and dielectric layers of the meta-tribomaterial matrix will get involved in the contact-separation process, which will result in generating higher electrical output. The electrical output signals can be used for active sensing of the external mechanical excitation applied to the meta-tribomaterial structure. On the other hand, the generated electrical energy can be harvested and stored to empower sensors and electronics at low power.
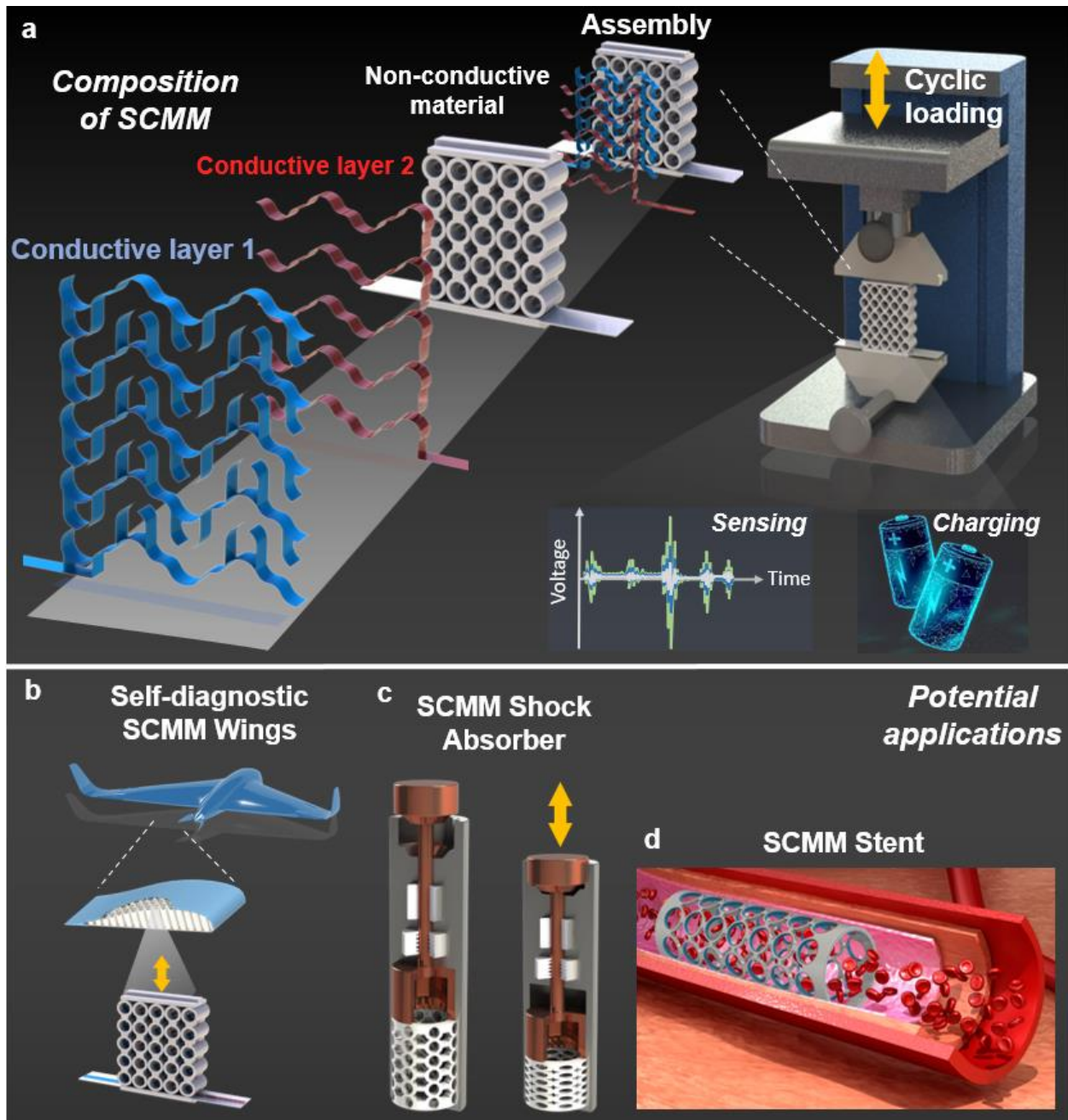
Figure 1 Vision for the proposed multifunctional mechanical metamaterial concept for active sensing and energy harvesting: (a) Composition of a snapping mechanical metamaterial designed based on the meta-tribomatrial concept. Broad applications of the proposed concept including (b) A flying wing aircraft with self-diagnostic and energy harvesting wings. (c) Self-sensing meta-tribomatrial shock absorber with energy harvesting capabilities. (d) Self-powered and self-sensing cardiovascular meta-tribomatrial stent for continuous monitoring of the artery radial pressure changes due to tissue overgrowth.

2.0 Objective and Significance

The goal of this Ph.D. research is to advance the knowledge and technology required to create a new class of multifunctional mechanical metamaterial systems that offer self-sensing, self-monitoring, and energy harvesting properties along with boosted mechanical performance due to their composite structure. For this purpose, this study introduces an architected mechanical metamaterial containing parallel snapping curved (semicircular-shaped) segments with elastic snap-through instability mechanism. In order to incorporate the sensing and energy harvesting features into the metamaterial functionality, the triboelectric nanogenerator concept is introduced into its architecture design. The stated goal decomposed into the following objectives:

- Design an architected mechanical metamaterial with elastic snap-through instability mechanism and characterization of the mechanical response.

- Incorporate the sensing and energy harvesting features into the metamaterial functionality and characterization of the electrical performance.

- Integrate multiscale systems for real-life engineering applications.

- Fabricate and test the integrated multiscale systems.

The research work will lead to discoveries of materials with new properties and functionalities in the fields of aerospace (morphing/deployable space structures), biomedical devices (medical implants, stents, artificial muscles), civil infrastructure and construction. From a sensing perspective, introducing the self-sensing functionality into the mechanical metamaterial design could in theory lay the foundations for living structures that respond to their environment and self-monitor their condition. This is the first step for a grander vision of "self-aware structures"

4

where structural systems utilize their entire constituent components as a sensing medium to directly infer multiple types of hidden information relating to the structure. In addition to its "inferring itself" aspects, the proposed concept could have numerous applications in the structural health monitoring arena. Traditional structural health monitoring approaches use dedicated sensors which often results in dense and heterogeneous sensing systems that are difficult to install and maintain in large-scale structures (Alavi et al., 2016a). On the other hand, it is not always possible embed a traditional sensor (such as a strain gauge) inside structures such as, in which cross-sectional or interlaminate failures may not be observable at the surface (Seifert et al., 2019). Another bottleneck limiting the structural health monitoring applications is that permanent monitoring systems often require extensive maintenance as a consequence of the limited durability of traditional sensors and of the limited robustness and exposure to failures of typical structural health monitoring architectures. The proposed concept can address most of these challenges because it is a paradigm shift in technology where "structure can a sensing medium itself" through a rational architectural design and choice of constituent materials. In addition to its self-sensing features, a meta-tribomaterial system is intrinsically sensitive to the applied stresses, and therefore, it can be implemented as a sensor in various materials or structural systems.

From an energy harvesting perspective, this research work will offer new concepts and mechanisms for materials and structures that utilize the energy that develops within them (strain and kinetic energy) for self-powering or local powering of sensing and actuating devices. Incorporating the triboelectric materials as a constituent material into the texture of mechanical metamaterials will expand the useable range of these materials as power harvesters. A nanogenerator meta-tribomaterial would naturally inherit the outstanding features of the triboelectric nanogenerators. It uses neither magnets nor coils; it is light in mass, low in density,

low in cost, highly scalable, and it can be fabricated using inorganic and "most of the organic" materials. Triboelectric nanogenerators have shown a significantly higher power density in comparison with other competitive technologies such as piezoelectric materials and electromagnetic generators (S. Wang et al., 2015; Yu et al., 2017).

Figure 2 shows the typical energy density for different types of energy harvesting devices that are currently available (Dziadak et al., 2016; Indira et al., 2019) (research projects and commercial devices). The current volume power density of triboelectric nanogenerators has reached more than 400 W/m^2 (Wang, 2013), while the highest reported volume power density of piezoelectric materials is 4.4 W/m^2 (Indira et al., 2019). The high power-to-volume ratio and power-to-weight ratio that could be potentially offered by the proposed meta-tribomaterial could be crucial issues for embeddable/implantable electronics. Similar to the triboelectric nanogenerators, meta-tribomaterial would work the best at low frequencies (<5–10Hz) and therefore, it will be the unique choice for harvesting low-frequency energy from civil infrastructure systems.
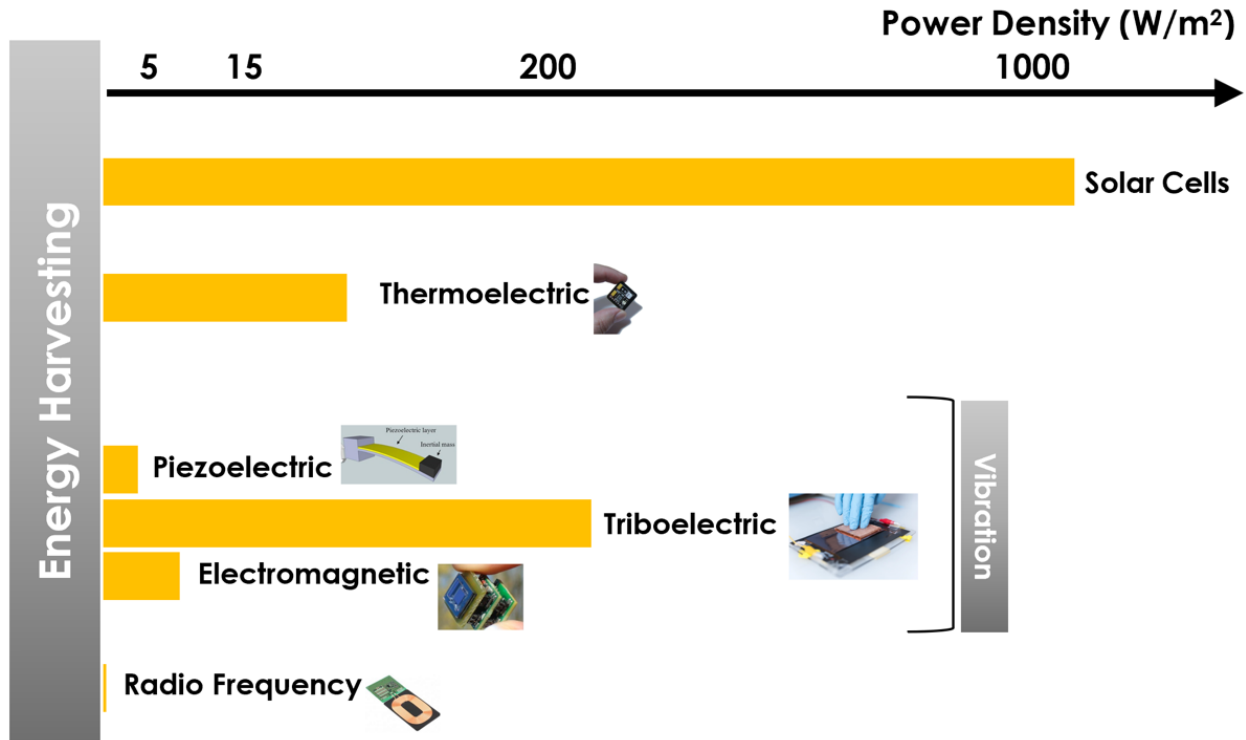
Figure 2 Power density for different available energy harvesting modalities (Dziadak et al., 2016; Indira et al., 2019).

From a mechanical perspective, meta-tribomaterials are composed of different materials that are organized in a periodic manner. Therefore, meta-tribomaterial s not only inherit all features of classical mechanical metamaterials, but could also offer significantly boosted mechanical properties due to their composite structure by overcoming the "rule of mixtures" (Deng et al., 2018; Dimas and Buehler, 2013; Munch et al., 2008). The theoretical models that have been developed in this research enable predicting and tuning the mechanical properties of meta-tribomaterial s to make them programmable tools for various engineering applications.

3.0 Background and State-of-Knowledge

3.1 Mechanical Metamaterials

3.1.1 Metamaterials

The mechanical properties of materials are the foremost basic concept in material sciences. They have been widely studied due to their essential importance for real-life applications. For hundreds of years, only the composition of materials has been modified in order to develop their mechanical properties (Ashby et al., 1992). In general, based on Power Law, for most natural materials, there is a direct relationship between their physical and mechanical properties. For instance, in general, the density and strength of specific classes of materials are related to each other, where the higher the strength of the material, the higher the density (Zadpoor, 2016). On the other hand, there are a lot of materials in nature that exhibit special properties that are not achievable with natural or manmade common materials. Cellular materials, such as bones, sponges, and honeycombs, which have evolved over a period of several million years, develop an optimized architecture and are good examples of this type of natural material with intriguing properties. The extremely complex porous structure of a bone core, including the density gradient and complicated formed ligaments, allows it to attain a far higher structural efficiency compared to most the human-made artificial cellular materials (Surjadi et al., 2019).

Metamaterials are artificial structures that are architecturally engineered to have specific properties that do not exist in a natural state. Although incorporating architecture into material development is not a new concept, advanced fabrication techniques such as 3D printing have

8

enabled the manufacturing of metamaterials with complicated designs in different sizes for a wide range of materials. Metamaterials have been used for the first time in electromagnetism and optics (Chen et al., 2010), but the concept of "Mechanical Metamaterials" has recently emerged and is comparatively less researched. For decades, only a few categories of mechanical metamaterials were explored. Nowadays, benefiting from novel geometrical designs of micro and nano structures, different types of mechanical metamaterials with uncommon mechanical properties have been innovated. Considering different topologies for mechanical metamaterials enables them to exhibit unique mechanical and physical properties such as tunable stiffness, negative Poisson's ratio, negative compressibility, and zero shear modulus (Surjadi et al., 2019).

3.1.2 Metamaterial Types

3.1.2.1 Electromagnetic Metamaterials

Electromagnetic metamaterials are newly considered as a part of physics and electromagnetism. Considering the microscopic parameters of material contains permeability and permittivity, the electromagnetic field of that material can be classified into four groups which are shown in Figure 3 (Singh et al., 2015).
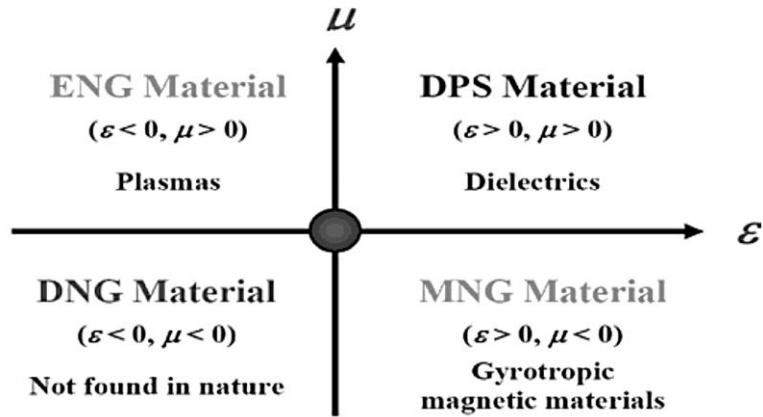
Figure 3 Classification of metamaterials in terms of permittivity ε and permeability μ. (Singh et al., 2015)

Negative permittivity and high or negative magnetic permeability in the range of radio and microwave frequencies are the special properties of Electromagnetic metamaterials. These properties are directly related to the type of structural elements, dimensions, geometric properties, and the operation frequency (Grimberg, 2013).

3.1.2.2 Photonic Metamaterials

Photonic metamaterials or optical metamaterials are the types of metamaterials that work with optical frequencies and emit the source of optical wavelengths. Zero and negative values for the reflection index are some samples for these types of metamaterials (Singh et al., 2015). Figure 4 shows the difference in the light beam reflection between positive index material, which is ordinary material, and negative index material, which is artificially enhanced material, such as photonic metamaterials.
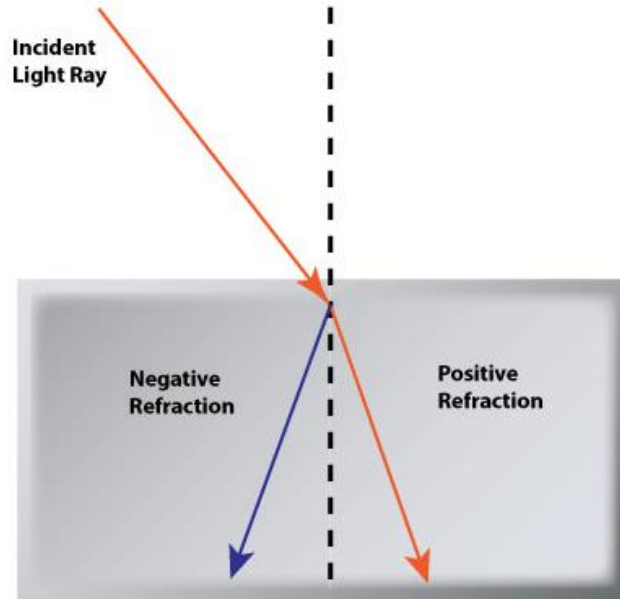
Figure 4 Positive index (ordinary material) and negative index materials

3.1.2.3 Mechanical Metamaterials

Mechanical Metamaterials are artificial structures that are architecturally engineered to have specific properties that do not exist in the natural state and their mechanical properties are defined by their structures instead of material compositions (Surjadi et al., 2019).

3.1.2.3.1   Extremal Mechanical Metamaterials

Extremal materials refer to materials that are substantially stiff in a certain deformation mode, while extremely flexible in the other modes. The behavior of the extremal materials is determined by the eigenvalues of the elasticity tensor. A very small eigenvalue in the given deformation mode indicates that the material is very flexible in the same direction of that specific eigenvalue. The elasticity tensor of extremal materials can have one or more very small eigenvalues. Based on the number of these very small eigenvalues, the extremal metamaterials can

11

be categorized. Unimode extremal material has only one very small eigenvalue. Bimode, trimode, quadramode and pentamode have two, three, four and five very small eigenvalues, respectively (Milton and Cherkaev, 1995). Among these five different modes, researchers have more attention to the unimode and pentamode extremal material.

Pentamode metamaterials with five very small eigenvalues in the elasticity tensor are very flexible in five out of six principal directions. It means that these types of metamaterials have a very large bulk modulus compared with their shear modulus. Therefore, subject to deformation, the volume of these type of material becomes constant. In other words, the Poisson ratio of the pentamode metamaterial can be reached to 0.5 which is the maximum theoretical amount for the Poisson's ratio. Milton and Cherkaev in 1995, proposed a specific design of pentamode metamaterial, which is depicted in Figure 5 (Milton and Cherkaev, 1995).
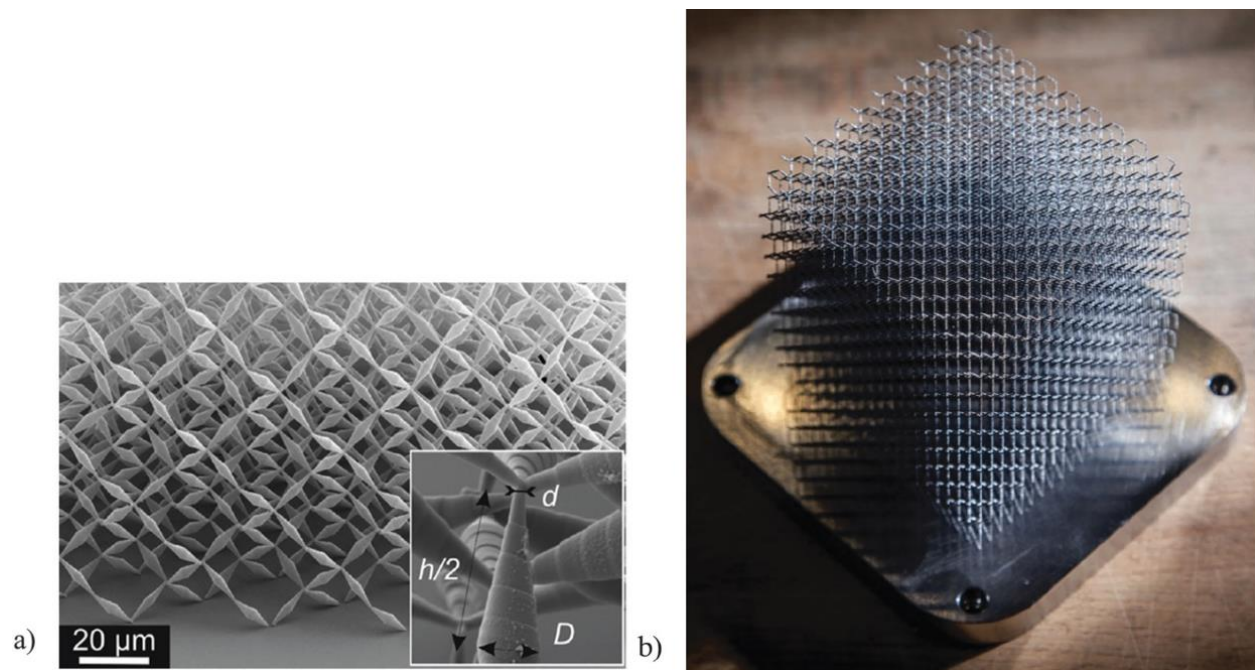
Figure 5 (a) A specific design of penta-mode meta-materials proposed by Milton and Cherkaev. (b) A metallic penta-mode meta-material based on the same design (Zadpoor, 2016).

Auxetic material is a sample of unimode metamaterial, which has the opposite properties compared to pentamode metamaterial. In this case, the bulk modulus is extremely high, and the shear modulus is extremely low, therefore the Poisson's ratio becomes -1, the lowest theoretical amount for Poisson's ratio. It means that as a result of deformation, the general shape of the auxetic metamaterial does not change, and it is only scaled (Zadpoor, 2016). These two categories of metamaterials, pentamode and unimode metamaterials, are exactly the opposite. Figure 6 shows the samples of three-dimensional auxetic metamaterials.
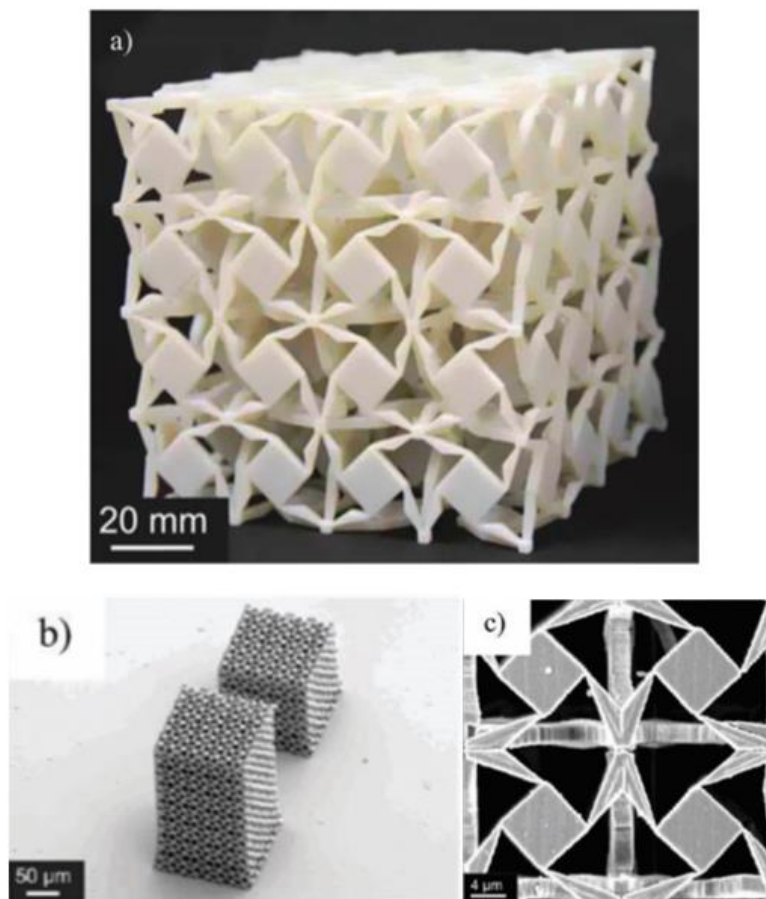
Figure 6 (a)A three dimensional auxetic metamaterial (unimode metamaterial) at macroscopic scale (b and c) at microscopic scale (Zadpoor, 2016).

3.1.2.3.2 Negative Mechanical Metamaterials

Negative metamaterials are types of metamaterials that have negative elastic modulus or negative bulk modulus. This condition is contrary to the theory of continuum mechanics. Based on continuum mechanics, the elasticity tensor should be positive definite, therefore both elastic modulus and bulk modulus should be positive to have a stable condition. Although the negative stiffness or negative compressibility leads to having unstable materials, by considering appropriate constraints, these types of material can be very stable.

Material with negative compressibility is one type of negative metamaterial, and it refers to the material which expands when the hydrostatic pressure is applied. In other words, when expansion occurs, negative metamaterials can have negative volume compressibility. Material with a cellular structure such as hexagonal honeycombs is a sample of this type of metamaterial (Zadpoor, 2016). Figure 7 shows the positive and negative compressibility of a conventional system in comparison with negative metamaterial (Gatt and Grima, 2008).
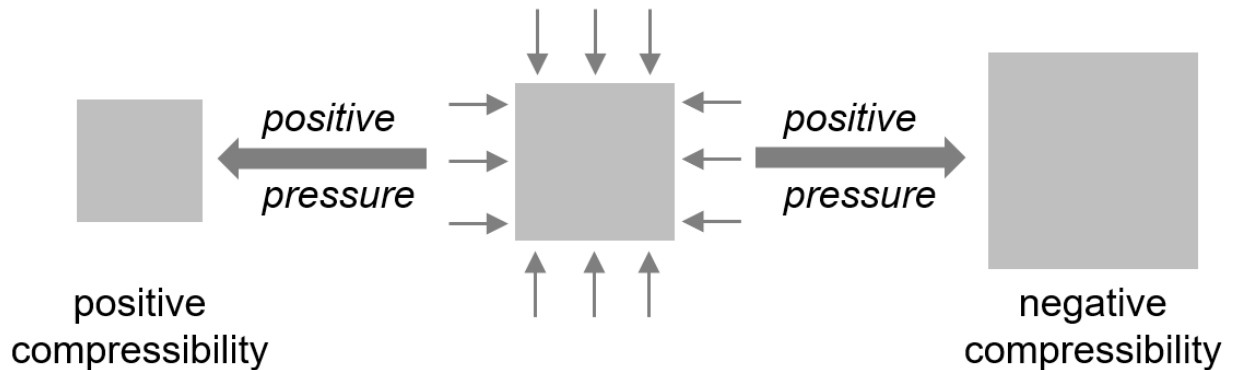
Figure 7 Unlike conventional systems (left) which shrink when subjected to an increase in pressure, systems with negative compressibility (right) expand in size when the external pressure increases (Gatt and Grima, 2008).

Another type of metamaterial with negative compressibility can be made with a combination of two materials with different mechanical properties. Gatt and Grimma proposed an example (Figure 8) of using multiple materials to show negative compressibility (Gatt and Grima, 2008).
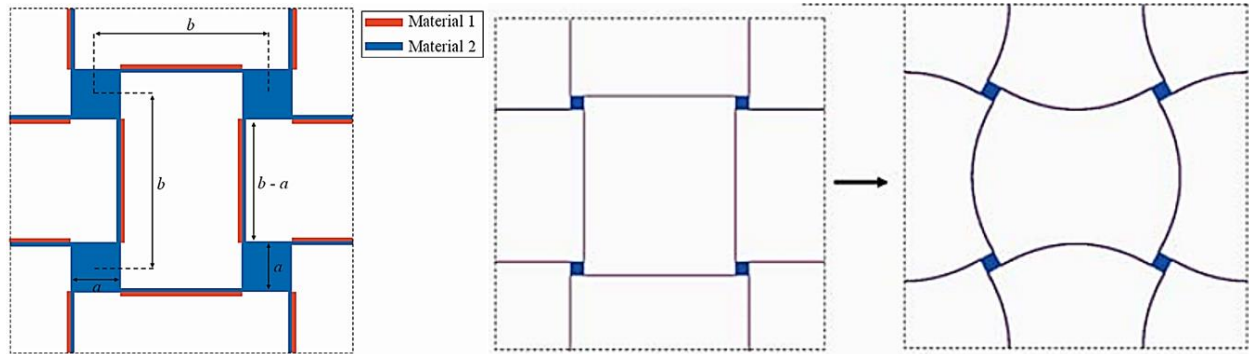
Figure 8 example of using multiple materials to show negative compressibility (Gatt and Grima, 2008).

Materials with negative stiffness are in the same category as negative metamaterials. For conventional materials with positive stiffness, deformation occurs in the direction of the applied force, and the internal forces try to preserve the original geometry. On the other hand, for materials with negative stiffness, the directions of the applied force and deformation are the opposite. In these materials, the internal forces and the applied load are in the same direction and assist each other to make a bigger deformation. Therefore, at similar load conditions, negative stiffness materials have greater deformation than positive stiffness materials. These types of materials which alone are considered unstable can show extraordinary properties such as high damping coefficient by being combined with a positive stiffness material. For conventional engineering materials, higher stiffness leads to having lower damping properties. Contradictory, high damping ratio materials are generally not very stiff. Therefore, having high stiffness and a high damping

ratio at the same time for one material is not applicable. Using a composite material containing both types of the above-mentioned materials is a solution to have both high stiffness and high damping ratio in one composite, and it could be used as a vibration isolator.

Considering a series of a negative stiffness material (k-) with a positive stiffness material (k+), the equivalent stiffness of the composite material would be:

$$Equivalent\ K = \cfrac{1}{\cfrac{1}{k_-} + \cfrac{1}{k_+}}$$

<div align="right">3-1</div>

If the absolute value of both k- and k+ approach the same value, the equivalent k of this combination approaches infinity. Practically it means that the overall stiffness of the new composite material is extremely high, but this combination is not stable and should be stabilized using appropriate constraints (Zadpoor, 2016).

3.1.2.3.3 Ultra-property Mechanical Metamaterials

For many structural applications, a material which has high stiffness, high toughness, high strength, and low mass density at the same time, is a perfect and ideal material. Considering the nature of these properties it is almost impossible to have some of these properties simultaneously in one material. For example, there is a conflict between strength and toughness. Recently, researchers have been trying to develop metamaterials with ultra-properties such as ultra-stiff, ultra-strong, ultra-light, and ultra-tough metamaterials (Zadpoor, 2016). Figure 9 shows an example of an ultra-light metamaterial with excellent recoverability (Surjadi et al., 2019).

Figure 9 Ultra-light metamaterial demonstrating ultra-low density and excellent recoverability (Surjadi et al., 2019).

3.1.2.4 Fabrication Methods

There are different fabrication techniques that could be used to synthesize mechanical metamaterials, but most applicable and acceptable of them benefiting from the Additive Manufacturing technique (AM). Additive manufacturing, also called 3D printing, refers to different processes that can build parts by adding raw material layer by layer. There are three main

classes for additive manufacturing techniques; 3D printing through ink extrusion, photopolymerization and powder fusion methods.

3.1.2.4.1 Ink Extrusion 3D Printing

The ink extrusion technique is one of the most common 3D printing methods of Metamaterial fabrication. In this method, the raw material is directly deposited via a nozzle onto a bed or a substrate. It can be done with melting a solid filament or depositing ink droplets onto a substrate. Fused Deposition Modeling (FDM) is one of the well-known Ink extrusion methods for 3D printing. In this method, the solid filament, typically made of a thermoplastic material like Polylactic Acid (PLA), Polycarbonate (PC), Acrylonitrile Butadiene Styrene (ABS) and so on, is heated up to the melting point and is extruded onto a bed from a heated nozzle. The extruded layer rapidly cools down and is ready to deposit the next layer (Surjadi et al., 2019). The schematic illustration for FDM is depicted in Figure 10a, and the object printing in the FDM machine is shown in Figure 10b.

The other technique in this category is Direct Ink Writing (DIW). In this method, a polymer solution or melt which is viscoelastic or viscoplastic material, called ink, is extruded through a micro nozzle onto the substrate or bed surface using an external force. This external force can be a hydraulic pressure, pressurized gas, screw or other types of mechanical pressure sources (Xu et al., 2019). Figure 10c shows the simple illustration of the DIW method and a multi-material DIW system is depicted in Figure 10d.
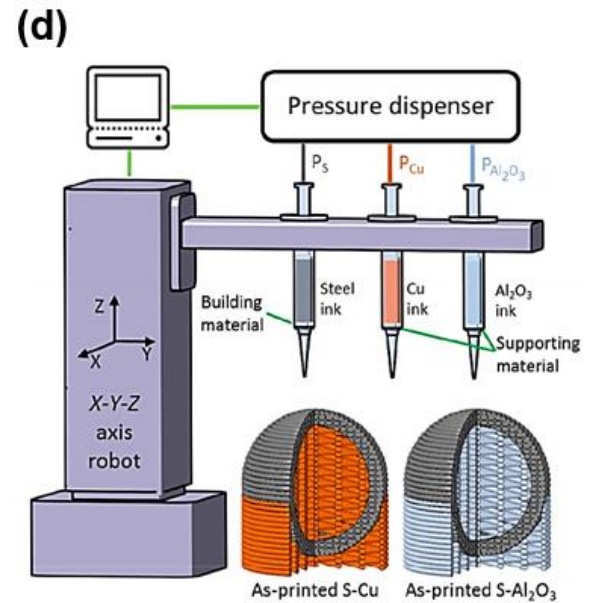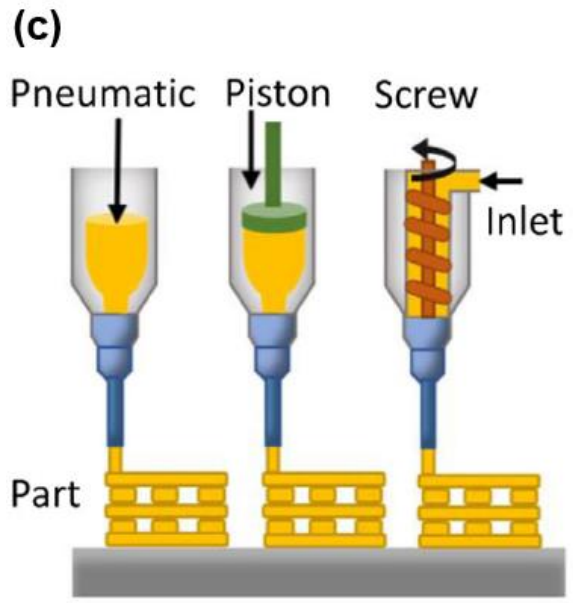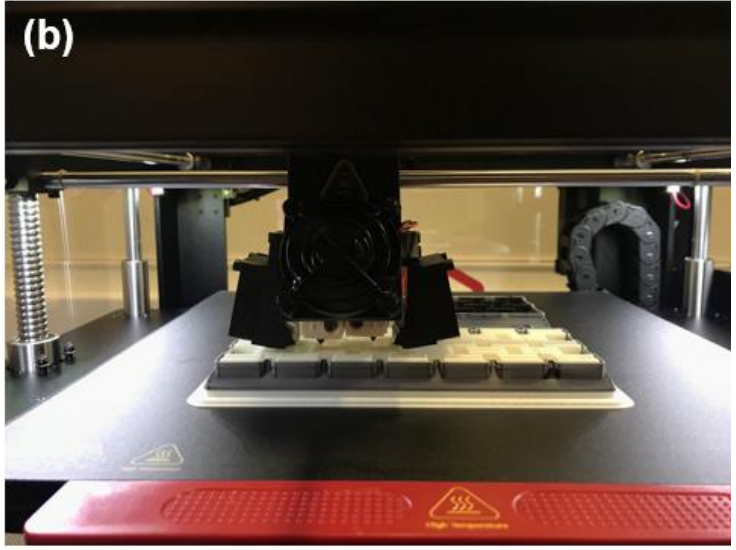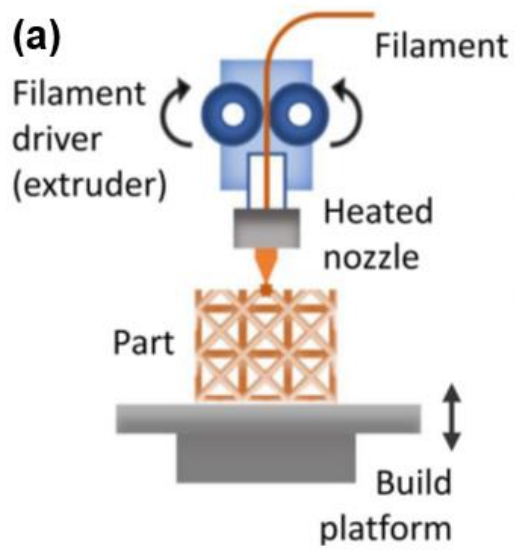
Figure 10 a) The schematic illustration for FDM (Surjadi et al., 2019). b) The object printing in FDM machine (Raise 3d Pro2 3D printer, iSMaRT Lab). c) Schematic illustration of the DIW method (Surjadi et al., 2019). d) A multi-material DIW system (Xu et al., 2019).

3.1.2.4.2 Photopolymerization 3D printing

The photopolymerization technique is a light-based 3D printing method and is capable to create solid structures in the micro and nanoscale. Compare to the Ink extrusion techniques that dimension of the nozzle cause some limitations in the quality and overall size of the objects, the light-based techniques are not restricted by these types of dimensional restrictions, therefore the finer features can be produced using this method (Surjadi et al., 2019).

In the Light-based 3D printing technique, a photopolymer resin is excited directly with a laser source or UV light to fabricate the 3D structures. Stereolithography (SLA) is one of the earliest and well-known 3D printing methods. A photocurable resin is cured and hardened layer by layer using a high-powered UV laser to fabricate the high-quality solid parts. Recently the new techniques of the photopolymerization method are widely used to make highly complex structures with higher qualities and finer details. Two-Photon Lithography (TPL), Projection Micro Stereolithography (PμSL), and Continuous Liquid Interface Production (CLIP) are some of these new techniques (Surjadi et al., 2019). The basic mechanics of stereolithography 3D printing is shown in Figure 11 (Formlabs, 2022).

Upside-Down (Inverted) SLA
1. Printed Part
2. Supports
3. Resin
4. Build Platform
5. Laser
6. Galvanometers
7. X-Y Scanning Mirror
8. Laser Beam
9. Resin Tank
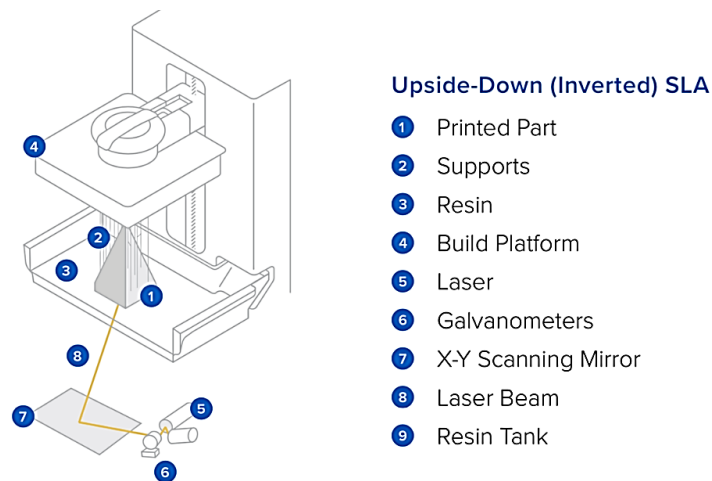
Figure 11 The basic mechanics of STL (Formlabs, 2022).

20

3.1.2.4.3 Powder Fusion 3D printing

Powder fusion method is typically benefited from a laser source to melt or sinter the powder particles in order to fuse them. In this method, a binding agent can be used in the fusion process. A combination of a powder-based technique with a light-based method provides an integrated 3D printing technique called Selective Laser Sintering (SLS). In the SLS technique, the polymetric powders are distributed on top of the previously fused layer in the powder bed and become ready to fabricate a new fused layer. The shape, size, and distribution of powder directly affect the print quality. The smaller powder size, the thinner fused layer, and the higher resolution. Direct Metal Laser Sintering (DMLS) technique is another type of SLS method which is used metallic powders instead of polymer or ceramic powders. Electron Beam Melting (EBM), Direct Energy Deposition (DED), and Selective Laser Melting (SLM) are also other types of Powder Fusion techniques (Surjadi et al., 2019). Figure 12 shows a schematic of the Selective Laser Sintering process (Leary, 2017).
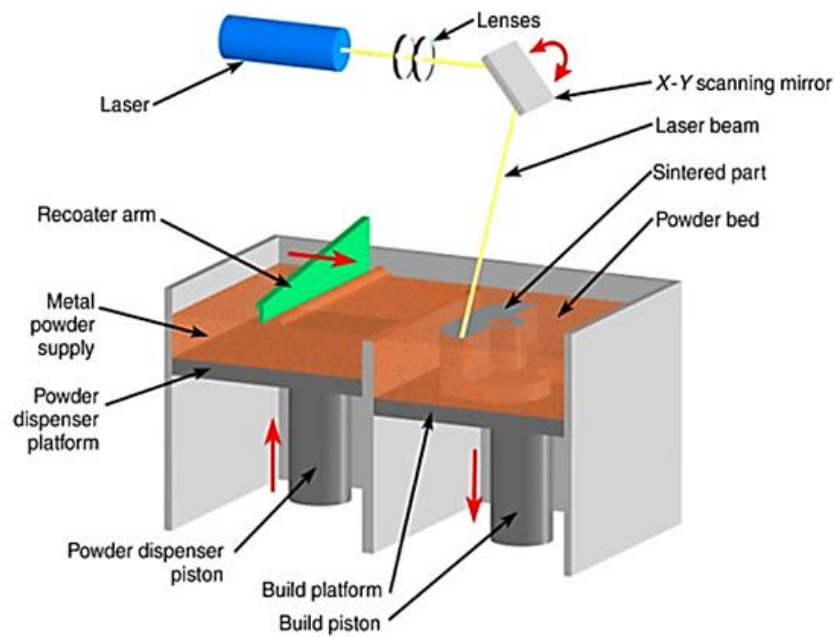
Figure 12 Schematic of Selective Laser Sintering process (Leary, 2017).

3.2 Multifunctional Mechanical Metamaterials

Metamaterials were initially used in the context of optics and electromagnetism (Chen et al., 2010, 2008). That is why the term metamaterial is sometimes understood as a specific term referring to optical and electromagnetic metamaterials. The concept of ''mechanical metamaterials'' has emerged during the last few years and is relatively less explored. Mechanical metamaterial refers to a class of new materials that their properties can be tuned through the design and assembly of microstructures. Mechanical metamaterials enable the development of advanced materials with novel functionalities that originate from their unusual mechanical properties (Zadpoor, 2016). The unusual mechanical properties often include either negative properties or extreme properties. Examples of negative properties are negative Poisson's ratio (Bertoldi et al., 2010; Grima et al., 2015), negative thermal expansion coefficient (Qu et al., 2017), negative compressibility (Nicolaou and Motter, 2012), and negative stiffness (Duoss et al., 2014; Hewage et al., 2016). Extremely high stiffness to mass ratio (Zheng et al., 2014), and extremely high (low) resistance against deformation in specific directions (Kadic et al., 2012) are examples of the extreme properties. Such otherwise ''impossible'' material properties allow for new approaches to material design. The mechanical metamaterial concept is appealing in its potential to accelerate the materials discovery and development by satisfying the requirements of specific and desired mechanical properties. Research efforts have been dedicated to exploring the performance of mechanical metamaterial and obtaining superior mechanical properties using the structure strategy (Jiao et al., 2019; Jiao and Alavi, 2019; Meza et al., 2015). Figure 13 presents a general overview of the types and functionalities of the mechanical metamaterials proposed in the last decade. More details about the previous studies in this arena can be found in comprehensive review papers done by Lincoln et al., Yu et al., and Zadpoor (Lincoln et al., 2019; Yu et al., 2018; Zadpoor, 2016).

Studies have been carried out to unveil the mechanisms governing the geometric nonlinearity of the mechanical metamaterial and to precisely design and optimize the microstructures for desirable characteristics (Yu et al., 2018). Recent interest has been shifted to utilize multifunctional mechanical metamaterial in devices and techniques in energy absorption, artificial muscles, drug delivery, and soft robots (Zadpoor, 2016).
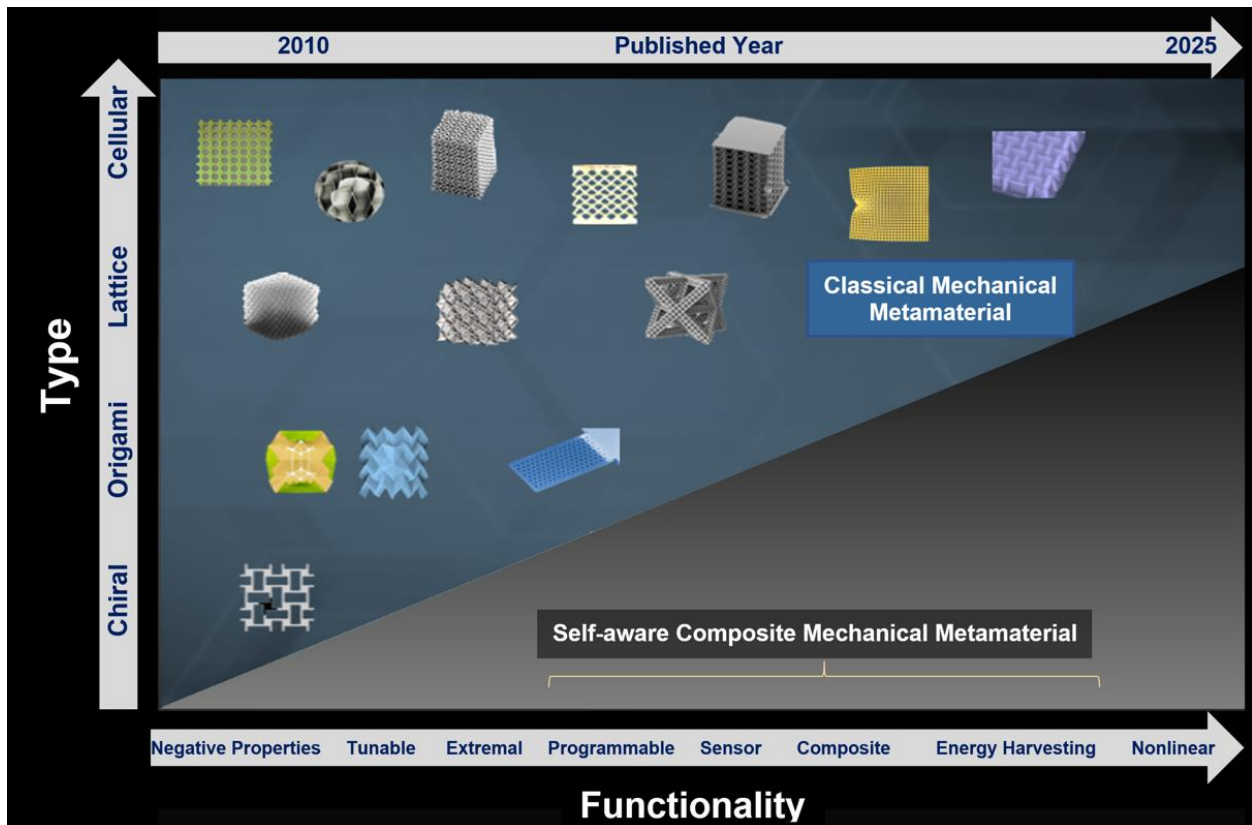
Figure 13 Review of the types and functionalities of the mechanical metamaterials in the existing studies.

However, a limitation of most of the published studies in the arena of multifunctional mechanical metamaterial is that they merely deal with the topology optimization and architecture tailoring to improve/identify the mechanical properties, and no other functionalities. The concepts proposed

in this work will introduce new self-sensing and self-powering functionalities in addition to the enhanced mechanical properties offered by such classical mechanical metamaterials.

Paralleling the rise in multifunctional metamaterial is the blooming field of additive manufacturing. Specifically, composite additive manufacturing continues to be a hot topic in labs, where 3D printing holds strong potential for the formation of a new class of multifunctional mechanical metamaterial composites through embedding of microstructures and nanomaterials (Ivanova et al., 2013; Seifert et al., 2019). For the purpose of this research, a multifunctional composite metamaterial will be defined as a metamaterial made of two or more materials that perform two or more functions in a manner that is constructive to the overall purpose of the structure. However, novel micro/nano architectures have been built by both composite materials' design and nanoscale 3D architecture tailoring (Meza et al., 2014; Schaedler and Carter, 2016). Metal-based (e.g., Ni, Cu) microstructure via electroless plating (Schaedler et al., 2011; Zheng et al., 2014), and ceramics (e.g., TiN and Al2O3) nanostructures via atomic layer deposition (ALD), were fabricated on 3D truss structures (Meza et al., 2014). 3D hollow architectures are featured with properties like ultra-light, ultra-stiff, and recoverable (Davami et al., 2015). More recently, unique ceramic/ carbonized mussel-inspired bio-polymer (C-PDA) nanolayered composite bending-dominated hollow lattice (B-H-lattice) has been developed with recoverability, high strength/weight ratio, optimal scaling factor, and good cyclic performance (Deng et al., 2018). In addition, a successful attempt has been made to show how an insertion of non-uniformly distributed magnetic inclusions into an otherwise uniformly designed mechanical metamaterial can make it act like a composite composed of a number of topologically different materials (Dudek et al., 2019). Despite its capacity to open new horizons for mechanical metamaterials, the entire concept of composite mechanical metamaterials is still in its infancy. Nearly all of the studies in

this arena deal only with improving the mechanical aspects of the mechanical metamaterials. Yet, a major challenge ahead is to how to develop a multifunctional composite mechanical metamaterial with novel functionalities. The proposed meta-tribomaterial concept could be a viable solution to this challenge. Besides, a practical aspect of this concept is that it enables designing layered composite systems using "a wide range of the organic" and inorganic materials from the triboelectric series.

The metamaterial "Tree of Knowledge" reveals that sensor applications is one of the pillars of the metamaterials future research (Zheludev, 2010). Figure 14 presents the "Mechanical Metamaterial Tree of Knowledge" complied by Dr. Amir Alavi in 2021. This tree of knowledge schematically shows the progression and future of mechanical metamaterials research, and is inspired by studies done on the future of the entire metamaterials family (Bertoldi et al., 2017, 2010; Lincoln et al., 2019; Pishvar and Harne, 2020; Yu et al., 2018; Zadpoor, 2016; Zheludev, 2015, 2010; Zheludev and Kivshar, 2012). As seen, the concepts of negative, chiral and lattice mechanical metamaterials are ripe and now moving into the domain of application. Origami and cellular mechanical metamaterials are also well researched. The only study related to quantum mechanical metamaterials proposes a generic tight-binding platform for mechanical, electromagnetic and optical metamaterials (Matlack et al., 2018). Emerging directions of investigation are composite, sensor, energy harvesting, and actuation mechanical metamaterials.
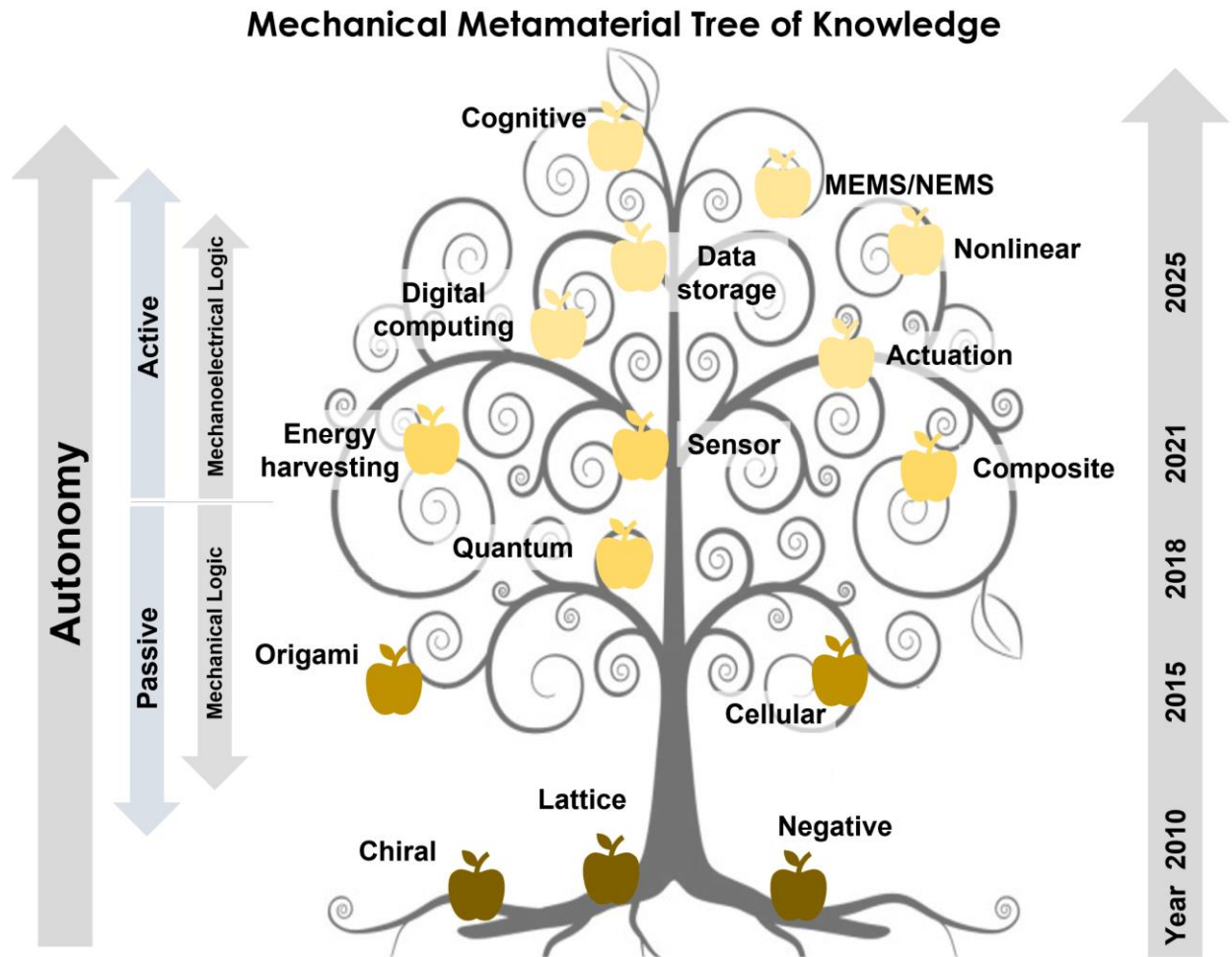
Figure 14 The Mechanical Metamaterial Tree of Knowledge compiled at the iSMaRT Lab. The tree shows the progression and future of mechanical metamaterials research.

A number of studies with focus on metamaterial sensors have emerged over the last years. Schueler et al. (Schueler et al., 2012) reviewed the metamaterial inspired composite right/lefthanded transmission line microwave sensors. Chen et al. (Chen et al., 2012) reviewed metamaterials application in sensing with an emphasis on split ring resonator-based sensors. Yang et al. (Yang et al., 2013) reviewed the current status of metamaterial sensors, with an emphasis on the evanescent wave amplification and the accompanying local field enhancement characteristics. A substantial portion of the research in the area has been dedicated to optical, electromagnetic and

acoustic metamaterial sensors (Yang et al., 2013). So far, there are very few studies with focus on developing mechanical metamaterial sensors (Chen et al., 2019; Jiang et al., 2018). All instances do not use the mechanical metamaterial structure as a sensing medium. Instead, they use the mechanical metamaterial simply as a frame that carries active sensing materials (e.g. conductive carbon nanotube (CNT) or graphene-based microstructure layers) to transform the mechanical stimuli into readable electrical signals. For example, Jiang et al. (Jiang et al., 2018) designed a highly sensitive stretchable strain sensor by attaching a conductive single-wall carbon nanotube (SWCNT) network to a one-unit auxetic mechanical metamaterial structure (see Figure 15). Arguably, there is a critical shortage in research needed to unleash the sensing capabilities of mechanical metamaterial. The proposed concept will convert the mechanical metamaterials into sensing systems to directly collect information about their operating environment. This is particularly important because of the difficulties in embedding an external sensor (such as a CNT strain sensor) in the microstructure of mechanical metamaterials (Seifert et al., 2019; Talreja and Singh, 2012).
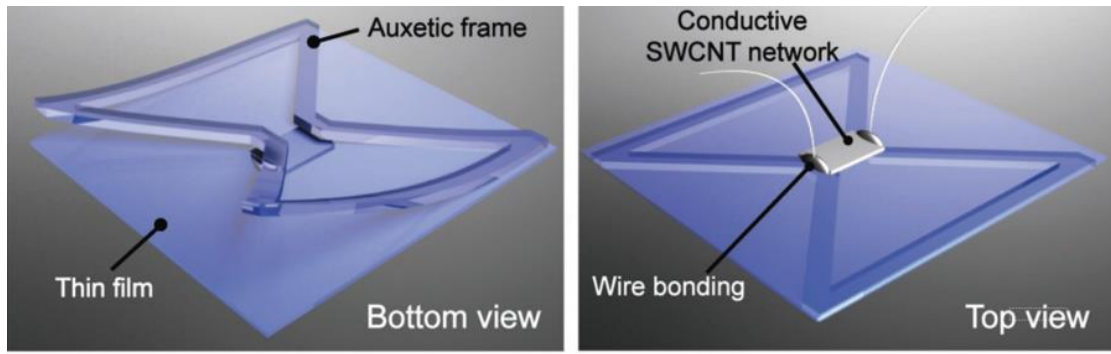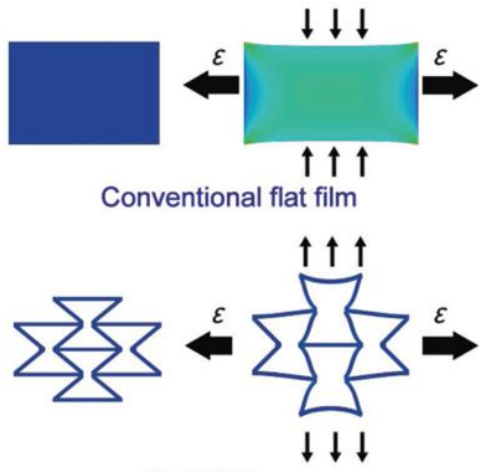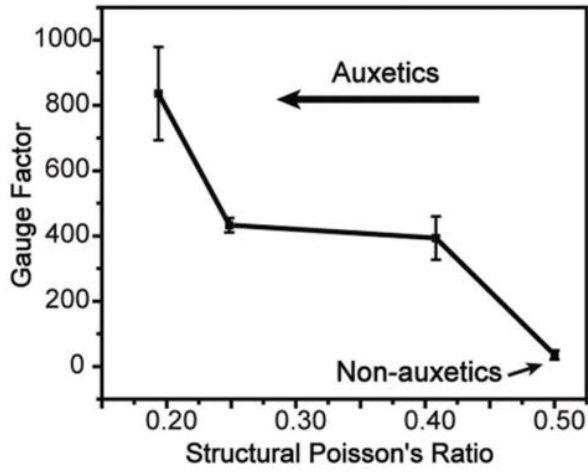
Figure 15 Stretchable strain sensors based on auxetic mechanical metamaterials composed of: auxetic frame, thin film, and conductive SWCNT network (Jiang et al., 2018).

3.3 Energy Harvesting

One of the major obstacles that is limiting the development of deployable integrated sensing and actuation solutions in smart structures is the scarcity of power. Several applications require the use of miniaturized low-powered sensing and actuation systems. These applications include civil and mechanical structures monitoring, biomedical implantable devices, machinery/equipment monitoring, home automation, efficient office energy control, surveillance and security, agricultural management, long range asset tracking, and remote patient monitoring. As a result, the power consumption, speed and size of integrated circuits have dramatically decreased. It is now becoming feasible to embed electronics in everyday objects to potentially enhance their performance. Table 1 shows the approximate energy consumption of commercial and research electronics. The power consumption shown in Table 1 corresponds to a continuous energy supply. The actual power consumption in real applications strongly depends on the complexity of the processed signal quantity and on the number of times per second it has to be transmitted. Several recent practical implementations of sensor nodes showed that 20 μW to 100 μW is enough to process and transmit data (Cook et al., 2006; Paul D Mitcheson et al., 2008). The value of 100 μW is considered representative of the latest developments of relatively complex nodes for systems operating at relative high data-rate. In spite of the significant developments in the area of localized sensing and actuation (Andrew Swartz et al., 2010; Lynch and Loh, 2006; Wilson et al., 2007), most of the developed systems to date still rely on batteries thus limiting the lifetime of the device as well as the diagnosis possibilities. Thus, energy harvesting has been a topic given great attention in recent years as a viable alternative (Najafi et al., 2011; Park et al., 2008).

Table 1 Approximate energy consumption in a wireless sensor node.

Volatile memory (VM) is assumed to be replaced by low-power non-volatile memory (NVM) (Chakrabartty et al., 2006; Elvin et al., 2006; Huang et al., 2010).

Operation	Commercial	Research
Microprocessor Operation[+]	350 µW (TI)	20µW
Receive 1 bit	200nJ (Telos)	12pJ
Transmit 1 bit	200nJ (X-bow)	16pJ
Retain VM – 1 bit	100pW (TI)	Replaced by NVM
Write 1 bit to NVM	200nJ (Micron)	25pJ
Analog-Digital (A/D) Conversion – 1bit	2nJ (TI)	50pJ
Sleep	300nW (TI)	5nW
Digital Signal Processing[+]	200µW (LSI)	20µW
Pin Leakage	100nW (TI)	2.2nW
+ Operation is scaled to processor speeds of 500 kHz		

A myriad of potential energy sources have been identified (solar, thermal gradient, piezoelectric, triboelectric, radio frequency, etc.). The key parameter of any energy harvesting device is its conversion efficiency that depends strongly on the conversion medium. In the past, natural materials were often chosen as conversion media for different energy harvesting devices. However, the conversion efficiency is limited by the properties of natural material and structures. For example, vibration energy harvesting often requires materials to response at frequencies lower than 300 Hz, which are not available from natural materials. Moreover, the current focus of vibration energy harvesting is to create small, lightweight structures that couple very well to mechanical excitation (Cook et al., 2006). To address these issues, metamaterials have been

introduced for energy harvesting in recent years (Chen et al., 2014). In fact, metamaterials with non-traditional physical behaviors provide innovative mechanisms for energy harvesting. A survey of the literature reveals that metamaterials used for energy harvesting mainly include electromagnetic metamaterials, phononic crystals and acoustic metamaterials (Chen et al., 2013; Cottone et al., 2009; Gonella et al., 2009). A number of researchers have used electromagnetic metamaterials for energy harvesting from radio frequency waves available in free space (Fowler and Zhou, 2017; Wang et al., 2011). According to basic properties of phononic crystals, phononic bandgaps have the ability of forbidding elastic waves from propagating within specific frequency ranges (Ferrari et al., 2011). Phononic crystal-based energy harvesters convert the strongly localized energy into electrical energy using proper media as long as the vibration or acoustic frequencies fall in the band gap (Chen et al., 2014; Gonella et al., 2009). The general idea in acoustic metamaterial energy harvesting is to confine the strain energy originating from an acoustic incidence and convert it into electrical energy. Carrara et al. (Carrara et al., 2013) leveraged the concepts of wave focusing, localization, and funneling to establish novel acoustic metamaterial energy harvesting configurations. Qi et al. (Qi et al., 2016) reported an acoustic energy harvester based on attaching an energy harvester into the defect area of an acoustic metamaterial. The energy harvesting component in all of the existing phononic and acoustic metamaterial energy harvesting studies has been piezoelectric materials. So far, there are only two studies in the area of using mechanical metamaterials for energy harvesting (Li et al., 2017; Tao and Gibert, 2020). The energy harvesters proposed in these studies are simply based on attaching external polyvinylidene difluoride (PVDF) piezoelectric and triboelectric transducers to the structural frame of the metamaterial to convert its localized deformations into electric energy (see Figure 16). A major issue with such segregated designs is that added mass and increased drag due to attaching an

external energy harvesting component may significantly degrade the structural performance of the mechanical metamaterial system. The concepts proposed in this work will tackle this issue by using the mechanical metamaterial fabric as the energy harvesting medium.
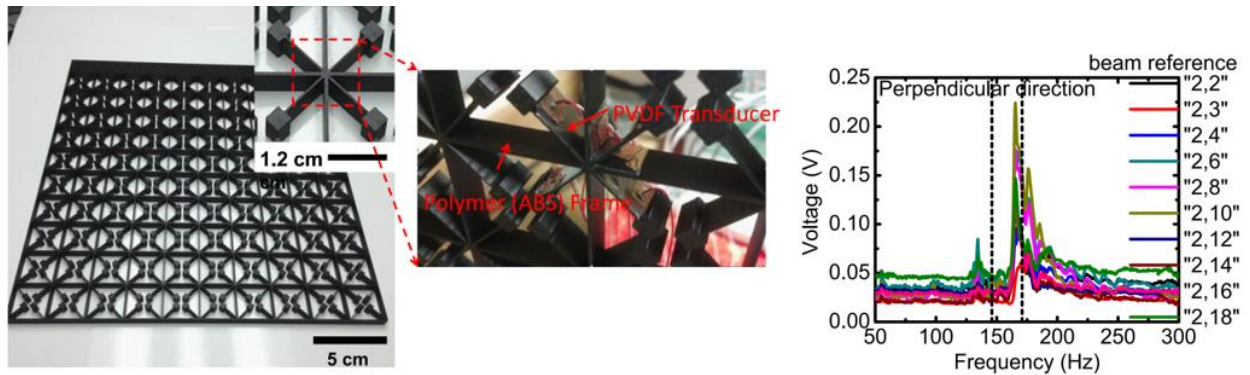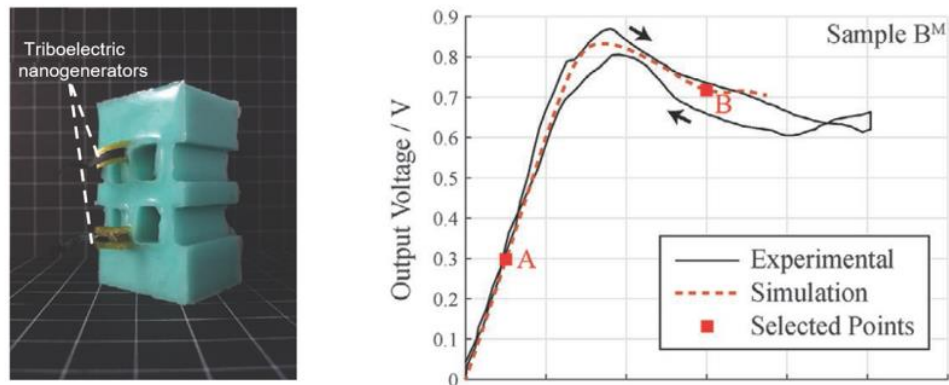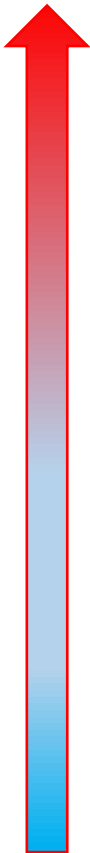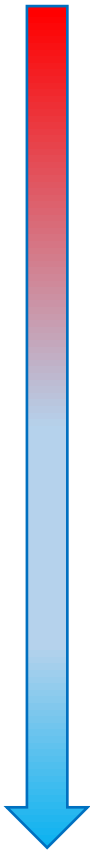
Figure 16 Mechanical metamaterials energy harvester: (a) Piezoelectric transducer attached to the surfaces of an auxiliary structure (cantilevers) within the metamaterial frame (Li et al., 2017), and (b) Triboelectric transducer bonded to a metamaterial-inspired frame (Tao and Gibert, 2020).

3.3.1 Triboelectric Nano generators (TENGs)

The use of nanogenerators has revolutionized harvesting energy and sensing techniques. In 2006 the first concept of nanogenerators was introduced by Z. L. Wang et al. as piezoelectric nanogenerators (Askari et al., 2018; Wang and Song, 2006). Several years later in 2012, a new method of energy harvesting was proposed based on the triboelectrification effect. This innovative technology is called triboelectric nanogenerators (TENGs) (Wang et al., 2018). Recent studies have provided useful information on TENG technology progress in different areas, including theory and modeling (Dharmasena et al., 2017; Niu et al., 2015, 2014, 2013; Niu and Wang, 2014; Pan and Zhang, 2019), energy harvesting (Fan et al., 2016; Hinchet et al., 2015; Wang et al., 2017; Zi and Wang, 2017), and active sensing (Chen and Wang, 2017; S. Wang et al., 2015; Wen et al., 2018). Triboelectricity is the phenomenon caused by friction between different materials when they are rubbed or pressed together. It is contact-induced electrification. When two different materials come into contact, the electrical charge is transferred at the interface of the two materials to maintain the electrochemical equilibrium. After separation, some extra electrons remain on the bonded atoms. Releasing those extra electrons results in the flow of charge (Niu and Wang, 2014; Yang et al., 2015). Almost any materials have triboelectrification effect, such as wood, metal, paper, plastic, etc. Because all of these materials can be used to make TENGs, the material options for TENG are vast. However, the ability of a material to gain or lose electrons is dependent on its polarity. Table 2 shows a triboelectric series for some common materials (Wang et al., 2018). When a material at the bottom of the series (negative side) is contacted by a material towards the top of the series (positive side), the material gains a larger charge. The greater the distance between two materials in the series, the more the charge transmitted.

Table 2 Triboelectric serirs for different material whit a tendency of lsing electrons (positive) and gaining electrons (negative) (Wang et al., 2018).

Positive			Negative
	Glass	Polyvinyl alcohol	
	Mica	Polyester (Dacron) (PET)	
	Polyamide 6-6	Polyisobutylene	
	Rock salt (NaCl)	Polyuretane flexible sponge	
	Wool, knitted	Polyethylene terephthalate	
	Furr	Polyvinyl butyral	
	Silk, woven	Polychlorobutadiene	
	Polyethylene glycol succinate	Butadiene-acrylonitrile copolymer	
	Cellulose	Natural Rubber	
	Cotton, woven	Polybisphenol carbonate	
	Polyurethane elastomer	Polychloroether	
	Steel	Polystyrene	
	Wood	Polyethylene	
	Hard rubber	Polypropylene	
	Amber	Polydiphenyl propane carbonate	
	Acetate, Rayon	Polyimide (Kapton)	
	Polymethyl methacrylate (Lucite)	Polyethylene terephtalate	
	Polyvinyl alcohol	Polyvinyl Chloride (PVC)	
	Copper	Polytrifluorochloroethylene	
	Silver	Polytetrafluoroethylene (PTFE, Teflon)	

As shown in Figure 17 four basic modes of TENGs were introduced by Z. L. Wang's group (Wang et al., 2018) as below:
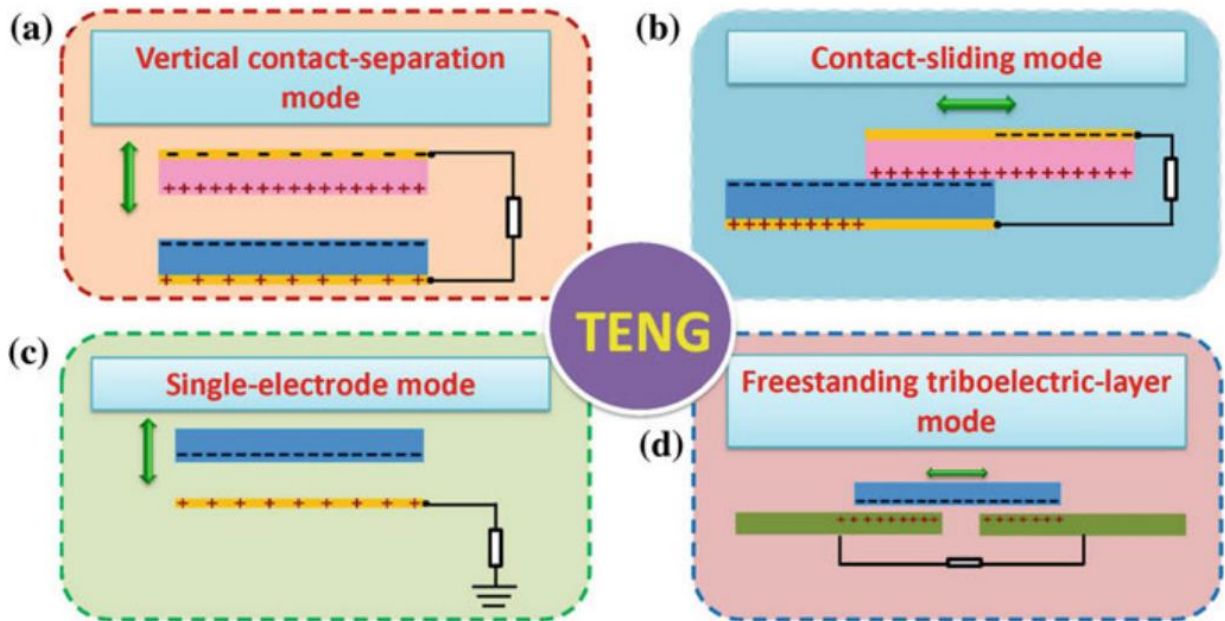
Figure 17 The four basic modes of TENgs: (a) contact-separation mode; (b) sliding mode; (c) single-electrode mode; and (d) freestanding mode. (Wang et al., 2018)

3.3.1.1 Contact-Separation Mode

Two different dielectric films face one other, and electrodes are being deposited on the layered structure's top and bottom surfaces (Figure 17a). Contact between the two dielectric layers results in oppositely charged surfaces. A potential drop is formed when two surfaces are separated by a tiny gap caused by the lifting of an external force. If the two electrodes are electrically connected by a load, free electrons from one electrode flow to the other to create an opposing potential in order to balance the electrostatic field. When the gap is closed, the potential generated by the triboelectric charge vanishes, and the electrons flow back.

3.3.1.2 Sliding Mode

Structure of the sliding mode TENG is the same as contact-separation mode (Figure 17b). Triboelectric charges are also produced on surfaces when two dielectric films slide on each other. Along the sliding direction, lateral polarization forces electrons on the top and bottom electrodes to flow. An AC signal is generated by periodic sliding. Disc rotation and planner motion are the potential options that can be used in sliding TENG mode.

3.3.1.3 Single-Electrode Mode

Both of the sliding mode TENG and contact-separation mode TENG have two electrodes connected to the load. In some cases, it is almost impossible to have both of the TENG parts electrically connected to the load. In this situation one electrode is connected to the load, and another one is grounded (Figure 17c), which is called single-electrode TENG mode. This mode is capable of working in both the contact-separation and sliding states.

3.3.1.4 Freestanding Mode

In a freestanding TENG mode, two symmetric electrodes are placed beneath a dielectric layer, while the distance between the electrodes and the electrode size are comparable to the size of the object moving in front of the electrodes (Figure 17d). As the object approaches and/or departs from the electrodes, asymmetric charge distribution in the media occurs, leading to an electron flow between the electrodes to balance the local potential distribution.

Triboelectricity has attracted a great deal of attention in recent years due to its potential for power generating to standalone devices and for energy harvesting (Wang et al., 2018).

4.0 Meta-tribomaterials

The presented objective in this part has been published in the Nano Energy Journal as well as a U.S. patent as (Alavi and Barri, 2022; Barri et al., 2021a):

Barri, K., Jiao, P., Zhang, Q., Chen, J., Wang, Z.L., Alavi, A.H., 2021. Multifunctional meta-tribomaterial nanogenerators for energy harvesting and active sensing. Nano Energy 86, 106074. https://doi.org/10.1016/J.NANOEN.2021.106074

Alavi, A., Barri, K., 2022. Self-aware composite mechanical metamaterials and method for making same. US Patent 2022/0011176 A1.

4.1 Physics mechanism of meta-tribomaterials

In order to develop the meta-tribomaterial system, self-recovering mechanical metamaterial and triboelectric energy harvesting paradigms should be integrated into the matrix of a multi-stable lattice. Meta-tribomaterial are composed of snapping mechanical metamaterial unit cells built-in contact electrification mechanism, as shown in Figure 18. Under uniaxial loading, the sample undergoes a large deformation caused by stiffness mismatch between snapping (buckling instabilities) and supporting (relatively stiffer/thicker) components, exhibiting very small transverse deformation after every snapping. Based on the multi-stable/self-recovering mechanism, phase transformation/shape-reconfiguration and zero (or close to zero) Poisson's ratio can be achieved up to large morphological change. As shown in Figure 18, when a normal vertical

37

force applied in the middle of the curved beams, the semicircular-shaped segment is mechanically deformed (buckled), snapping from first/original stable state (State I) to fully compacted/deformed stable state (State III) at a critical applied force. In a very ideal situation, the constrained conditions at both ends are strong and the two stable states are symmetric, the reaction force will be symmetric from one to the other stable state under displacement control which means that an identical reverse force is needed that allows the deformed beams to return to their original configuration. In the case of a self-recovering snapping, the constant positive force means that the fully compacted segments (State III) automatically return to their initial stable configuration (State I) after the load is removed.
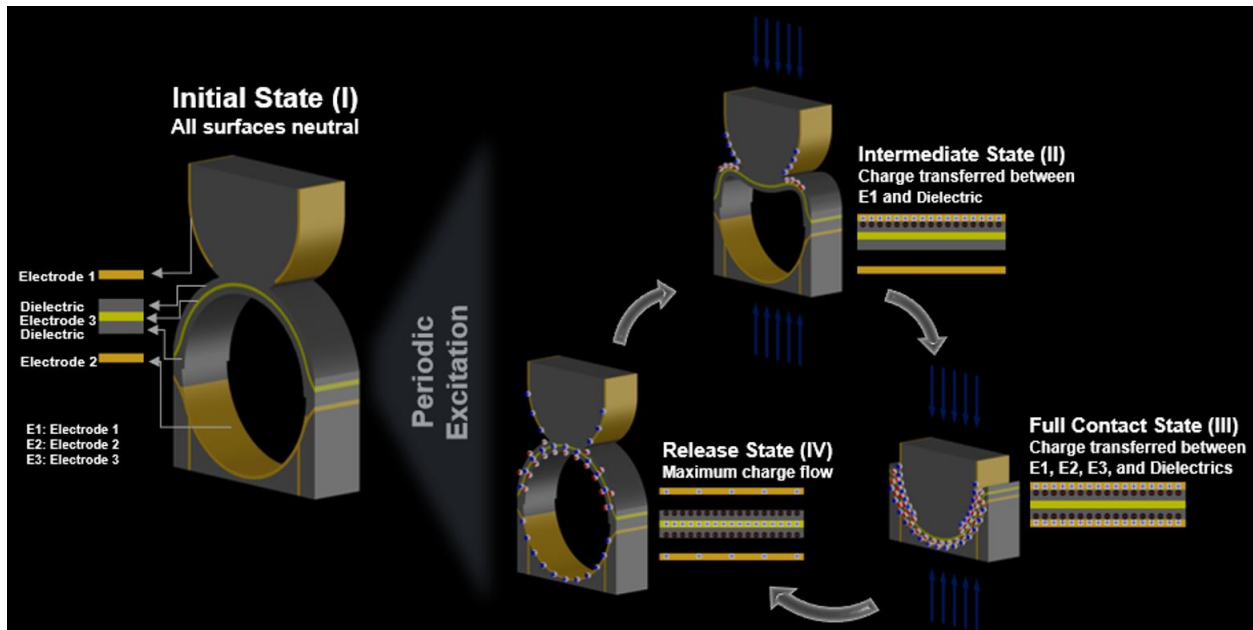
Figure 18 Design of snapping mechanical metamaterial unit cell

The proposed system servs as a triboelectric nanogenerator (TENG). As it explained in chapter 3, TENGs have four fundamental working modes: vertical contact-separation mode, lateral sliding mode, single-electrode mode, and freestanding triboelectric-layer mode (see Figure 17). The

vertical contact-separation mode is integrated into the unit cell design in this study. As shown in Figure 19, the physical contact of two different materials' surfaces with distinct electron affinity creates oppositely charged surfaces. A potential drop is created when two surfaces are separated by a gap. Free electrons in one electrode would flow to the other electrode in order to balance the electrostatic field when the two electrodes are electrically connected by a load. The potential drop created by triboelectric charges disappears when the gap is closed, and the induced electrons will flow back (Wang et al., 2012; Zhu et al., 2012). Under compressive loads, the snapping mechanical metamaterial structure undergoes periodic deformations and contact electrification occurs between the conductive and non-conductive surfaces (see Figure 18). By unloading the structure, a potential difference is formed between the conductive layers. Higher loading amplitude results in larger deformations. Consequently, more conductive and dielectric layers of the matrix get involved in the contact-separation process. This leads to higher rate of the electrostatically-induced electron transfer and generating higher voltage.
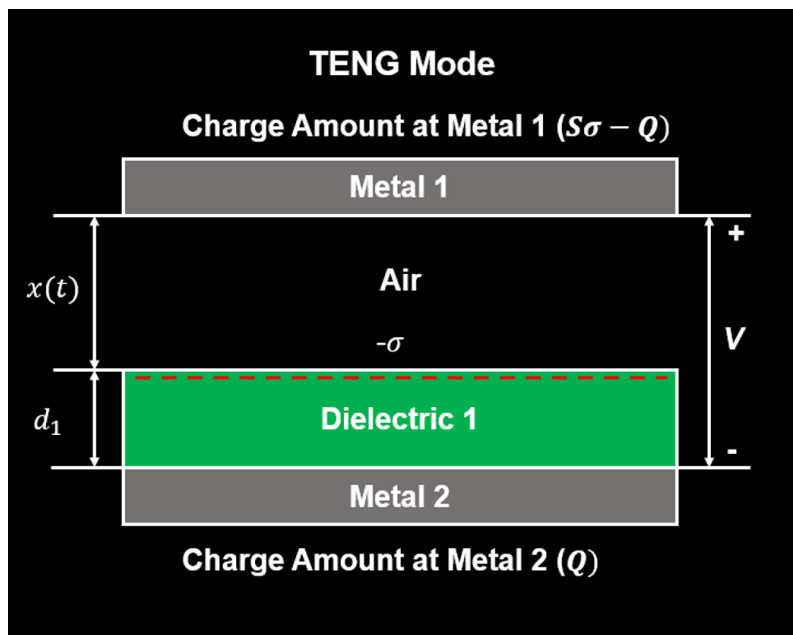
Figure 19 Working mechanisim of teng system

To show the feasibility of creating meta-tribomaterial-based mechanisms, two-dimensional (2D) snapping mechanical metamaterials are studied first. An architected mechanical metamaterial containing parallel snapping curved (semicircular-shaped) segments with elastic snap-through instability mechanism was fabricated as the test structure. The design of mechanical metamaterials with snap-through instabilities has been the focus of active research in recent years (Che et al., 2017; Haghpanah et al., 2016; Rafsanjani et al., 2015; Yang and Ma, 2019). Multi-stable/self-recovering snapping metamaterials have advantages in the applications such as the development of tunable metamaterials with switchable properties (Che et al., 2017; Yang and Ma, 2019). In this study, the metamaterial was made up of multiple bi-stable unit cells. The unit cell consisted of thick horizontal and vertical elements and a thin curved part. In order to incorporate the sensing and energy harvesting features into the metamaterial functionality, the triboelectric nanogenerator concept was introduced into its architecture design. The design process is shown in Figure 20. Triboelectric nanogenerators can produce electrical output based on triboelectrification and electrostatic induction in response to an external mechanical stimulation (Wang, 2013). The contact electrification is a universally-existing phenomenon in the nature and people's living life, and has been known for thousands of years. It describes a phenomenon that a material/surface becomes electrically charged after it gets into contact with a different material/surface (S. Wang et al., 2015). Four fundamental modes of triboelectric nanogenerators are vertical contact-separation mode, single-electrode mode, lateral-sliding mode, and freestanding mode (S. Wang et al., 2015). However, in order to fabricate the 2D structure of the snapping composite mechanical metamaterial, three constituent layers were defined. The first two layers were conductive (electrode) layers created as periodic repeatable segments (Figure 20a). The aligned conductive layers act as opposite electrodes that are embedded inside a thicker non-conductive (dielectric)

40

layer serving as the skeleton of the mechanical metamaterial (Figure 20b). All conductive and non-conductive layers of the prototypes are printed simultaneously. Therefore, the 3D printed samples are ready to test immediately after finishing the printing process without a need to post-printing modifications. In Figure 20, h, g, l, L, W, and R, are 15.5 mm, 6.5 mm, 82.6 mm, 119.35 mm, 100 mm, and 7.76 mm, respectively. The thicknesses of the conductive and non-conductive layers are 0.65 mm and 0.3 mm, respectively. In order to fabricate this complex design as one integrated unit, Raise3D Pro2 Dual Extruder 3D Printer was used as it supports printing with a variety of multi-material filaments. There is a wide range of organic and inorganic materials from the triboelectric series that can be used to fabricate the conductive and dielectric layers. To maximize the electrification between the two layers, materials with large differences in triboelectric polarity were chosen. Polylactic Acid (PLA) with carbon black (Young's modulus $E = 3000$ MPa, Poisson's ratio $v = 0.25$) and Thermoplastic Polyurethane (TPU) ($E = 12$ MPa, $v = 0.48$) were used as the conductive and non-conductive layers, respectively. As seen in Figure 20c,d, the entire snapping composite mechanical metamaterial structure forms composite matrix composed of the conductive and dielectric layers in a periodic manner. The semicircular-shaped snapping segments include both conductive and non-conductive layers. The semicircular-shaped snapping segments were centrally clamped by relatively thicker (stiffer) supporting segments with a connection platform, as illustrated in Figure 20b. The curved elements were specifically designed in mathematical/trigonometric function form to achieve smooth snap-through transition and symmetrical stable configurations before and after large deformation. The clamped conditions of the snapping beams at both ends were released and connected to supporting segments to create periodic repeatable unit cells and provide local support to prevent lateral displacement and bending at the ends of the semicircular-shaped slender elements.
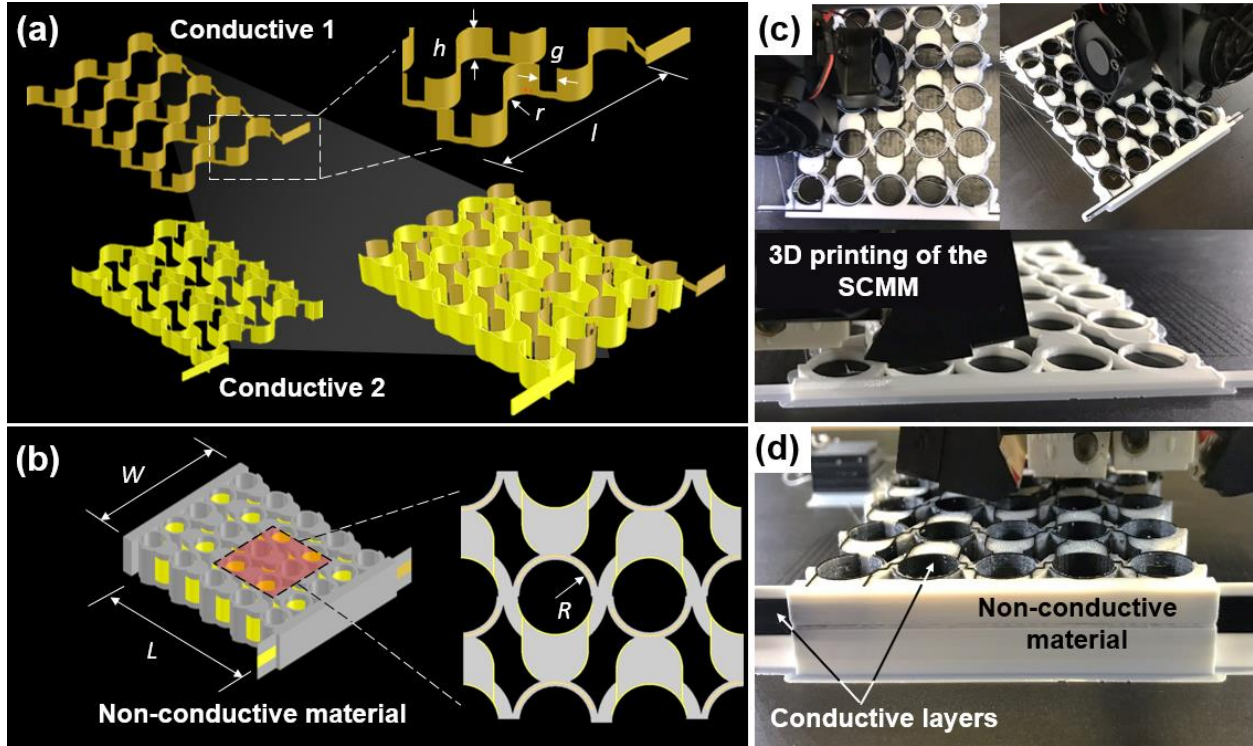
Figure 20 Designing a 2D mechanical metamaterial with parallel semicircular-shaped snapping segments under the meta-tribomaterial concept: (a) Segments of the two conductive layers (Conductive 1 and 2) created as 5 periodic repeatable segments, and the aligned conductive layers, (b) Schematic representation of the composite matrix composed of the conductive and non-conductive layers in a periodic manner, and (c), (d) 3D printing of the meta-tribomaterial prototypes composed of the conductive and non-conductive layers that are involved in the contact–separation process.

The test setup and the fabricated prototype are shown in Figure 21. Uniaxial loading experiments were performed on the 3D printed metamaterial specimen with a TestResources testing machine. Cycling loading at 0.5 Hz frequency was applied to the specimen under displacement control until it was fully compacted. The displacement range was controlled to be between 5 mm to 10 mm. The applied load changed between 15 N and 45 N.
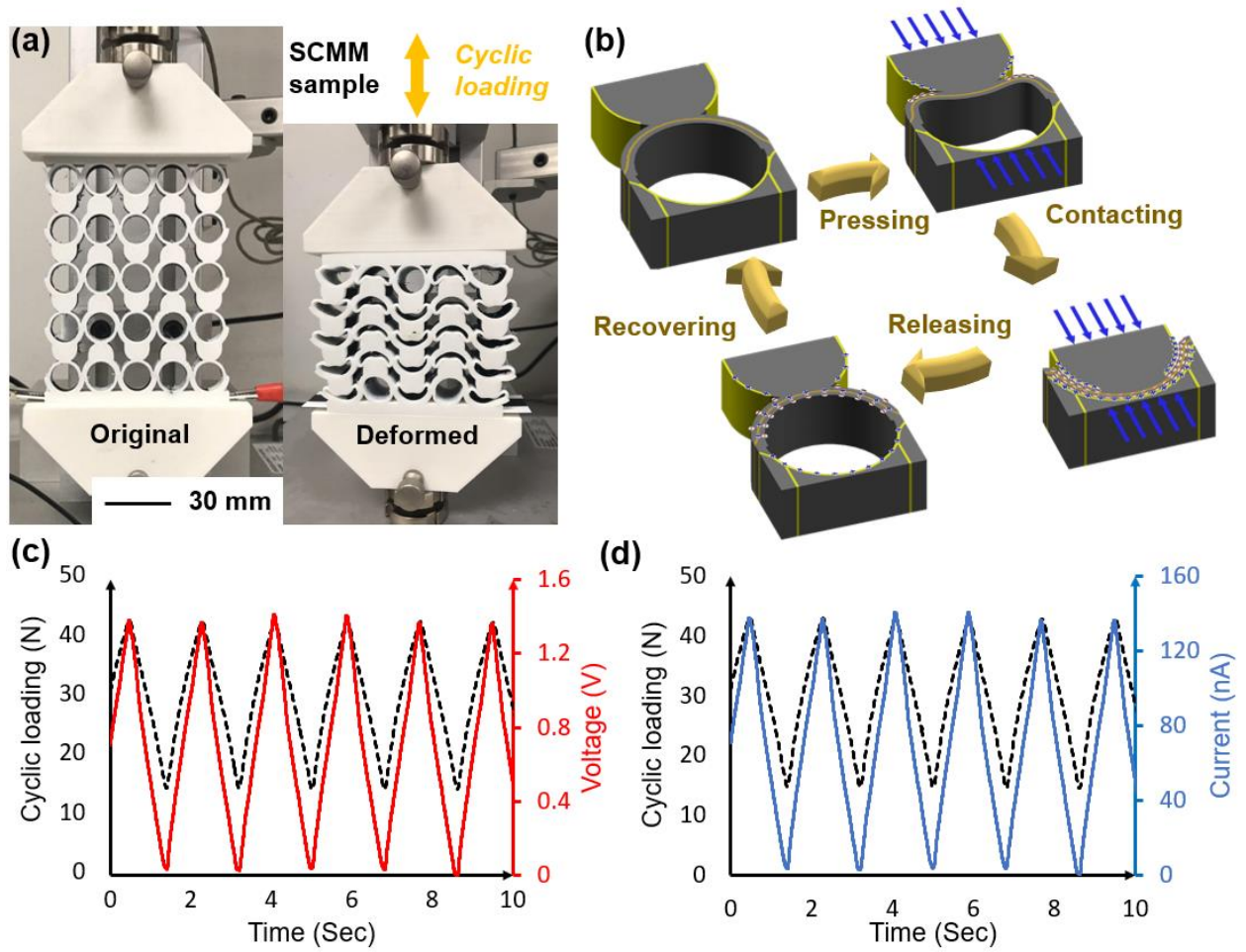
Figure 21 A self-sensing and self-charging 2D mechanical metamaterial: (a) 3D printed meta-tribomaterial sample comprised of 5×5 unit cells at the original and deformed states under cyclic loading. (b) Snapping mechanisms of the elastic bulking semicircular-shaped snapping shells, and the operating principle of the meta-tribomaterial unit cells in the contact-separation mode triboelectric nanogenerator. Applied cyclic loading and the corresponding (c) voltage and (d) current generated by the proposed meta-tribomaterial (in red and blue, respectively).

In order to record the voltage generated due to the applied mechanical excitations, wires were connected to the extended parts of the conductive layers, as shown in Figure 21a. The voltage values were read using a National Instruments 9220 DAQ module with 1 GΩ impedance. A low-noise current amplifier (SR570, Stanford Research Systems) was used to measure the currents

generated by the meta-tribomaterial prototypes. The applied cyclic loads and the corresponding voltage and current generated by the proposed mechanical metamaterial structure are, respectively, shown in Figure 21c,d. As seen, the voltage and current values are proportional to the applied force. The maximum generated voltage and the corresponding measured current were 1.35 V and 140 nA respectively. Also, the generated electrical energy can be readily stored using an energy harvesting circuit.

Figure 22 illustrates the meta-tribomaterial charging characteristics under periodic mechanical motion. Figure 22a,b show the voltage-time and the stored charge-time relationships at different load capacitances, respectively. As seen in Figure 22a, the capacitors are charged at the maximum speed at t = 0. Thereafter, the speed of charging decreases gradually until it reaches the saturation voltage. The saturation voltage is about 0.85 V, which is almost 0.5 V less than the maximum voltage shown in Figure 21c. Figure 22c shows the influence of the capacitance on both final voltage and stored charge in the capacitors after 40 s. For the small capacitor, the voltage on the capacitor is almost equal to the saturation voltage, while the stored charge, which is proportional to capacitance, is close to zero. By increasing the capacitance, the stored charge increases and the voltage decreases. Figure 22d shows the voltage and current output for different load resistances. When the resistance is low enough (less than 100MΩ), the current is at its peak value and the voltage is at its minimum level. When the resistance value is large enough (more than 1GΩ in this study), the voltage is almost at its peak value and the current is close to zero.
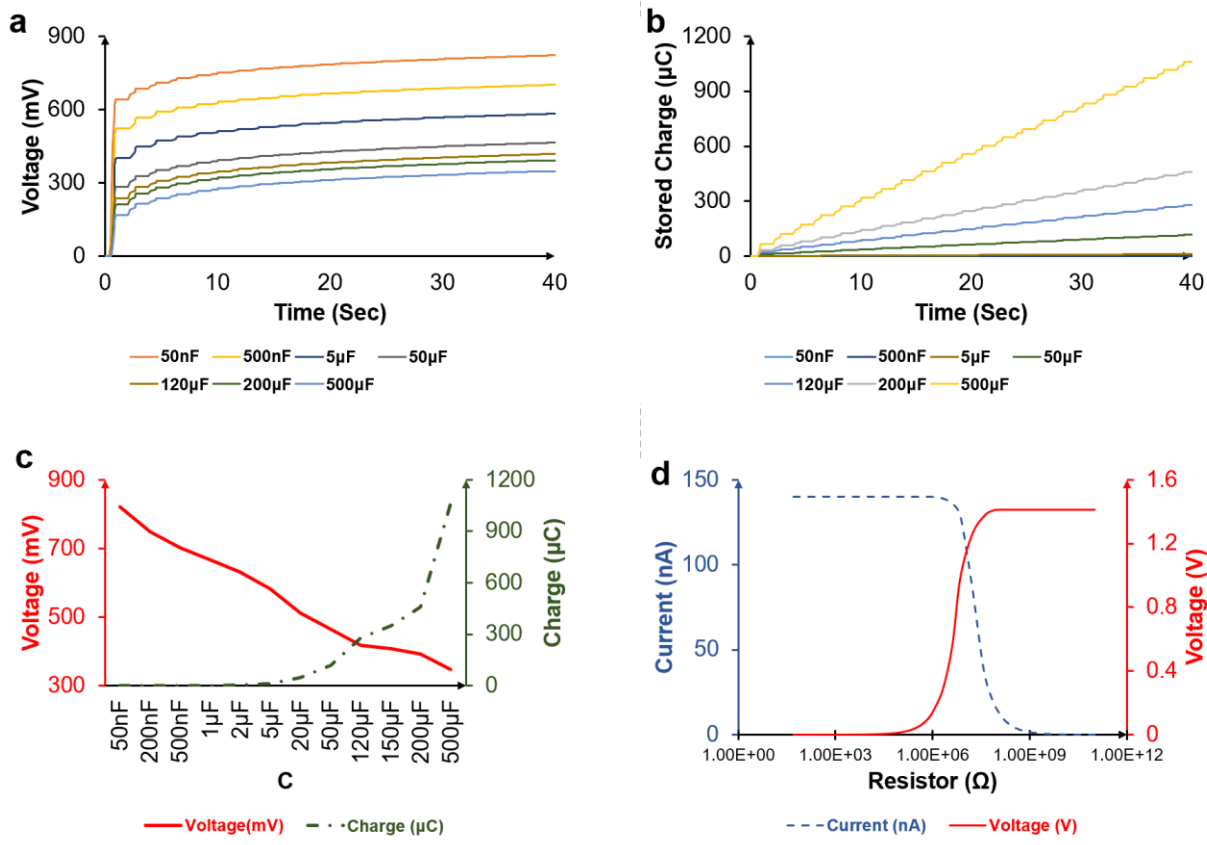
Figure 22 meta-tribomaterial charging characteristics under periodic mechanical motion. a, Voltage-time relationship at different load capacitances. b, Stored charge-time relationship at different load capacitances. c, Voltage and charge stored in the load capacitor at 40 seconds. d, Load resistance effects on the output voltage and current.

4.2 Mechanical and Electrical Characterizations of the meta-tribomaterial

Figure 23 presents the force-displacement relations of the cylindrical unit in the meta-tribomaterial. It can be seen that the curve has three stages, including the stable, unstable and strengthened. It can be seen that the unstable stage of the semi-cylinder contributes the majority of the contact-separation motions, which accounts for the triboelectric effect in the V-Q-x theory.

45
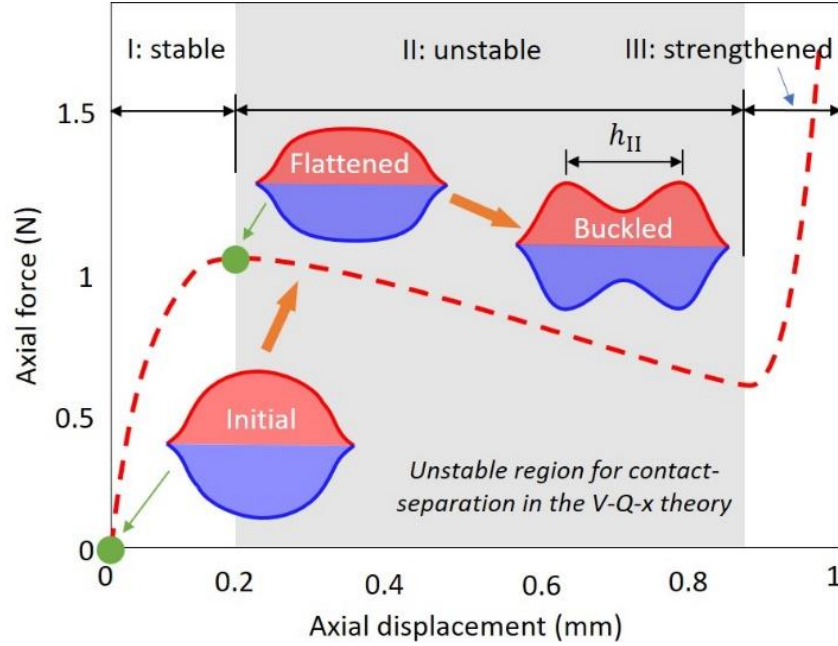
Figure 23 Force-displacement relations of a cylindrical unit in the meta-tribomaterial and the corresponding original and deformed shape configurations in the stable and unstable regions.

4.2.1 Characterization of the Electrical Performance of meta-tribomaterials

In the proposed snapping meta-tribomaterial, the thickness of the dielectric layer is d_1, and the relative dielectric constant is ε_{r1}. Therefore, the equivalent thickness of the dielectric layer can be written as:

$$d_0 = \frac{d_1}{\varepsilon_{r1}}$$

4-1

and the *V-Q-x* relationship is expressed as (Zhang and Quan, 2019):

$$V = -\frac{Q}{S\varepsilon_0}[d_0 + x(t)] + \frac{\sigma x(t)}{\varepsilon_0}$$

4-2

46

ε_0, σ, $x(t)$, and S denote the vacuum permittivity, charge density at the contact surface, varying gap distance, and the effective contact area, respectively. To determine the voltage V in Equation (4-2), it is necessary to obtain $x(t)$ and S. Since the cyclic compression applied to the meta-tribomaterial was displacement-control, the varying gap distance was determined by the loading conditions in the experiments as:

$$x(t) = \frac{\Delta(t)}{n_y}$$

<div align="right">4-3</div>

$\Delta(t)$ is the displacement and n_y is the number rows. Connecting the meta-tribomaterial with a load resistance R to form a circuit, the generated voltage V can be obtained using the Ohm's law as:

$$V = R\frac{\mathrm{d}Q}{\mathrm{d}t}$$

<div align="right">4-4</div>

where Q is the charge. Substituting Equations (4-3) and (4-4) into Equation (4-2):

$$\frac{\mathrm{d}Q}{\mathrm{d}t} = -Q\Gamma + \frac{\sigma\Delta(t)}{n_y R \varepsilon_0}$$

<div align="right">4-5</div>

$$\Gamma = \frac{d_0 + x(t)}{RS\varepsilon_0} = \frac{n_y d_0 + \Delta(t)}{n_y SR\varepsilon_0}$$

<div align="right">4-6</div>

Solving the ordinary differential equation in Equation (4-5) leads to:

$$Q(t) = e^{-\int \Gamma \mathrm{d}t} \int \frac{\sigma\Delta(t)}{n_y R \varepsilon_0} e^{\int \Gamma \mathrm{d}t}\, \mathrm{d}t + c e^{-\int \Gamma \mathrm{d}t}$$

<div align="right">4-7</div>

where c is the integration constant that can be determined by the initial conditions. Deriving

Equation (4-7), the voltage can be obtained as:

$$V(t) = R\frac{dQ}{dt} = -R\Gamma e^{-\int_0^t \Gamma d\tau} \int_0^t \frac{\sigma\Delta(\xi)}{n_y R\varepsilon_0} e^{\int_0^\xi \Gamma d\tau} d\xi + \frac{\sigma\Delta(t)}{n_y\varepsilon_0} - c\Gamma e^{-\int_0^t \Gamma d\tau} \qquad \textbf{4-8}$$

According to the boundary conditions:

$$V|_{t=0} = -\frac{Q|_{t=0}}{S\varepsilon_0}\left(d_0 + \frac{\Delta|_{t=0}}{n_y}\right) + \frac{\sigma\Delta|_{t=0}}{n_y\varepsilon_0} = \frac{\sigma\Delta|_{t=0}}{n_y\varepsilon_0} - \frac{c}{S\varepsilon_0}\left(d_0 + \frac{\Delta|_{t=0}}{n_y}\right) \qquad \textbf{4-9}$$

and

$$Q|_{t=0} = 0 \qquad \textbf{4-10}$$

which leads to: $c = 0$. As a consequence, Equations (4-7) and (4-8) can be rewritten as below equations. To determine the charge and voltage, it is necessary to obtain the effective contact area S in Γ.

$$Q(t) = e^{-\int \Gamma dt} \int \frac{\sigma\Delta(t)}{n_y R\varepsilon_0} e^{\int \Gamma dt} dt \qquad \textbf{4-11}$$

and

$$V(t) = -R\Gamma e^{-\int_0^t \Gamma d\tau} \int_0^t \frac{\sigma\Delta(\xi)}{n_y R\varepsilon_0} e^{\int_0^\xi \Gamma d\tau} d\xi + \frac{\sigma\Delta(t)}{n_y\varepsilon_0} \qquad \textbf{4-12}$$

4.2.2 Characterization of the mechanical response of meta-tribomaterials

The deformation configuration of the meta-tribomaterial unit under the axial compression can be calculated as (Che et al., 2017):

$$EI\left(\frac{\mathrm{d}^4w}{\mathrm{d}x^4} - \frac{\mathrm{d}^4w_0}{\mathrm{d}x^4}\right) + p\left(\frac{\mathrm{d}^2w}{\mathrm{d}x^2}\right) = -f\delta\left(x - \frac{l}{2}\right) \qquad \text{4-13}$$

where w, $w0(x)$, p, E, I, f, δ, and l are the deflection of the beam, the initial shape of the beam, the compression force of the beam, the Young's modulus, the area moment of inertia of the beam, the transverse force, the Dirac delta function, and the total length of the beam, respectively. The boundary conditions are:

$$\begin{cases} w_0(x) = \dfrac{h}{2}W_1(x) \\ W_1(x) = 1 - \cos\left(\dfrac{2\pi x}{l}\right) \end{cases} \qquad \text{4-14}$$

where h is the maximum height of the initial beam (i.e., radius of the meta-tribomaterial unit). The general solution can be written as:

$$w(x) = \sum_{i=1}^{\infty} A_i W_i(x) \qquad \text{4-15}$$

Where the symmetric buckling mode and the antisymmetric buckling mode are shown in equations 4-16) and (4-17) respectively:

$$\begin{cases} W_i(x) = 1 - \cos\left(N_i \dfrac{x}{l}\right) \\ N_i = (i+1)\pi \end{cases}, i = 1, 3, 5 \ldots \qquad \text{4-16}$$

$$\begin{cases} W_i(x) = 1 - 2\dfrac{x}{l} - \cos\left(N_i \dfrac{x}{l}\right) + \dfrac{2}{N_i}\sin\left(N_i \dfrac{x}{l}\right) \\ N_i = 2.86\pi, 4.92\pi \ldots . \end{cases}, i = 2, 4, 6 \ldots \qquad \text{4-17}$$

and A_i are the weight coefficients that determine the contribution of each buckling mode to the shape function. The effective contact area S in Equations (4-11) and (4-12) are obtained as:

$$S = \varphi \cdot 2\pi h \cdot B \qquad \text{4-18}$$

where B is the width of the electrode and dielectric layers in the meta-tribomaterial. φ is the contact-separation factor give as:

$$\varphi = \frac{h_{\mathrm{II}}}{2h} = \frac{1}{6} \qquad \text{4-19}$$

where h_{II} is the radius of the cylindrical units in the buckling region (i.e., unstable). Taking Equation (4-19) into Equation (4-18), the effective contact area yields:

$$S = \frac{1}{3}\pi h B \qquad \text{4-20}$$

50

Finally, substituting Equation (4-20) into Equations (4-11) and (4-12), the total charge and voltage of the meta-tribomaterial can be calculated as:

$$Q_{\text{total}} = n_x n_y Q(t) \qquad \text{4-21}$$

$$V_{\text{total}} = n_x n_y V(t) \qquad \text{4-22}$$

Table 3 summarizes the geometric and material properties of the meta-tribomaterial (Zhang and Quan, 2019). Figure 24 presents the comparison of the output voltages between the theoretical and experimental results.

Table 3 Geometric and material properties of the meta-tribomaterial.

Geometric properties (mm)	Cylindrical unit radius h	7.45
	Width B	15.5
	Thickness of the electrode layer ($E = E1 = E2$)	0.3
	Thickness of the dielectric layer ($d = d1$)	0.65
Material properties	Relative permittivity of the dielectric layer (TPU) ε_{r1}	7.2
	Permittivity of vacuum ε_0	8.854×10^{-12}
	Surface charge density σ (C/m²)	20×10^{-6}
	Load resistance R (Ohm)	7.5×10^{10}
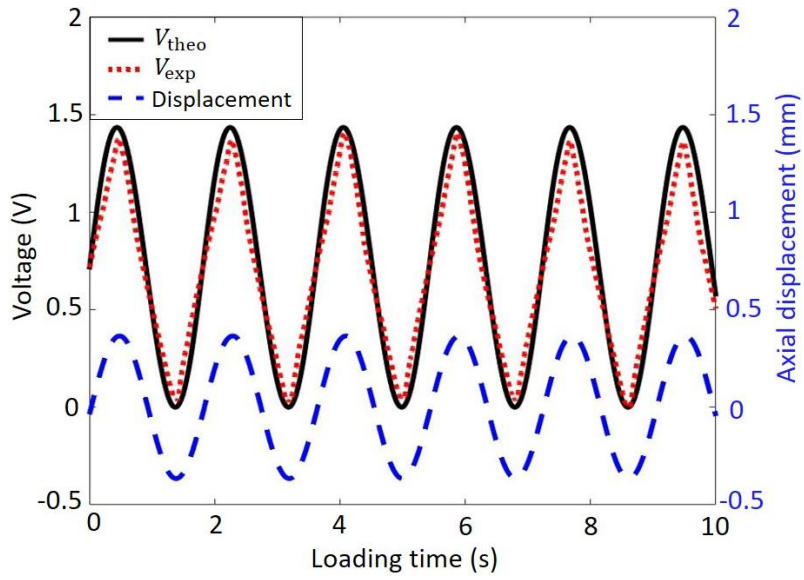
Figure 24 Comparison of the output voltage between the theoretical and experimental results under the cyclic displacement.

5.0 Scaled 3D Hierarchical Structures/Configurations

The results obtained for 2D metamaterials reveal the feasibility of creating composite multifunctional mechanical metamaterial systems with sensing and energy harvesting functionalities via introducing the contact electrification into the fabrication process. It is possible to measure the force/pressure applied to the metamaterial structure by monitoring the generated voltage. The kinetic energy harvested from the external excitations by the nanogenerator metamaterial prototype can be stored for self-powering or empowering other sensing devices. Moreover, the study reveals that it is possible to create mechanical metamaterials whose electrical and mechanical responses can be programmed. The snapping mechanism or the layered design of the composite matrix of the tested structure can be engineered to deform in specified order or prevent random snapping, which will result in programmed triboelectrification and mechanical behaviors. Accordingly, the meta-tribomaterial concept can be applied to design a variety of programmable mechanical metamaterials with sensing, energy harvesting properties.

In order to emphasize the broad range of applications of the meta-tribomaterial concept, it is deployed to create multifunctional biomedical, automotive/aerospace, and civil engineering systems. A series of 3D hierarchical configurations have been developed by taking advantage of the proposed 2D self-recovering meta-tribomaterial design. The first application is patient-specific medical devices which contains spinal fusion cage, cardiovascular stent, and esophageal stent. The other application in automotive/aerospace, and civil engineering systems contains meta-tribomaterial shock absorber, multifunctional composite beam, and metamaterial concrete nanogenerator.

Figure 25 shows the scaled 3D hierarchical structures/configurations under the meta-tribomaterial concept from nano scale to macro scale for the wide range of applications in biomedical, automotive/aerospace and civil engineering.
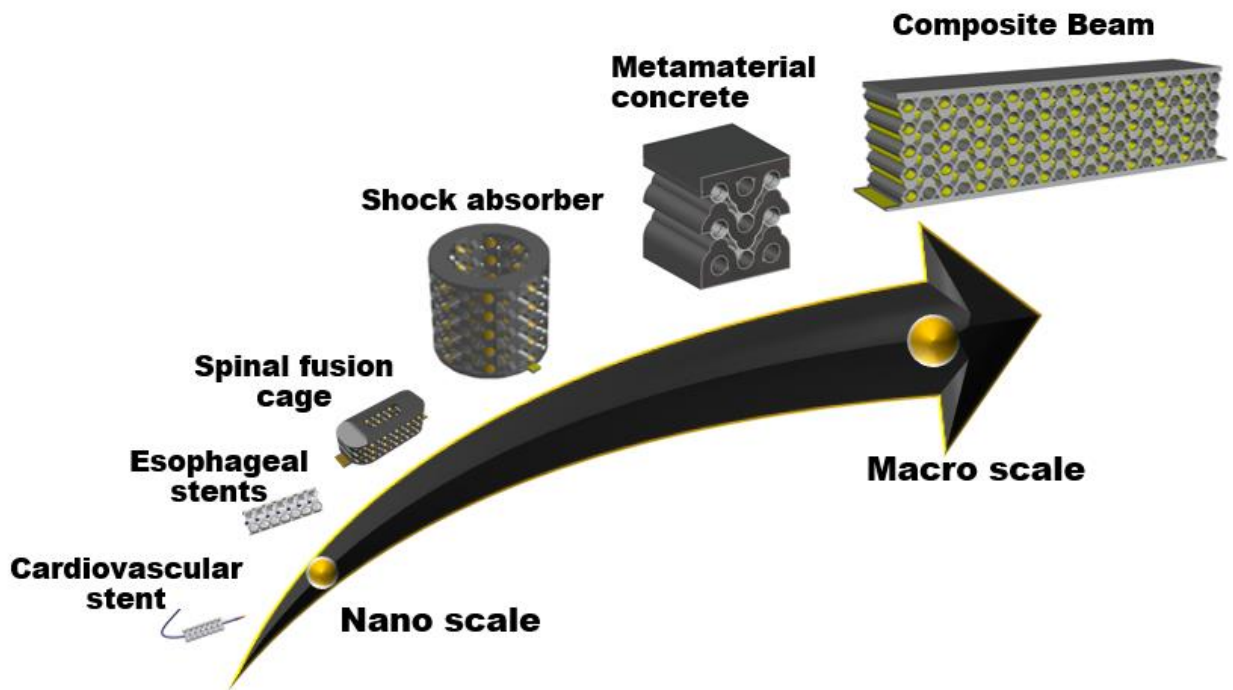
Figure 25 Scaled 3D hierarchical self-sensing and self-powering multifunctional mechanical metamaterial systems

5.1 Patient-specific Self-aware Implants

The presented objective in this part has been published in the Advanced Functional Material Journal as (Barri et al., 2022c):

Barri, K., Zhang, Q., Swink, I., Aucie, Y., Holmberg, K., Sauber, R., Altman, D.T., Cheng, B.C., Wang, Z.L., Alavi, A.H., 2022c. Patient-Specific Self-Powered Metamaterial Implants for Detecting Bone Healing Progress. Adv. Funct. Mater. 2203533.

5.1.1 Introduction

Smart implants with therapeutic benefits and diagnostic capabilities have shown a remarkable potential to revolutionize the healthcare system. For decades, smart implants have been deployed to measure and analyze various physical parameters from inside the body such as patients' pH and hormone levels, electrical activity, forces, strains, displacements, blood glucose, and temperature (Ip and Yang, 2015). Real-time biofeedback provided by smart implants can play a key role in achieving better surgical outcomes. Data collected by smart implants can be used to refine the implant design and to improve surgical techniques and strategies. Despite the significant research carried out in the arena of smart implants, only a small fraction of them have become a part of our daily clinical practice. Two key issues constraining a wide application of the smart implant technologies are the device size for sensor integration and synthesis of scalable biomaterials for fabricating implantable devices (Barri et al., 2022b; Ip and Yang, 2015). Advanced wireless sensors offer new opportunities for designing smart implants. Unlike wired

smart implants that are merely practical for preclinical research, wireless sensors foster development of implants that can take several measurements and communicate in real-time post-surgery (Barri et al., 2022b). Most of the current implantable telemetry systems utilize batteries or capacitors for operation. The use of energy storage devices in biomedical implants is associated with many issues such as short lifetime, size limitations, and chemical risks (Barri et al., 2022b). Passive or battery-free sensors are limited by the implantation depth and cannot record the data continuously unless they are powered by an external inductive/ultrasonic energy source (Alazzawi and Chakrabartty, 2016; Barri et al., 2022b). Many of these passive implants use radio-frequency identification (RFID) technology to interrogate the sensor, which faces severe limitations inside the tissue (Alazzawi and Chakrabartty, 2016). Furthermore, signal corruption commonly occurs in the sensing circuits of the passive implants without sufficient filtering of the power supply voltage. Multiple circuit boards are required for sensing, power transfer, energy storage and wireless communications in active and passive smart implants (Barri et al., 2022b). The implants should be significantly modified in order to integrate these components into their very small area. Creating a new class of smart implants with intrinsic sensing and self-powering mechanisms could be the key to translating innovative implantable devices from lab to the operating rooms.

The other challenge ahead of smart implant technology is the lack of new biomaterials capable of achieving properties similar to human tissue (Zadpoor, 2020). Over the past five decades, researchers have been improving the composition of these metallic or polymeric materials to develop single-functional biocompatible implants mainly with better mechanical performance (Zadpoor, 2020). In order to mimic the extraordinary properties of the biological tissues, more attention has been recently paid to developing implants using novel classes of composites and nanomaterials (Zadpoor, 2020). The most recent innovation in the area of biomaterials for medical

implants is the designer biomaterials concept, where rational geometrical design is used to build mechanical metamaterial systems with desired mechanical, physical, and biological properties (Zadpoor, 2020). Mechanical metamaterials are artificial structures, typically periodic, which are architecturally engineered to have specific properties that do not exist in a natural state (Chen et al., 2010; Zadpoor, 2016). Although incorporating architecture into material development is not a new concept, advanced fabrication techniques such as 3D printing have enabled the manufacturing of mechanical metamaterials with complicated designs. A recent study by Zadpoor (Zadpoor, 2020) has revealed the remarkable potential of mechanical metamaterials to replace biological tissues via facilitating their regeneration. However, the entire concept of metamaterial for biomedical application is still in its infancy. So far, the only effort in the area of metamaterial implants has been a study on rational design of femoral stems with promising mechanical properties and biocompatibilities (Kolken et al., 2018). With the rapid development of smart materials and structures, more intelligent features are being incorporated into mechanical metamaterials (Barri et al., 2021a; Gibson, 2010; Tao and Gibert, 2020). Currently, there is urgent need for exploring new class of multifunctional metamaterial implants with novel properties and functionalities.

5.1.2 Spinal Fusion Cage

Here, the striking concept of "self-aware metamaterial implants" is introduced, where multifunctional implants with built-in TENG mechanisms can utilize their constituent components to achieve advanced functionalities. Without loss of generality, this concept is deployed to create a new generation of multifunctional interbody fusion cage implants with self-sensing,

self-powering and mechanical tunability functionalities for post-operative biomechanical evaluation of lumbar spinal fusion. This study shows how a self-aware metamaterial fusion cage can detect various levels of spinal fusion through continuous stability and load-sharing measurements directly at the intervertebral disc space level. These features could provide physicians the ability to assess the progress of fusion without the need for advanced radiographic imaging. The experiential studies are performed using synthetic and human cadaver spine models to verify the performance of the self-aware fusion cage system. Also, the capacity of this scalable and cost-effective concept in changing the landscape of the patient-specific smart implantable technologies is discussed.

5.1.2.1 Results and Discussion

In this dissertation, the first-of-its-kind mechanically tunable multifunctional metamaterial implant that can sense and harvest energy from body motions is demonstrated. The self-aware implant concept is inspired by the recent study on meta-tribomaterial sensor and nanogenerators which is explained in chapter 4 of this dissertation. A self-aware implant can be seen as a composite mechanical metamaterial system with multi-stable/self-recovering snapping segments. Different rationally-designed triboelectric auxetic microstructures are used to build a self-aware implant. The entire implant structure serves as an energy harvesting medium as well as an active sensing system. The implant is capable of collecting information about the operating environment directly. This metamaterial implant with a built-in TENG mechanism can offer unprecedented mechanical properties such as ultra-high strength-to-density ratios and high resilience. These properties are crucial for designing a mechanically robust implant.
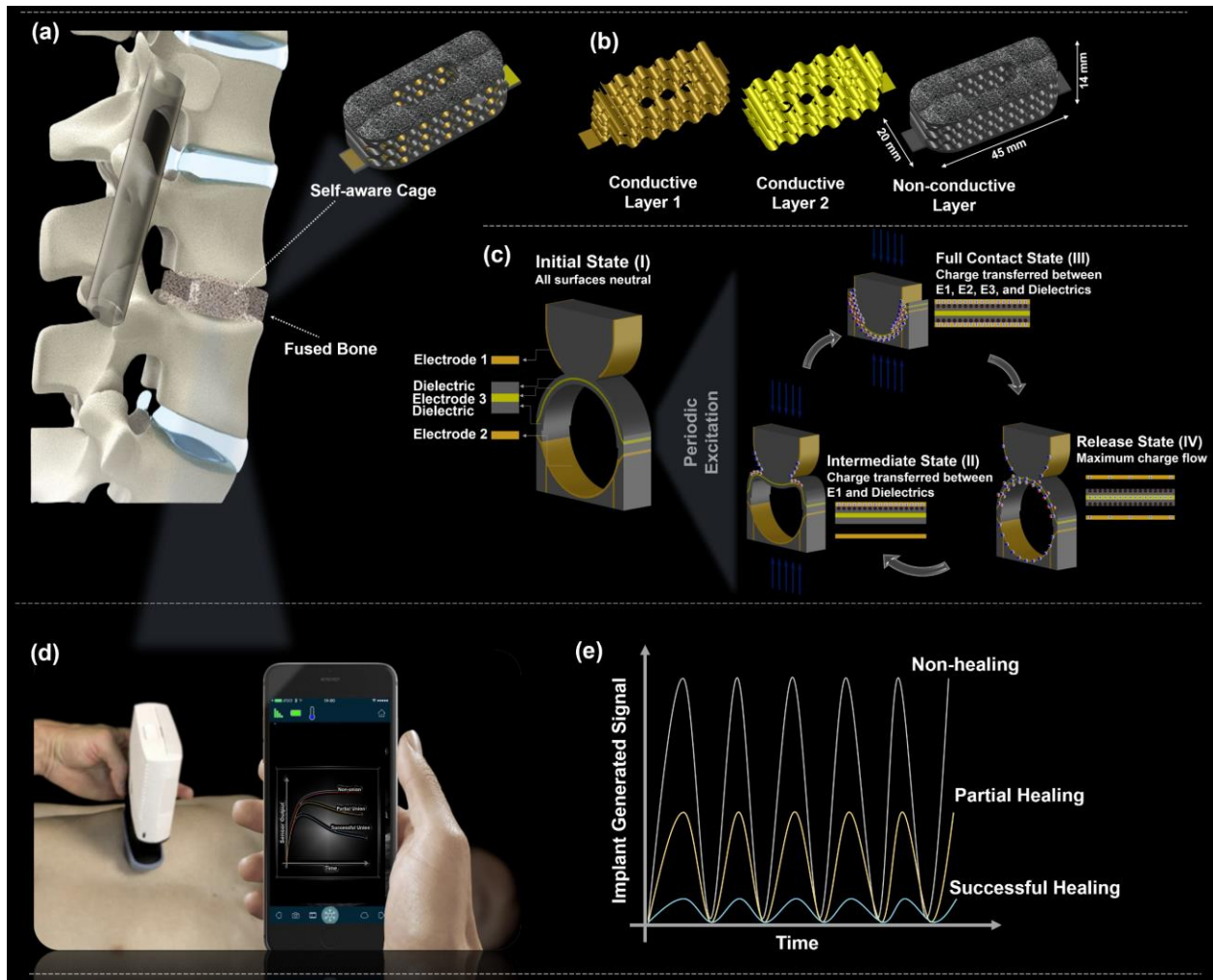
Figure 26 Vision for the proposed research showing a self-aware implant that can be used for reliable determination of spinal fusion development post-surgery directly at the intervertebral level. (a) A multifunctional nanogenerator interbody fusion cage with self-recovering, self-sensing and energy harvesting functionalities implanted during spinal fusion surgery. (b) Composition of a self-aware cage implant. The implant generates electrical signals due to spine micro-motions using its built-in contact-electrification mechanism. The signal can be used for sensing and energy harvesting purposes. (c) Physics mechanisms of the built-in contact-electrification in self-aware implants. (d) The recorded data will be retrieved using an FDA-compliant portable ultrasound scanner. This figure shows a Clarius Tri-Scanner™ ultrasound scanner. (e) The sensor output signals represent various healing stages and can be correlated with the changes of FSU stiffness due to the healing process.

A proof-of-concept spinal fusion cage prototype highlights the features and underlying mechanics of the proposed technology. The reason behind this choice is that interbody fusion cages are widely used in treating conditions with lumbar spinal instability. Lumbar spinal fusion surgery is performed to treat spinal disorders such as degenerative conditions, deformity, trauma, and tumors. The number of lumbar spinal fusion surgeries performed each year in the United States exceeds 400,000 (Chaichana et al., 2014). The energy absorption functionality of the cages makes them relevant case studies for validating the self-aware implant concept. Current technology (i.e. radiography-based imaging techniques, wired load cells, active and passive sensors attached to the spine fixation rods) is limited and does not have the specificity nor the sensitivity to determine spinal fusion (Barri et al., 2022b; Kanayama et al., 1997; Lin et al., 2011, 2007). In current commercialized devices, the progress of the fusion has limited means of confirmation. In most instances, follow-up radiographic observations including the use of plain film x-ray or dynamic flexion extension films may be ordered. It can be difficult to assess fusion on plain radiographs, and often computed tomography (CT) scans are employed. Even with advanced imaging, fusions still, at times, are difficult to fully confirm. Furthermore, common complications with spinal fusion procedures such as implant subsidence are difficult to evaluate using these techniques. A self-sensing interbody fusion cage can properly assess the progression of fusion by enabling measurement of the forces transmitted through the anterior column at the index level. Also, the implant subsidence could potentially be identified as a sharp decrease in the load applied to the device after endplate violation. Figure 26 shows the vision for diagnosis of spinal fusion development directly at the intervertebral level using the proposed self-aware fusion cage. Spinal fixation devices are used to stabilize vertebrae movement. They allow bone graft materials to be packed inside interbody cages that fuse with the adjacent vertebra (Figure 26a). In this process,

60

the interbody cage provides immediate stabilization of the functional spinal unit (FSU), transfers the loads between the fused vertebrae, promotes bone growth, and thereby improves fusion rates (Kanayama et al., 1997). Figure 26b shows the composition of a self-aware interbody fusion cage. As seen, the implant is composed of rationally-designed conductive (electrode) and non-conductive (dielectric) triboelectric layers arranged in a periodic manner. The implant architecture is composed of parallel snapping curved segments with elastic snap-through instability mechanisms. These curved elements are designed to exhibit snap-through transition before and after deformation. The local support is provided by the clamped conditions of the snapping elements to prevent lateral displacement and bending at the ends of the semicircular-shaped slender elements. Figure 26c visualizes the physics mechanisms of the built-in contact-electrification in the implant. The spine force mechanically deforms (buckles) the semicircular-shaped segments of the implant. At a critical spine force, these segments snap from State I (stable) to State III (compacted). The implant microstructure is designed to induce a "self-recovering" snapping under spine loading. As a result, the fully compacted segments automatically return to their initial stable configuration after the load is removed. Under spine micro-motions, contact-electrification will occur between the conductive and non-conductive layers of the implant. This contact-electrification process will generate an electrical output. Spinal fusion rods and cages typically share the load applied to the spine post-surgery. During the initial stages of the healing process, the cage and rods carry the majority of the spine load, but eventually, the fusion hardware becomes obsolete once the arthrodesis occurs (Kanayama et al., 1997; Lin et al., 2007). The changes in the loading conditions of the smart cage can be used for the long-term assessment of the healing process. The voltage signal generated by the cage is proportional to the forces applied to its structure. Higher loading amplitudes create larger deformations. Consequently, the number of

layers engaged in the contact–separation process increases leading to a larger voltage. The proposed diagnostic mechanism is based on a "relative healing" diagnostic approach. The term relative healing implies that the signal generated during the healing process should be compared with the previous stage and a "reference baseline". During the spinal fusion surgery, the surgeon will pack the bone graft inside the purposely designed large opening/cavity in the middle of the cage (see Figure 26a). The reference baseline voltage will be the initial voltage generated by the cage filled with the graft. This is the first stage of the fusion representing an "unhealed" fusion stage. As the bone starts forming inside and around the cage, it will start interfering with more unit cells, making the cage stiffer and reducing the stress on the cage and the corresponding voltage. As bone heals, the load will be transferred to the fused vertebrae and the amplitude of forces exerted to the cage will continuously decrease. As a result, the voltage generated by the cage will decline over the course of fusion. The changes in the loading conditions (mechanical usage) of the cage would shift the voltage from the reference baseline during the course of the fusion. Upon osseous union, the spine load will be carried mostly by the fused bone. In this stage, the deformation of the cage will be at its minimum (close to zero) and will not be enough to generate any voltage. These changes in the signal patterns during the healing process can be coupled with available miniaturized wireless data logging technologies (e.g. (Barri et al., 2022b)) to record its mechanical usage over time. As seen in Figure 26d, the collected data by data loggers can be wirelessly retrieved using an FDA-compliant portable ultrasound scanning system, as shown in (Alazzawi and Chakrabartty, 2016). The data could be correlated with the changes of FSU stiffness due to the healing process (Figure 26e).

However, one of the advantages of the proposed implantable technology is that the implants can be fabricated using a wide range of biocompatible (e.g. Au, Al, Ti, ethyl cellulose

(EC), polylactic acid (PLLA), polydimethlysiloxane (PDMS), etc) and bioresorbable metallic or polymeric (Magnesium, poly (3-hydroxybutyric acid-co-3-hydroxyvaleric acid) (PHB/V), poly (caprolactone) (PCL), and poly (vinyl alcohol) (PVA), etc.) materials with triboelectric properties. The self-aware implants are structure-dominated, scale-independent multifunctional mechanical metamaterials. Thus, depending on the targeted application, their shape, size and stiffness can be readily tuned by changing the number and deformation sequence of auxetic cells, assembly of microstructures, and layers material. This could result in design of personalized and patient-specific implants (PSIs) facilitated by many of the existing additive manufacturing (AM) techniques. A PSI that exactly matches the patients' anatomy could potentially improve primary stability and increase the lifetime of the implants (Haglin et al., 2016). Furthermore, a self-aware cage implant serves as a bony modulus matched expandable cage because of the self-recovering mechanism integrated into its design. Compared to the commercially available expandable cages, the cage offers higher bone fusion area and ease of insertion, as well as a more efficient biomimetic design capturing native bone porosity for better bone growth because of its customizable auxetic structure. The porous, self-recovering and tunable structure for the cage or similar self-aware implants could effectively reduce the stiffness to "mitigate the stress shielding effect", to minimize cage subsidence and to obtain more comparative strength for the surrounding tissue.

Here, proof-of-concept PSI fusion cage porotypes are fabricated and tested using synthetic biomimetic and human cadaver spine models. Based on the arrangement of conductive and nonconductive parts, and also the geometry of the metamaterial, the dominated triboelectric mode is contact-separation. Figure 27 shows the fabrication process of the self-aware metamaterial implants. Two porotypes with different dimensions were fabricated.
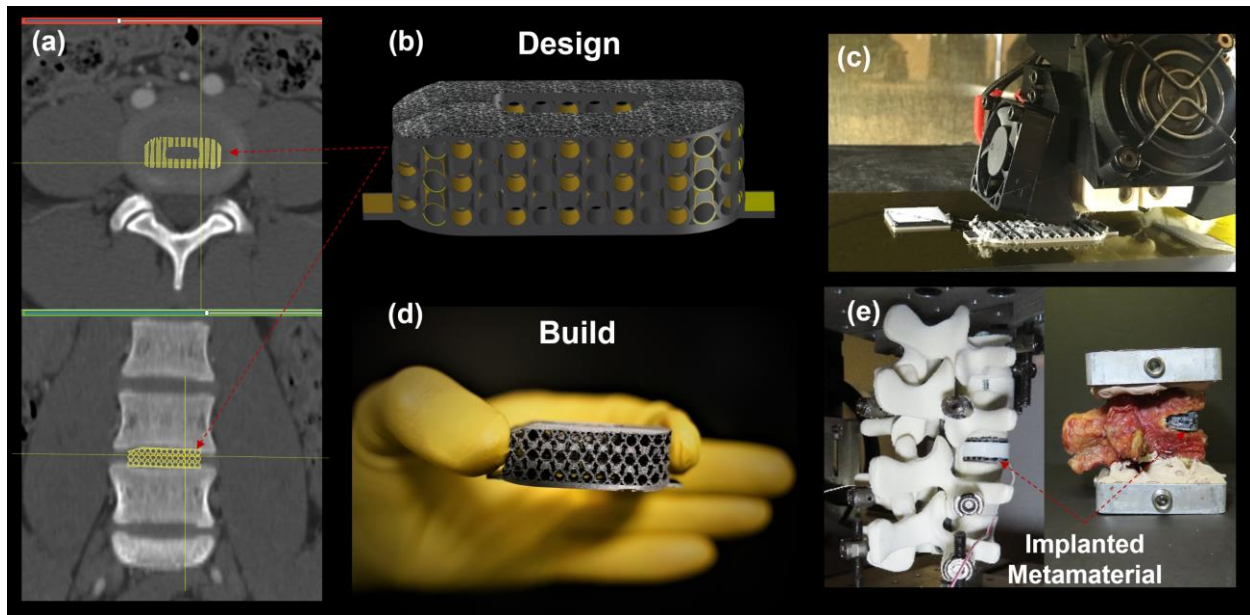
Figure 27 Fabrication process of the proposed self-aware metamaterial implants. (a) CT scans showing the cadaver spine segments (Photo courtesy of Allegheny General Hospital). The implantable self-aware interbody fusion cage is schematically shown on the radiographs. The PSI cage implants are designed based on the geometry of the spinal motion segments derived from the CT scans. (b) The 3D model of the prototype interbody fusion system matching the patient's anatomy. (b) 3D printing of the fusion cage. (c) The fabricated patient-specific fusion cage. (d) The self-aware fusion cage implanted inside synthetic and human cadaver spine models.

The first sample was designed to fit within the synthetic spine disc space for preliminary studying of the implant performance (Figure 27e). The second sample was fabricated according to the geometry of the spinal motion segments derived from the CT scans of the lumbar spine of a 55-year-old male (weight: 86.6 kg, height: 165.1 cm) (Figure 27a,e), while its elastic material properties were designed to be within the ranges reported for lumbar intervertebral discs (Ahn et al., 2008; Argoubi and Shirazi-Adl, 1996; Kamel, 2018; Nikkhoo et al., 2015, 2013). The length, width, and height of the first sample were 45 mm, 20 mm, and 14 mm, respectively. These dimensions were, respectively, 32 mm, 16 mm, and 13 mm for the second cage implant designed for the human cadaver spine model. Surgeons are generally recommended to use fusion cages with

maximal surface area to enable packing more bone graft (Fogel et al., 2009). Accordingly, a fairly large cage to disc surface area ratio (~ 0.6) for the samples was considered. In clinical practice, a patient may even require wider cage because of circumstances found at the time of surgery (Fogel et al., 2009). The thickness of the conductive layers was ranged between 0.1mm-0.2 mm during the numerical simulations. The inside radius of the circular segments was set to 1.4 mm. In this study, TPU and PLA with carbon black were considered to fabricate the dielectric and conductive layers, respectively. TPU and PLA are both biocompatible with the human body (Carvalho et al., 2020; Mi et al., 2017). Also, they are, respectively, on the negative and positive sides of the triboelectric series (Kim et al., 2020), which is an important factor for increasing the triboelectrification. The human lumbar spine has low-frequency vibrations normally within a range of 1–8 Hz (Fan et al., 2020; Patterson et al., 2021). A relatively low frequency (0.25 Hz and 0.5 Hz) was considered to ensure the sensing capability even under quasi-static or very low-frequency condition, as well as persevering the spine models under the loading cycles. Also, the axial force on spine usually ranges from 200 N (in relaxed sitting or lying position) to 1000 N (during upright standing or sitting) (Kettler et al., 2000). Furthermore, in tests using synthetic spines, a maximum non-destructive axial compression of 350 N is recommended (Kubosch et al., 2016; Liu et al., 2020). Accordingly, 325 N was considered, which corresponded to 3 mm displacement. The first set of experiments were carried out using a synthetic biomimetic lumbar spine model (Sawbones, WA, USA) at the L3-L4 vertebrae level. The first cage specimen was implanted on the posterior segment. As shown in Figure 27e, the synthetic spine model was securely attached to the top and bottom plates using special fixtures. Tests were performed under displacement control condition with displacements ranging from 0 mm to 3 mm. Figure 28 shows the results of the experimental studies on the spine cage implanted inside the synthetic spine model

at the initial stage of the healing process. As seen in Figure 28a,b, the self-aware cage is capable of generating 9.2 V and 4.9 nA under compressive loading. Low-power electronics can be empowered using the electrical energy generated by the nanogenerator cage implants. Hence, it is of utmost importance for the prototype to demonstrate its charging capability. Since the output signal of the sensor under the cyclic mechanical compression load has a periodic characteristic, it can be referred to as an AC signal. To that end, the main objective of energy harvesting applications is to charge some form of storage (i.e., a battery or a capacitor). With a simple full bridge rectifier circuit, the self-aware implant has the ability to charge the output capacitor with the behavior modeled in Figure 28c. As soon as the loading starts, the capacitors are charged at maximum speed. Gradually, the charging speed decreases until it is fully charged. As seen in Figure 28c, the saturation voltage is approximately 8 V, which is about 1 V less than the maximum voltage shown in Figure 3a. The comparison of the stored charge in the capacitor over time, shown in Figure 28d, provides sufficient knowledge about the behavior of the sensor as a charging source. Figure 28e presents the voltage and charge stored in the capacitors after 30 seconds.
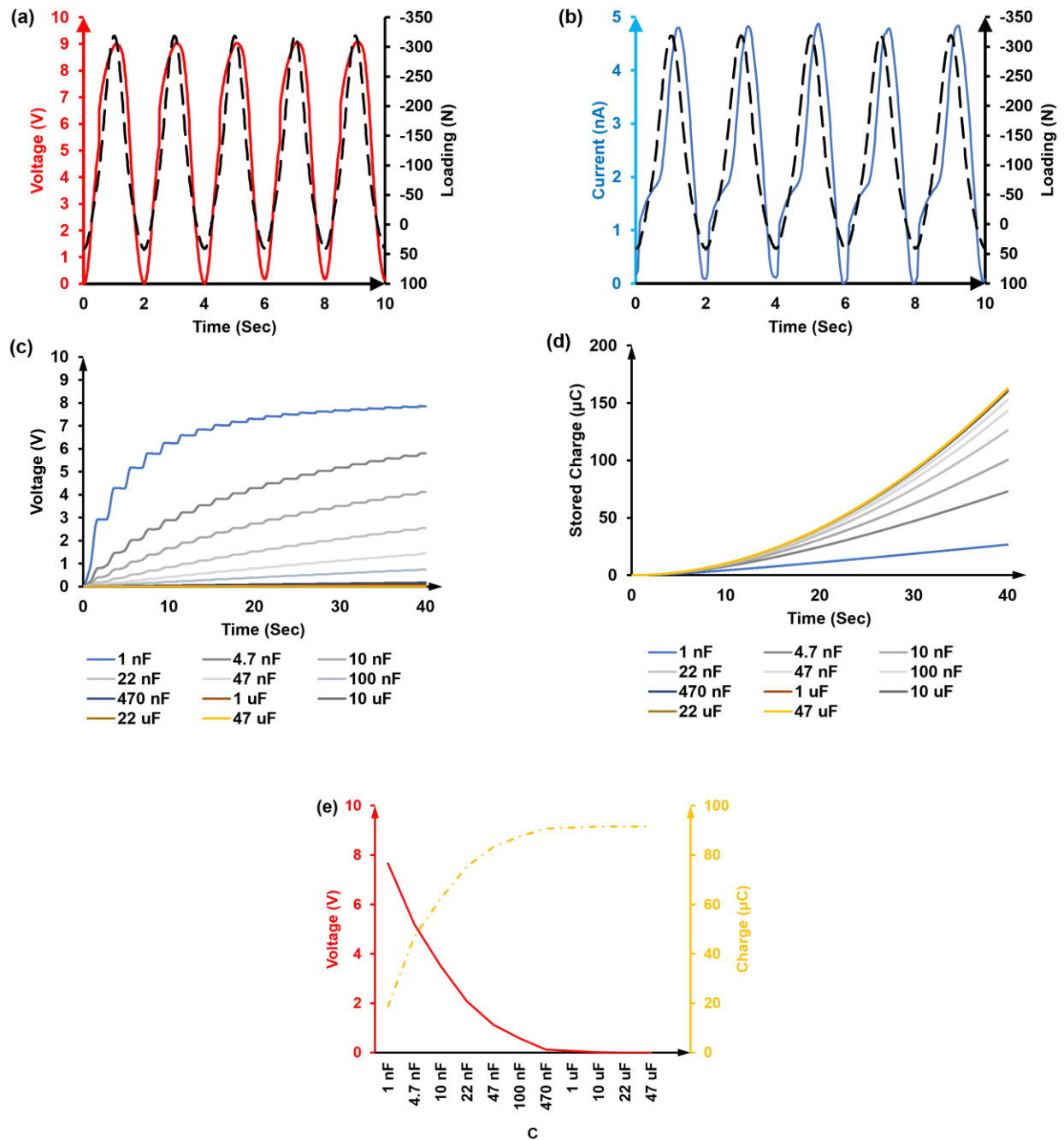
Figure 28 Synthetic spine model test results showing: (a) Voltage (in red) generated by the self-aware interbody fusion cage. (b) Current (in blue) generated by the self-aware interbody fusion cage, (c) Voltage-time for different capacitances. (d) Stored charge time for different capacitances. (e) Voltage and charge stored in the load capacitor at 30 seconds.

In addition, bench-top testing were performed using the synthetic spine model to evaluate the performance of the proposed smart cage system for detecting various fusion states. Figure 29 illustrates the test setup and self-aware interbody fusion cage placed inside different rings. The encapsulating rings were 3D printed using PLA with gradually increasing stiffness (10% to 100% infill density) to simulate the spinal fusion process. This simulated osseous union phase using filler materials, as reported in a recent study by the authors (Barri et al., 2022b), was merely designed to characterize the patterns of the voltage generated by the cage due to the FSU stiffening emulated by increasing the stiffness of the encapsulating rings. In fact, exact simulation of the fusion process has not been done in vitro so far due to complicated biological mechanism involved. While the simulated fusion does not represent the exact mechanical behavior of the fused bone, it provides important information about the correlation between the dynamics of the implant signal and the bone healing. The number of loading cycles, amplitude and frequency were 50, 300 N and 0.5 Hz, respectively. The fusion cage was first inserted inside the disc space without an encapsulating ring to investigate a non-healing state, where the entire spine load is carried by the implant. Then, different rings with increasing stiffness were placed around the spinal cage to simulate the healing progress. Fifty loading cycles were applied during each stage. Five spinal fusion states (FS) were considered as follows:

- •FS1: 10% infill
- •FS2: 25% infill
- •FS3: 50% infill
- •FS4: 75% infill
- •FS5: 100% infill
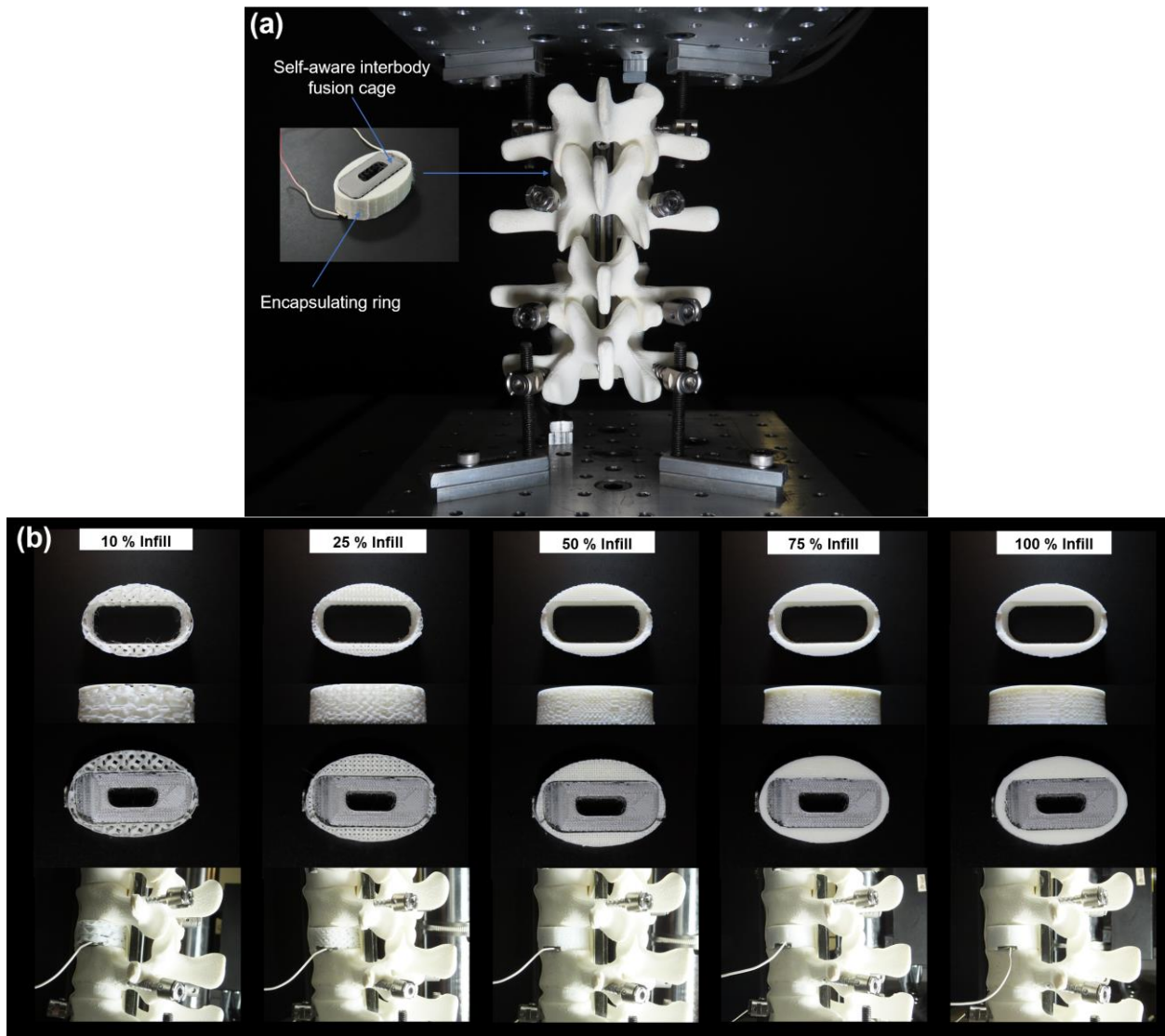
Figure 29 Spinal fusion monitoring process using the proposed self-aware fusion cage system. (a) Test setup including synthetic biomimetic spine model with the fusion cage and encapsulating ring implanted at the L3-L4 vertebrae level. (b) Simulated spinal fusion using the fusion cage encapsulated in rings with varying stiffness.

The voltage values generated by the cage during various fusion states are shown in Figure 30. During the non-healing state, maximum load is exerted on the fusion device. As seen in Figure 30a,b, the highest voltage is generated during the simulated non-healing state. Using rings with higher stiffness represents the healing progression. As the rings become stiffer, they carry larger

69

portions of the load. This reduces the level of load-induced strains inside the cage resulting in generating lower voltage values, as shown in Figure 30a,b. As the spine healing process continues, the cage voltage decreases proportionally. In FS5, a 100% infill density disc was used to simulate a successful osseous union. In this case, almost the entire load is carried by the ring. While the deformation of the cage is not exactly zero at this stage, it is small enough not to generate any signals. This successful osseous union state corresponds to the lowest measured voltage. This observation implies that load transfer gradually shifts from the fusion cage to the bony bridge within the fused segment.
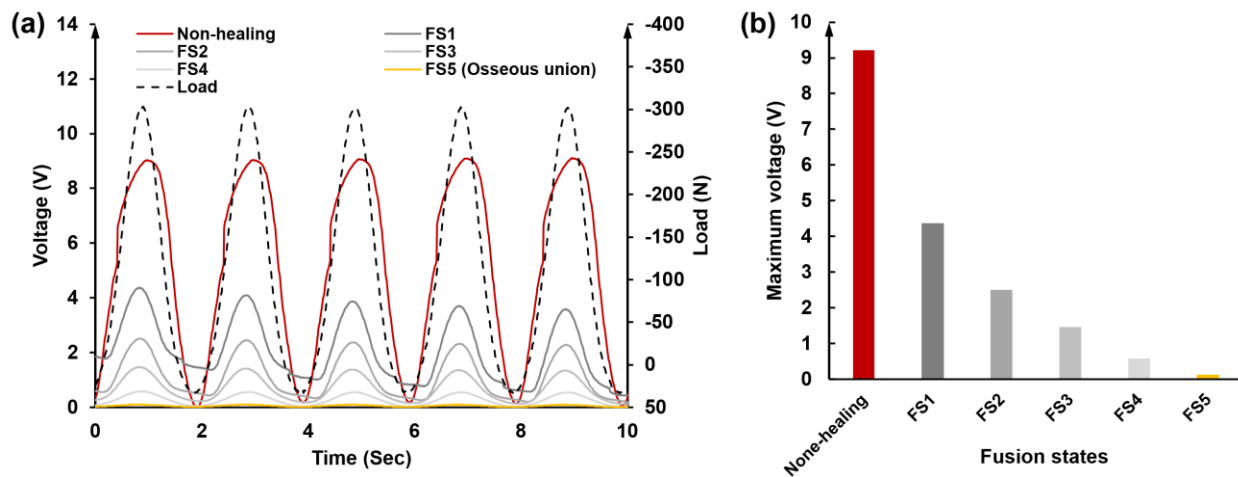
Figure 30 Self-aware fusion cage outputs corresponding to different fusion states for the synthetic spine model. (a) Generated voltage corresponding to different fusion states subjected to the cyclic loading. (b) Maximum generated voltage in each fusion state.

In order to evaluate the electrical and mechanical performance of the proposed spine fusion cages, fatigue tests were performed on the synthetic spine model. For the fatigue study, the second porotype was subjected to 40,000 axial loading cycles at 0.5 Hz frequency with a 350 N axial compression force. The fatigue test results are presented in Figure 31a. The cage elastic modulus

70

(E) decreased from 1.76 MPa to 1.4 MPa after 40,000 loading cycles (Figure 31a). The generated voltage dropped with a high slope from 2.69 V to 1.31 V during the initial 10,000 cycles (Figure 31b). The voltage remained close to 1 V over the rest of the fatigue test. The observed trend in voltage is the result of changes in both mechanical and electrical properties of the spinal fusion cage. Charge carrier density decreases over time in the proposed built-in TENG system. Decline of the electrical and mechanical performance under thousands of cycling loadings is expected and should be carefully studied to find calibration parameters for various classes of patient-specific implants.
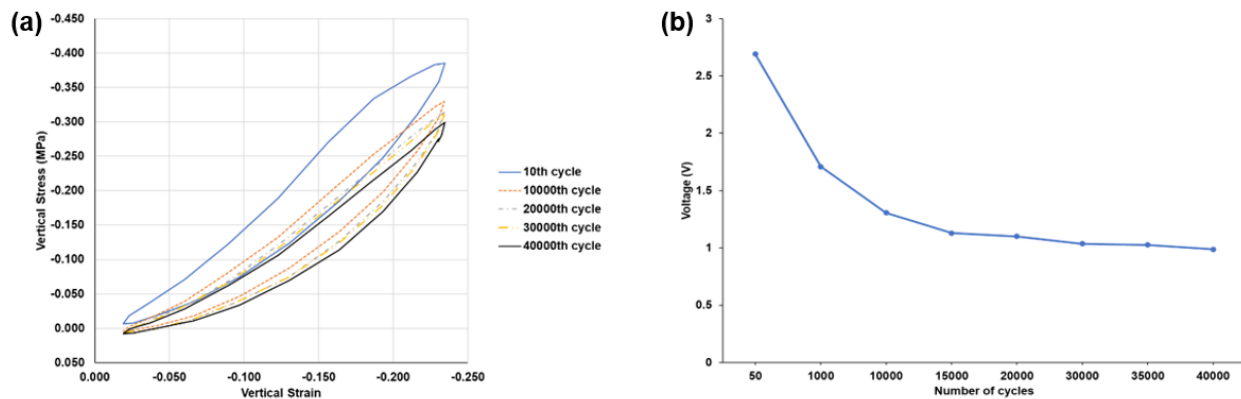
Figure 31 (a) Stress-strain hysteresis curves for 10th, 10000th, 20000th, 30000th, and 40000th cycles, (b) Voltage variations during the fatigue test.

It should be noted that a desirable performance for a spine fixation device varies case by case. The target performance does not necessarily need to be the maximum electrical output or mechanical performance and heavily depends on the clinical requirements. However, synthetic spinal constructs have different stiffness properties compared to the animal or human vertebral models. This issue causes difficulties in the measurement of realistic bone strains (Krammer et al., 2001; Szivek et al., 2002). Based on several biomechanical studies (Huang et al., 2010; Szivek et al.,

71

2005), human cadaver studies have provided the best indication of bone strains during loading of the spine. Arguably, the cadaver models are essential to allow evaluation of strain levels expected during spinal fusion in patients. Therefore, the performance of the proposed self-aware interbody fusion cage is studied for the in-vitro monitoring of spinal fusion in human cadaver models. To this aim, a fusion monitoring process similar to that considered for the synthetic spine was conducted using human cadaveric spinal segments. The fusion cage with stabilized voltage signal after the fatigue testing were used. The spinal segment used for testing was isolated from a 55-year-old male donor with a DEXA T-score of -1.4, indicating osteopenia. To simulate the entire bone fusion process, a complete discectomy was performed at the L4-L5 index level with care taken to remove all soft tissue down to the endplate (Figure 32a). Then, 3D printed rings with different infill densities were used to fill the intervertebral disc space. Fifty axial compression loading cycles with an amplitude of 500 N at 0.25 Hz frequency were applied to the cadaver spine with implanted fusion cage at each stage. Figure 32b presents the test setup with different filler rings with 10% to 100% infill density. The measured voltage values for different healing states are shown in Figure 33. Stiffer rings representing a fusing bone reduced the level of load applied to the cage. In this case, the spinal cage sensor produced a lower voltage (Figure 33a). Decrease in voltage indicates the progress of the spinal healing process. Similar to the synthetic spine tests, the lowest voltage recorded was at FS5 during the cadaveric tests. FS5 denote a ring with 100 percent infill density and accordingly a successful osseous union.
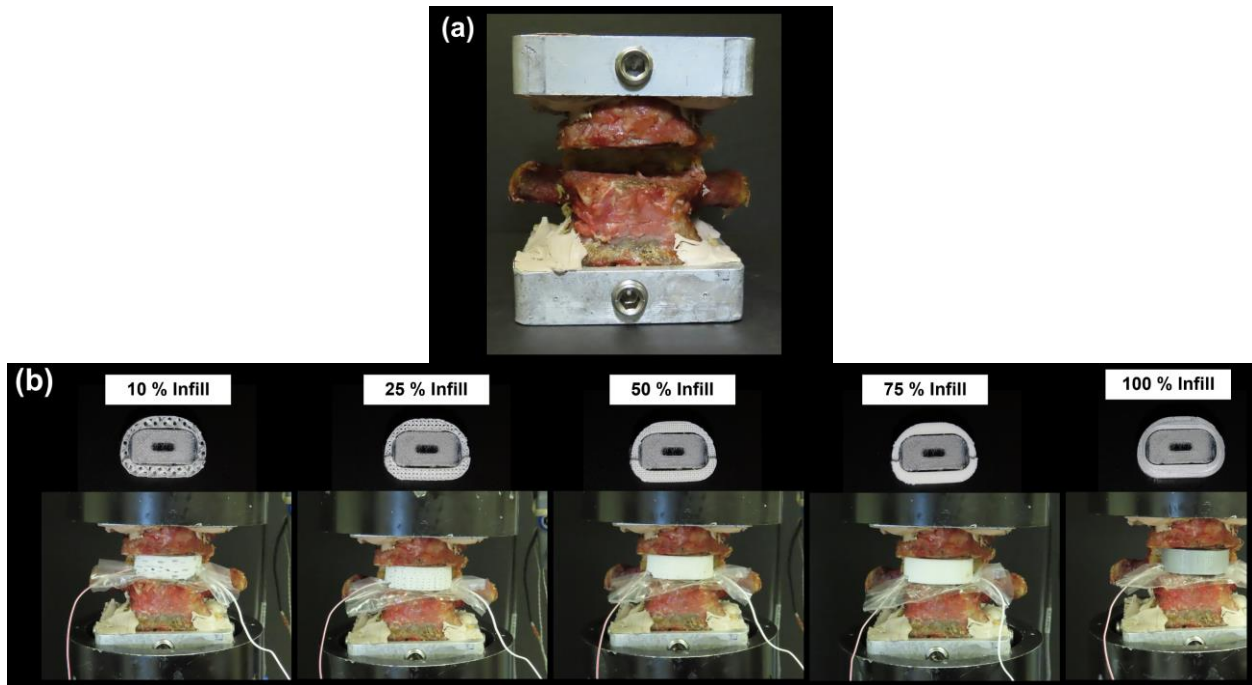
Figure 32 Spinal fusion monitoring process using the proposed self-aware fusion cage system implanted inside the human cadaver spine model. (a) Test setup including the fusion cage and encapsulating ring implanted inside the L4-L5 cadaver spine segments. (b) Simulated spinal fusion using the fusion cage encapsulated in rings with varying stiffness.
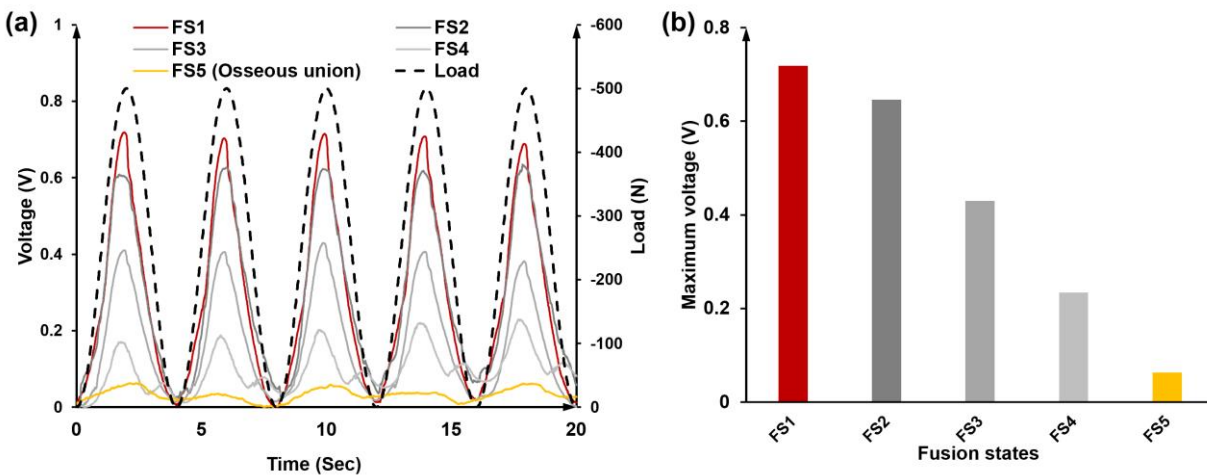
Figure 33 Self-aware fusion cage outputs corresponding to different fusion states for the human cadaver spine. (a) Generated voltage corresponding to different fusion states subjected to the cyclic loading. (b) Maximum generated voltage in each fusion state.

However, the presented proof-of-concept prototypes demonstrate the first application of the self-aware metamaterial implants for biomedical sensing, monitoring and energy harvesting. The mechanical and electrical performance of self-aware implants should be customized for each patient based on the clinical requirements and anatomical matching. The results reveal the capacity of the proposed concept in pushing the limits of medical implant technologies without using any external power source and bulky electronics. Since the implant itself could serve as a sensor and energy harvesting medium, little to no modification to existing implant designs would be required. The self-aware implants can continuously collect the data due to any mechanical stimuli. Wireless interrogation of the implant measured data is a challenging task. A viable solution is to couple the signal generated by the self-aware implants with ultra-low-power consumption (< 100 Nanowatts) wireless data logging technologies (e.g. (Alavi et al., 2016b, 2016a; Barri et al., 2022b; Huang et al., 2010; Mehta et al., 2020)) to create fully self-powered systems. This can be done through a passive strategy where a range of spinal motions will be induced by asking the patients to acquire a predetermined number of sitting and standing postures during therapy sessions. The voltage response of the cage implant corresponding to each posture can be recorded and will be assessed at various stages of the healing process. A limitation of this approach is that it evaluates the fusion condition at a given moment and presents only a "snapshot at the time" where the measurements are taken. It is also feasible to design a semi-active strategy by coupling the data-loggers with the cage electrical signal to continuously record its mechanical usage over time. This way, the data-logger serves as a non-volatile storage memory that can potentially record all in-vivo events and aggregate the short-term fluctuations. The signal patterns stored by the data-loggers in both passive and semi-active approaches can be retrieved using a telemetry interface. For instance, mm3 sized sonomicrometry crystals can be fully integrated with the data-loggers and an ultrasonic

74

encoder/driver on a single chip for wireless interrogation of the implant (Alazzawi and Chakrabartty, 2016; Kondapalli et al., 2018; Kondapalli and Chakrabartty, 2021).

Such a powerful experimental tool would enable design of the next-generation healing monitoring technologies for other treatments and therapeutics of fracture repair. A self-aware implant would naturally inherit the outstanding features of the TENGs, which have significantly high-volume power density (~500kW/m2) (S. Wang et al., 2015; Wang et al., 2018; Zi and Wang, 2017). This energy can be used to empower other miniaturized low-power consumption electronics in-vivo. Furthermore, electrical stimulation (ES) has proved to be an effective method to enhance bone healing (Griffin and Bayat, 2011). There are a number of FDA-approved invasive and noninvasive electrical stimulation devices currently being used for bone growth stimulation in a variety of orthopedic conditions (Griffin and Bayat, 2011). These devices administer electrical current to the bone which commonly include direct current (DC), pulsed electromagnetic field (PEMF), capacitive coupling (CC), or inductive coupling (IC). In this area, using the electrical signal generated by a self-aware implant to accelerate bone healing and changing growth factors could open the doors for widespread application of smart implants in therapy for fracture healing.

In this study, TPU (E = 12 MPa, ν = 0.48) and PLA with carbon black (Young's modulus E = 3000 MPa, Poisson's ratio ν = 0.25) were, respectively, used to fabricate the dielectric and conductive layers of the fusion cages. PLA and TPU are on the negative and positive sides of the triboelectric series, respectively. This combination maximizes the electrification between the layers. At first 3D models of the cages were created using AutoCAD and SolidWorks based on the geometries of the synthetic and cadaver spines. Three different segments of the proposed implants were fabricated using the FDM method and a Raise3D Pro2 Dual Extruder 3D Printer. All layers of the interbody fusion cages (i.e. electrodes and dielectric layers) were printed simultaneously.

After the printing process finished, and removing the supports and extra printed parts from implants, the implants without any additional post-printing modifications were tested.

An Instron 8874 universal testing machine was used to test the spine samples. The cadaveric specimen was mounted for testing using customized fixtures and a polyester resin and hardener (Bondo, 3M) to enable testing on a 6 degree-of-freedom spine tester (Bose Smart Series). The LabView software interfaced with an NI9220 module (1GΩ impedance) was used to record the generated voltage values. The current generated by the fusion cages was measured using SR570 amplifier (Stanford Research Systems).

5.1.2.2 Conclusion

In this chapter, the novel concept of self-aware metamaterial implants was presented. A novel concept of self-aware metamaterial implants was discussed in this study. Taking advantage of nanogenerators and metamaterials, new multifunctional aspects were introduced into the fabric of medical implants. First-of-its-kind interbody fusion cage prototype was fabricated and proof of concept for self-powered monitoring of bone healing was demonstrated without the need for external power sources and without any loss of data. The experimental studies performed on both synthetic spine and human cadaver spine models confirm the efficiency of the self-aware implants in assessing fusion process and harvesting energy from mechanical excitations. Under loading conditions similar to human lumbar spine, the fusion cage porotype can generate voltage and current values equal to 9.2 V and 4.9 nA, respectively. A series of fatigue tests using the synthetic spine model revealed that the cage elastic modulus drops from 1.76 MPa to 1.4 MPa after 40,000 loading cycles. The generated voltage drops from 2.69 V to around 1 V. The results imply the necessity to develop more robust fabrication and calibration methods for such patient-specific implants. The proposed concept could open avenue for the next stage of the revolution in smart

implantable devices, where a new generation of scalable, cost-effective, multifunctional, and personalized implants could be widely used by clinicians to achieve better surgical outcomes. The future research will focus on developing a series of mechanically and electrically-optimized self-aware metamaterial cage implants for in-vivo testing in large animal models.

5.1.3 Medical stents

As it shown in Figure 25 the orthopedic self-aware implants seem to be the most immediate application area. For instance, stents are extensively used in cardiac surgeries. Despite their clinical efficacy, they may cause a complication called in-stent restenosis (Chen et al., 2018). Currently, there are not any implantable system that can detect this complication at early stages. A biocompatible self-aware cardiac stent can be used to monitor any local hemodynamic changes due to in-stent restenosis. In a similar manner, a self-aware esophageal stent empowered by esophageal peristalsis can monitor the local esophagus wall radial compressive forces changes caused by stent migration and tumor overgrowth. However, rational design of such multifunctional smart implants requires targeting various physical property types. Accordingly, a multi-physics design approach should be adapted to mimic the complex properties of the biological tissues (Zadpoor, 2020).

5.1.3.1 Cardiovascular Stent

Incorporating the meta-tribomaterial concept into the design of the various devices enables continuous measurement of the applied forces and harvesting the energy form the external

mechanical excitations. These features are particularly important for designing advanced medical stents. Millions of cardiovascular stents are implanted every year because of their clinical efficacy. The presence of a stent within an artery can lead to excess growth of arterial tissue that may cause renarrowing within the stent. This complication known as in-stent restenosis can reach as high as 50% among stented patients (Chen et al., 2018). There is currently a serious need for a rapid, noninvasive, and easily accessible method to detect in-stent restenosis. A self-sensing, biocompatible and non-toxic meta-tribomaterial stent equipped with a miniaturized wireless interface self-powers itself by harvesting the energy from the arterial pulsations of the blood vessels. The stent can be deployed using a commercial balloon dilatational catheter for continuous monitoring of local hemodynamic changes upon tissue overgrowth and artery renarrowing condition.

In this section, a proof-of-concept cardiovascular medical stents has been developed. Figure 34a present the mechanism and fabrication process of the meta-tribomaterial-based 3D designs for the cardiovascular stent. As seen, the 3D metamaterials can be identified as hierarchical tubes composed of 2D parallel U-shaped snapping segments at the microlevel. The cardiovascular stent was first fabricated as auxetic meta-tribomaterial films and was then configured into tubular stent form.
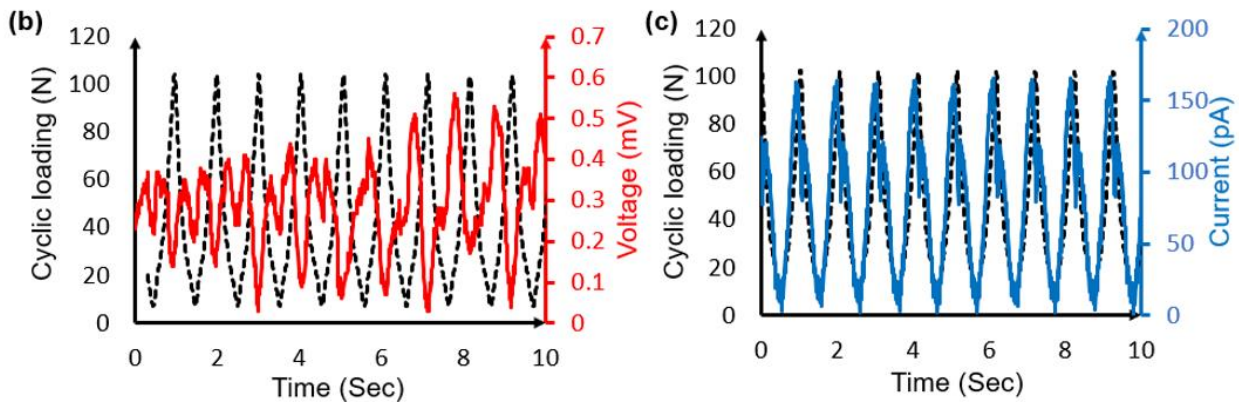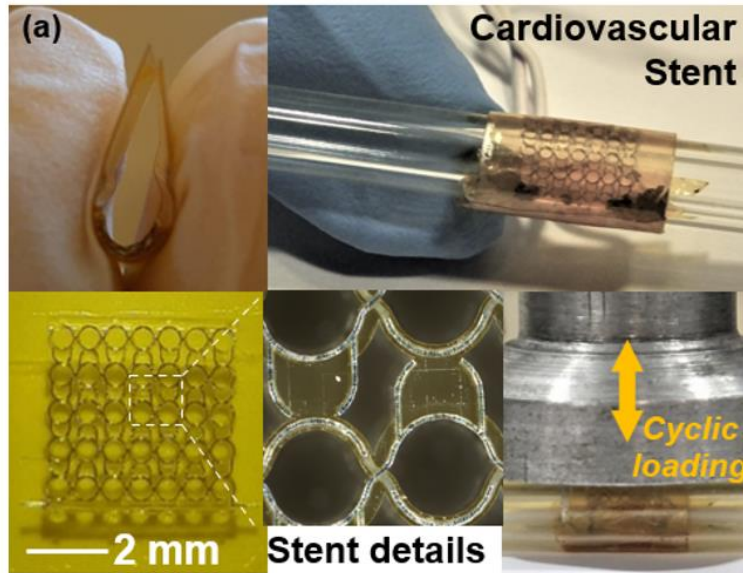
Figure 34 Multifunctional tubular 3D stents designed based on the meta-tribomaterial concept: (a) Design details and testing of the cardiovascular stent film comprised of 5×7 unit cells. Applied cyclic loading and the corresponding (b) voltage (in red) and (c) current (in blue) signals generated by the cardiovascular stent.

The nanoscale meta-tribomaterial cardiovascular stent prototype was fabricated using a 3D direct laser writer (Nanoscribe Photonic Professional, GT) as shown in Figure 35. The printing was done through two-photon polymerization of IP-S resist by a femtosecond pulsed laser at 780 nm. The Nanoscribe 3D printing system is equipped with a laser generator, an optical cabinet, an optical microscope/lens to focus the laser beam, a Galvo mirror system to control fast laser-beam

scanning, a piezoelectric stage for controlling precise movement and an operation software (Nanowrite) for controlling actual 3D printing. The whole system was placed on an anti-vibration table to reduce acoustic noise. The Nanoscribe 3D printing system uses a unique deep-in-liquid mode to print large-height pattern. The meta-tribomaterial was printed with 25× lens, NA 0.8 with a resolution of 1 μm.
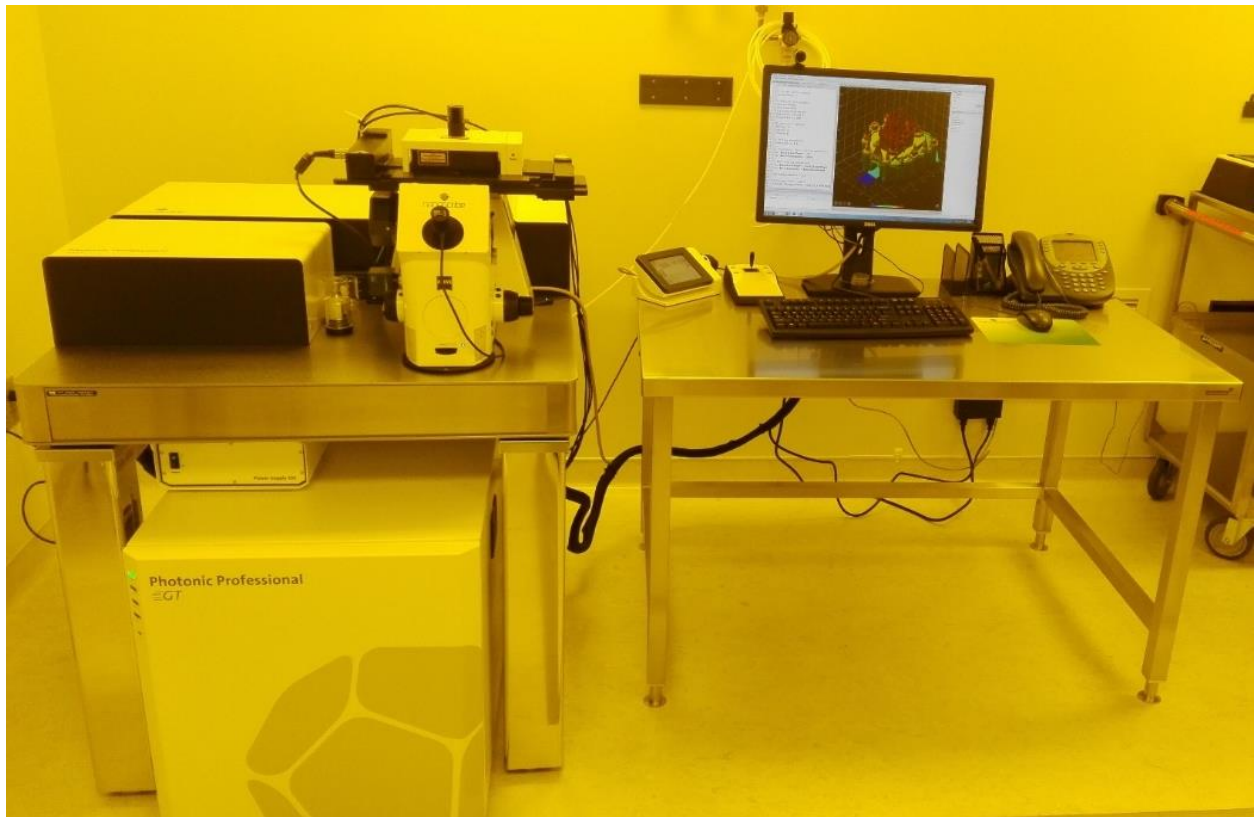
Figure 35 Nanoscribe printing system at Petersen Institute of NanoScience and Engineering.

The meta-tribomaterial stent consists of two conductive parts (E1 and E2) and one non-conductive part. Each part was printed separately in shell and Scafford mode, which print the boundary of the structure in solid but the body in a Scafford pattern. The whole structure had a dimension of 7.5 mm x 7.5 mm x 300 um, and were split into blocks of 220 μm × 220 μm × 200 μm , with a stitching

overlap of 4μm. The laser power was set to 90 mW, writing speed of 11 cm s-1, slicing distance

of 1 μm. After printing, the structures were developed in propylene glycol monomethyl ether

acetate (PGMEA) bath for 30 min followed by 5 min isopropyl alcohol (IPA) rinse. After the

structures were naturally dried in the air, they were placed under UV lamp for 30 min UV light

flood with 16 mW/cm2 intensity, which fully cross-linked the whole structure. As the direct-

printed parts were all non-conductive, parts E1 and E2 were then loaded into Denton sputter coater

for a conformal coating of 30nm Au/Pd metal film to make them conductive. All the three parts

were then placed under optical microscope for assembling. To make the assembling easier, a few

droplets of IPA was sprayed onto the structures to make the parts more flexible and easier to

assemble. Once assembled, the assembly was detached from the substrate and glued to a flexible

substrate, following by silver paste gluing of two wires to E1 and E2 electrodes for subsequent

electrical measurement. The fabricated auxetic meta-tribomaterial film was then configured into

tubular stent form. The cardiovascular stent was directly placed under the compressive loading

cycles. Figure 34b,c present a typical time-history response of the proposed meta-tribomaterial

cardiovascular stents to cyclic loading at 1 Hz frequency. The maximum generated voltage and the

corresponding measured current were 0.6 mV and 172 nA, respectively.

5.1.3.2 Esophageal Stent

Arguably, the same meta-tribomaterial-based approach can be used to design self-powered

diagnostic implants for pressure measurement in hollow internal organs and specifically

esophagus, where nearby tissue grows around the stent and changes the esophagus radial pressure

(Hindy et al., 2012; Kim et al., 2017). An esophageal meta-tribomaterial stent empowers itself by

harvesting the energy from contraction and relaxation of esophagus wall. The initial 3D model of meta-tribomaterial esophageal stent prototype with 7×5 unit cells is shown in Figure 36.
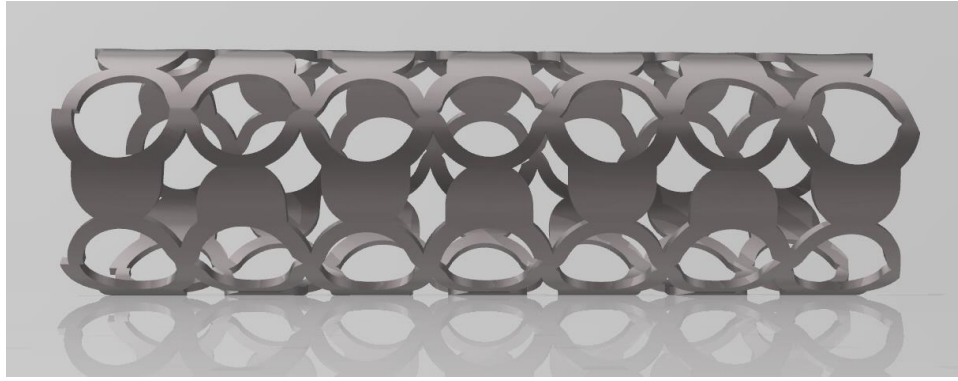
Figure 36 3D model of the meta-tribomaterial esophageal stent prototype with 7×5 unit cells.

In this study, the meta-tribomaterial esophageal stents prototypes were fabricated using the FDM 3D printing technique. Raise3D Pro2 Dual Extruder 3D Printer was used to fabricate the composite samples as one integrated unit using two conductive and non-conductive materials. The fabrication process can be divided into three steps: 1) 3D modelling of the proposed design using AutoCAD and SolidWorks, 2) 3D printing of the design using a dual extruder 3D printer, and 3) removing the supports and extra printed parts from the 3D printed object. Since all layers of the prototypes (i.e. electrodes and dielectric layers) are printed simultaneously, the 3D printed samples are ready to test immediately after finishing the printing process without a need to post-printing modifications. After several preliminary tests with various conductive and non-conductive filaments and checking the generated electrical signal, PLA and TPU were found to be optimal materials for the conductive and non-conductive layers, respectively. The non-conductive TPU layer provides sufficient flexibility in the entire system. The thickness of conductive layers within the TPU framework was ranged between 0.1 mm to 0.3 mm. The esophageal stent auxetic structure

had a dimension of 72 mm x 52.6 mm x 4 mm. The inner diameter of the tubular esophageal stent was 8.73 mm. A flexible polyurethane graft was inserted into the esophageal stent for testing its electrical properties. A 3D printed fixture and shaft was used to simulate the contraction and relaxation of esophagus wall during loading. Figure 37b,c present a typical time-history response of the proposed meta-tribomaterial esophageal stents to cyclic loading at 0.05 Hz frequency. The peak to peak generated voltage and the corresponding measured current were 3V and 7 nA, respectively.
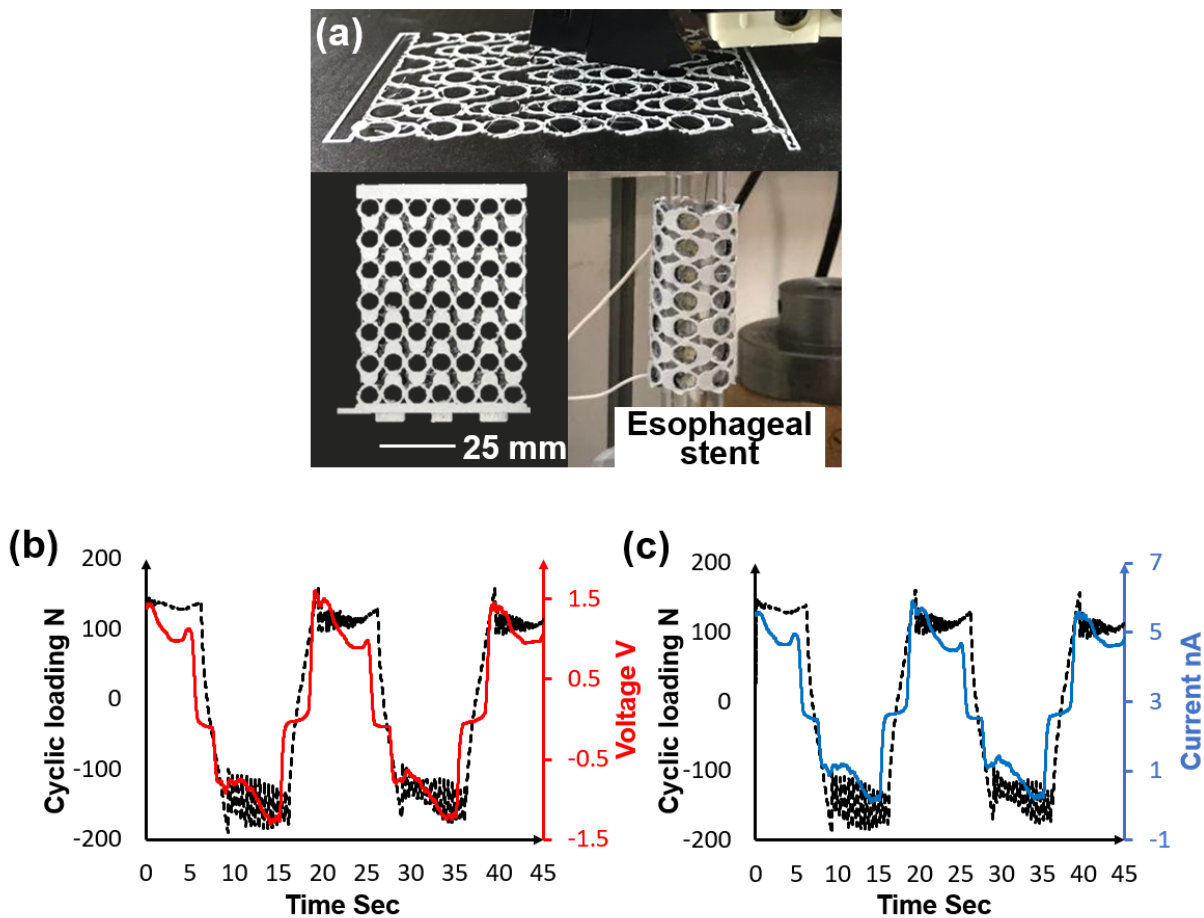
Figure 37 Multifunctional tubular 3D stents designed based on the meta-tribomaterial concept. a, 3D printing the composite matrix of the conductive and non-conductive layers in the esophageal stent prototype. b, voltage and c, current signals generated by the esophageal stent.

5.1.3.3 Conclusion

In this section, a new generation of meta-tribomaterial nanogenerators with energy harvesting and sensing functionalities was proposed and a proof-of-concept esophageal medical stent was developed. The broad application of the proposed meta-tribomaterial concept for designing proof-of-concept multifunctional material systems such as self-sensing, self-monitoring, and self-powering medical stents were highlighted. These demonstrations imply the remarkable potential of the meta-tribomaterial-based systems for various sensing, diagnostic, and energy harvesting applications. Results from these preliminary studies give confidence that it is feasible to create novel types of active and multifunctional mechanical metamaterials.

5.2 Self-Sensing and Self-Powering Civil and Mechanical Engineering Systems

The presented objective in this chapter has been published as a book chapter, two conference papers (Alavi et al., 2022; Barri et al., 2022a, 2022d) as well as a provisional patent:

Alavi, A.H., Zhang, Q., Barri, K., 2022. Advanced multifunctional structures for future smart cities. Rise Smart Cities 29–52. https://doi.org/10.1016/B978-0-12-817784-6.00004-7

Barri, K., Zhang, Q., Kline, J., Khazanovich, L., Alavi, A.H., 2022a. Super compressible multifunctional metamaterial concrete. https://doi.org/10.1117/12.2607689 12043, 382–389. https://doi.org/10.1117/12.2607689

Barri, K., Zhang, Q., Taylor, B.E., Sun, Z., Sachs, S., Khazanovich, L., Wang, Z.L., Alavi, A.H., 2022d. MULTIFUNCTIONAL NANOGENERATOR CONCRETE MATERIAL SYSTEMS, in: ASME 2022 Conference on Smart Materials, Adaptive Structures and Intelligent Systems SMASIS. Dearborn, Michigan.

Alavi A.H., Barri, K., Kline, J., Zhang, Q., Khazanovich, L., Super-compressive metamaterial concrete and methods for making same. U.S. Provisional Patent, June 7, 2021.

There is a critical need to develop multifunctional structural and mechanical elements with tunable mechanical properties. A new generation of lightweight, mechanically tunable composites is presented with sensing and energy gathering capabilities. The so-called self-aware structures are created by integrating metamaterial and triboelectric energy harvesting concepts. Proof-of-concept composite beam prototypes are fabricated using additive manufacturing methods. Experiments and theoretical analyses are conducted to quantitatively investigate the mechanical and electrical properties of the designed multifunctional beams. This study shows how these integrated structural elements can serve as nanogenerators and distributed sensing mediums without a need to

incorporating any external sensing modules and electronics. The feasibility of design self-sensing and self-powering structural elements at multiscale is discussed for next generation infrastructure systems. Furthermore, this chapter of dissertation presents a new class of lightweight reinforced composite metamaterial concrete with energy harvesting functionality. The proposed nanogenerator metamaterial concrete is created via integrating the mechanical metamaterial and triboelectrification paradigms. A metamaterial concrete system composed of an auxetic polymer lattice encapsulated in a conductive cement matrix is designed and fabricated. The metamaterial concrete structure is rationally designed to induce contact-electrification between its layers under mechanical excitations. The conductive cement enhanced with graphite powder serves as the electrode in the proposed system, while providing the desired mechanical performance. Experimental and numerical studies are conducted to investigate the electrical and mechanical properties of the designed prototypes. Furthermore, the potential applications of the proposed mechanically-tunable nanogenerator concrete system is discussed.

5.2.1 Self-Sensing and self-powering meta-tribomaterial shock absorber

The purpose of this part of the dissertation is to illustrate the broad applications of the meta-tribomaterial concept by designing multifunctional automotive and aerospace engineering systems. The potential application is designing self-sensing shock absorbers with energy harvesting capabilities. Figure 38a presents the 3D model of three different layers of the proposed shock absorber system, and Figure 38b shows the fabrication and testing process of the meta-tribomaterial-based 3D cylindrical designs for the shock absorber. As seen, the 3D metamaterials can be identified as hierarchical tubes composed of 2D parallel U-shaped snapping segments.

Experimental studies were performed for further evaluation of the electrical performance of the designed 3D configurations.

The meta-tribomaterial snapping, shock absorber prototypes were fabricated using the FDM 3D printing technique. Raise3D Pro2 Dual Extruder 3D Printer was used to fabricate the composite samples as one integrated unit using two conductive and non-conductive materials. Since all layers of the prototypes (i.e. electrodes and dielectric layers) are printed simultaneously, the 3D printed samples are ready to test immediately after finishing the printing process without a need to post-printing modifications. TPU and Conductive PLA are used for the non-conductive and conductive layers, respectively. The non-conductive TPU layer provides sufficient flexibility in the entire system. The thickness of conductive layers within the TPU framework was 0.3 mm. The shock absorber height, inner diameter and outer diameter were 92 mm x 16 mm x 34 mm, respectively.
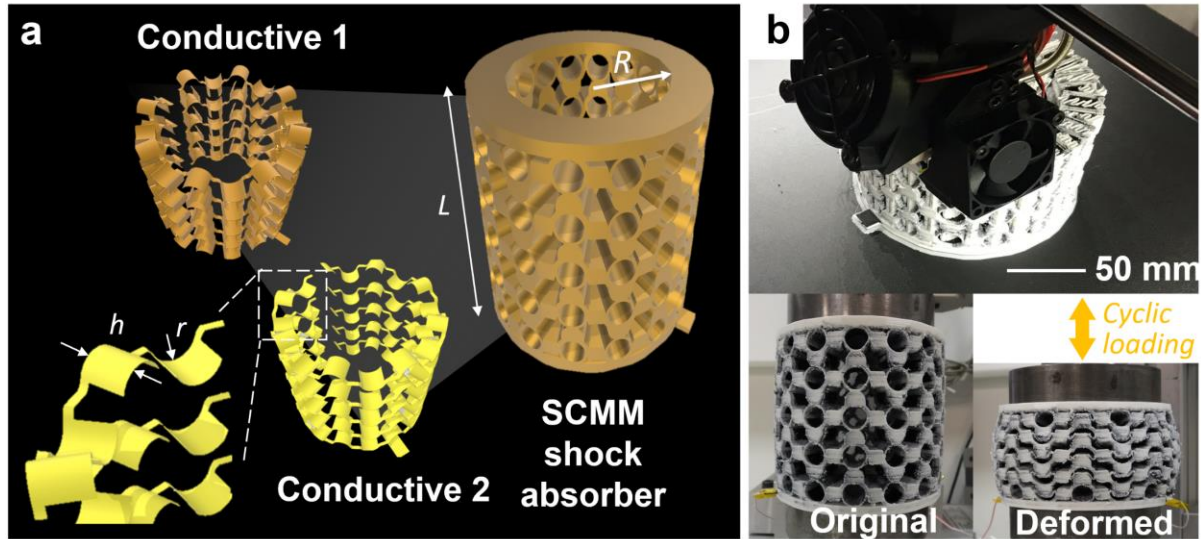
Figure 38 Multifunctional 3D shock absorber designed based on the meta-tribomaterial concept. a, Composite matrix of conductive and non-conductive layers in the meta-tribomaterial shock absorber. b, 3D printing of the meta-tribomaterial shock absorber prototype comprised of 80 unit cells under loading, and the shock absorber specimen at the original and deformed states under the cyclic loading. Applied cyclic loading and the corresponding c voltage (in red) and d current (in blue) signals generated by the proposed meta-tribomaterial shock absorber.

Figure 38c,d present a typical time-history response of the proposed meta-tribomaterial shock absorber to cyclic loading. Uniaxial loading experiments were performed on the 3D printed meta-tribomaterial shock absorber specimen with a TestResources testing machine. Cycling loading at 0.1 Hz frequency was applied to the specimen under displacement control until it was fully

compacted. The displacement range was controlled to be between 0 mm to 40 mm. The applied load changed between 5 N and 700 N. Under uniaxial loading, the sample undergoes a large deformation with very small transverse deformation after every snapping. The voltage values were read using a National Instruments 9220 DAQ module with 1 GΩ impedance. A low-noise current amplifier (SR570, Stanford Research Systems) was used to measure the currents generated by the meta-tribomaterial prototypes. A LabVIEW program was developed to control and synchronize measurements from all modules and store readings in the host computer. The applied cyclic loads and the corresponding voltage and current generated by the proposed meta-tribomaterial shock absorber are shown in Figure 38c,d respectively. The peak-to-peak generated voltage and the corresponding measured current were 4 V and 5 nA respectively.

The presented designs are proof-of-concept and are not optimized for best electrical and mechanical performance. However, incorporating the meta-tribomaterial concept into the design of the shock absorber enables continuous measurement of the applied forces and harvesting the energy form the external mechanical excitations. The proposed shock absorber system can be used as a smart base isolation system to protect structures against earthquake forces, as well as sensing and energy harvesting capabilities.

5.2.2 Multifunctional Structures for Smart Civil Infrastructure

5.2.2.1 Introduction

Smart cities aim to optimize the efficiency of city operations and services. Smart civil infrastructure systems form the backbone of smart cities. Advanced manufacturing, sensing, and automated control methods are integrated with information and communication technologies (ICT)

to improve the performance and maintenance of smart infrastructure systems (Al-TabbaaAbir et al., 2018; Albino et al., 2015; Berglund et al., 2020; Harrison et al., 2010). Enabling technologies for smart civil infrastructure have gained significant attention in recent years. In this area, many studies have been carried out to develop advanced data mining and informative algorithms, wireless sensing and monitoring technologies, cyber-physical systems, new material systems, and progressive construction methods (Al-TabbaaAbir et al., 2018; Queheillalt et al., 2008; Wang et al., 2014). Smart materials are arguably the key elements of smart civil infrastructure systems. In a truly intelligent system, the constituent materials are expected to offer both a designated structural behavior and a range of built-in functionalities such as sensing, tunability, autonomy, and programmability. Material systems with advanced functionalities build the foundation for multifunctional structures (MFSs). The MFS technologies combine a number of material subsystems to achieve functional integration and intelligence (MOMODA, 2004). With the rapid development of materials and manufacturing techniques, the performance-tailored MFS technologies have been blooming recently. Most of the studies in the area of MFSs are focused on improving certain functionalities, in particular mechanical and sensing properties. A major step forward is to explore new generation of MFSs with other advanced capabilities for smart civil infrastructure systems. Developing MFSs with functionalities such as sensing, energy harvesting, mechanical tunability, and digital computing functionalities can result in building intelligent structural systems that fit perfectly hand in hand with the smart city development. Embedding these functionalities directly into the texture of MFSs is a key to build a foundation for the so-called "engineering living structures". These are structures that can respond to their environment, self-monitor their condition, and self-program themselves. They can be self-powered and serves as self-diagnostic tools for distributed SHM of civil infrastructure systems. They can eliminate the

need for dense networks of dedicated sensors and major difficulties associated with installing and maintaining traditional SHM systems (Alavi et al., 2016a). Scalability is perhaps the most challenging issues ahead of MFSs for broader applications in smart cities. Developing new class of multifunctional metamaterials can address these challenges. Unlike natural materials, metamaterials gain their functionalities through a rational microstructural design. Accordingly, they can be designed to achieve desired functionality from a wide design space of potentially many configurations of representative microstructures. The concept of meta_tribomaterial which is introduced in chapter 4 of this study, transforms mechanical metamaterials into scalable nanogenerators and active sensing mediums. Meta-tribomaterials can be created using finely tailored and seamlessly integrated snapping microstructures. Meta-tribomaterials are capable of acting as triboelectric nanogenerators (TENGs) and generate electrical signals in response to the applied mechanical excitations. Success in trail of the meta-tribomaterial concept has opened a new era of MFSs. A breakthrough in this arena is the creation of multifunctional "engineered self-aware structures (ES^2s)" that are scalable integration of meta-tribomaterial structural units. ES^2s can be built using a single meta-tribomaterial unit, a series of meta-tribomaterial systems each with different configuration, or meta-tribomaterial units embedded within another macroscale structural systems. The entire ES^2 systems can then be deployed to perform a designated functionality.

5.2.2.2 Results and Discussion

In this section, the ES^2 concept is demonstrated through fabricating mechanically tunable multifunctional composite beam prototypes with sensing and energy harvesting functionalities. The design process for the ES^2 beam is shown in Figure 8. As seen, an ES^2 beam is composed of tailored and topologically different triboelectric auxetic microstructures. The entire MFS serves

as an energy harvesting medium as well as an active sensing system to directly collect information about its operating environment. The beam has a built-in TENG mechanism and inherit the enhanced mechanical properties offered by classical mechanical metamaterials such as lightweight, ultra-high strength-to-density ratios and high resilience. These properties are crucial for designing mechanically robust smart structures at large scales. As seen in Figure 39a, the layered architectural tailoring of triboelectric materials can form a multifunctional MM beam. Deformation mode of the fabricated layers are engineered so that contact-electrification occurs under periodic deformations. The contacting/sliding surfaces of the self-aware beam act as conductive and dielectric layers similar to a TENG system which is introduced in chapter 4 of this dissertaion. The semicircular-shaped snapping segments include both conductive and dielectric layers. Figure 39f,g show the signal generated by the ES^2 beam during bending and compressive testing. As seen, the voltage values are proportional to the applied force in both tests. The results reveal the feasibility of creating composite multifunctional ES^2 systems with sensing and energy harvesting functionalities via introducing the contact electrification into the fabrication process. Variations of the strains due to damage progression can be correlated with the changes of the generated voltage for SHM applications.

Furthermore, this capability was investigated by introducing three different structural damage detection states to the beam. First, the damage was introduced by making two groves (3 mm by 3 mm) at 1/3 and 2/3 lengths of the bottom of the composite ES^2 beam. Then, one middle unit cell of the second row from the top of the beam was randomly chosen and cut. Finally, the cut made in the previous stage was extended throughout the entire beam width.
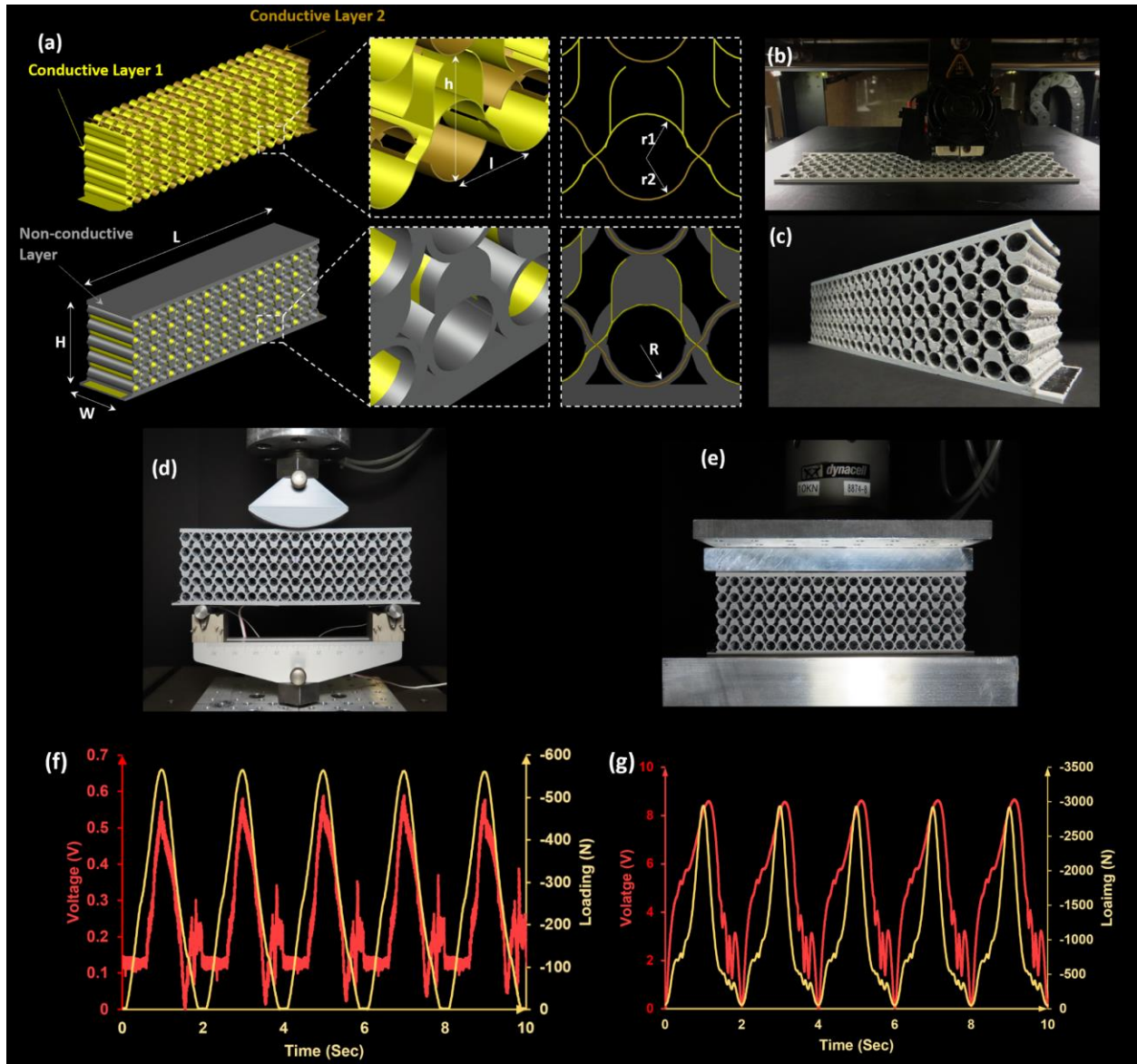
Figure 39 Designing a composite multifunctional ES^2 beam. (a) Segments of two conductive layers (Polylactic Acid (PLA) with carbon black) and a non-conductive layer (Thermoplastic Polyurethane (TPU)) (b) 3D printing of the ES^2 beam. (c) Fabricated composite beam. H, L, W, h, l, r1, r2 and R are 70 mm, 216.5 mm, 48.8 mm, 13.6 mm, 10.3 mm, 4 mm, 4.3 mm, and 4.1 mm, respectively. The thicknesses of the conductive layers are 0.16 mm. (d) Three-point bending test of the ES^2 beam. (e) ES^2 beam tested under uniaxial loading. Applied cyclic loading and the corresponding voltage (in red) generated by the ES^2 beam under (f) Three-point bending at 0.5 Hz frequency, and (g) Compressive loading at 0.5 Hz frequency.

Figure 40 shows the defined damage scenarios. A commercial uniaxial single-element strain gauge (Kyowa KFGS-5-350-C1-11 L3M3R) was glued to the bottom center of the beam. Three-point bending tests were performed under the cyclic loading of 0.5Hz during the intact and damaged modes. Figure 41a,b show the maximum measured voltage values and the maximum measured strain for four different states, respectively. The lowest voltage is measured in the intact beam while the strain was the highest. The highest voltage was recorded at the final damage state with two grooves and a full cut through the beam width. The results presented in Figure 41a proved that damage progression can be detected by tracking the changes of the voltage signal patterns.
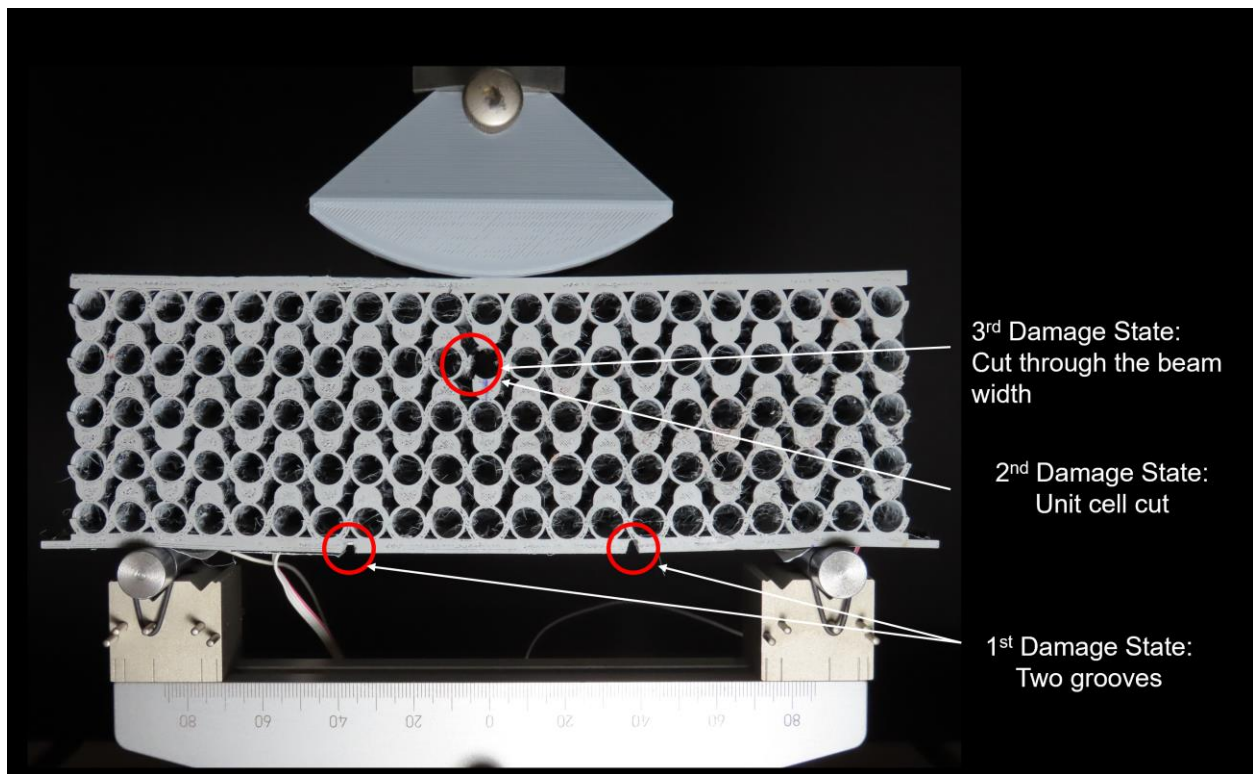
Figure 40 Damage state defined for the composite ES^2 beam
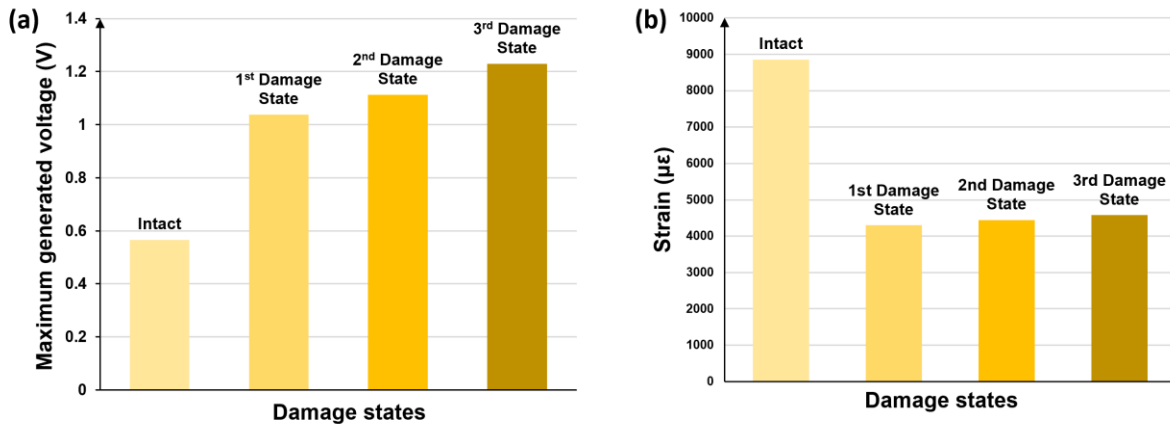
Figure 41 (a) Maximum measured voltage and (b) Maximum measured strain for different structural damage states introduced to the composite ES^2 beam.

The ES^2s offer other interesting features as well. For instance, the proposed beam became more flexible after creating two grooves at the bottom surface. A sharp increase in the measured voltage and a significant drop in the strains was observed by progression from the intact to first damage states. This observation indicates that more electrification occurs in the triboelectric layers due to larger deformations caused by the imposed cracks. The TENG modes developed during the intact and damaged states are shown in Figure 42a,b, respectively. In the intact and 1st damage states, the triboelectric layers are undamaged, and they act in their original contact-separation mode (Figure 42a). As the damage progresses, the change in strains at the bottom of the beam become less significant due to the redistribution of loads in the metamaterial after one cell was cut. Cutting one cell across the full beam width alters the displacement pattern within the metamaterial surrounding the damaged cell. For example, in the damaged row of the beam, the triboelectric mode was changed from contact-separation mode to single-electrode mode, and the integrated triboelectric metamaterial system continued to work efficiently in all damaged states mode (Figure 42b). This is while the strain gauge could not detect any internal damage on the proposed beam.

By embedding such self-sensing and self-diagnostic capabilities in the MFSs, the voltage variation can be readily used as a sign of damage progression with a need for external sensing modules.
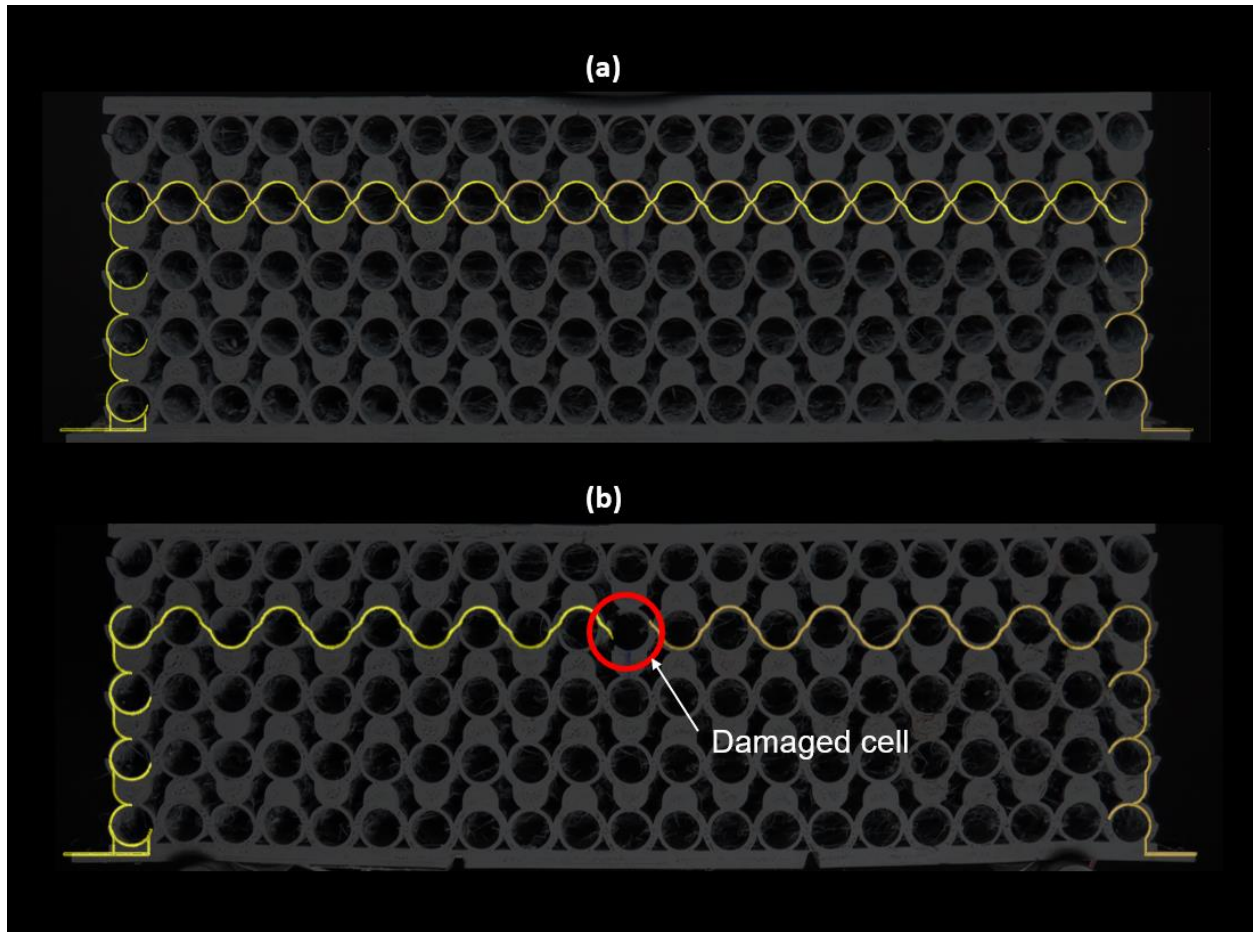
Figure 42 (a) Triboelectric layers of the selected part of the intact ES^2 beam in their original state working in a contact-separation mode. (b) Triboelectric layers of the damaged part of the ES^2 beam working in a single-electrode mode.

The next major step in this area could be embedding "digital computation" capability into the ES^2 systems. The ES^2 systems with computational functionality can be viable tools to create autonomous and intelligent smart infrastructure systems. Such ability can be integrated into the structure of the ES^2 systems through mechano-logic and performing local morphological

computations (Wang, 2013). One of the main limitations of the current embedded mechano-logic systems is lack of digital electrical outputs and a need for external power supply to pass electrical currents through the material structure. The ES^2 systems could address these challenges by serving as a "mechanoelectrical-logic gate" capable of transducing external signals directly into electrical outputs to perform digital computations. Since the output of a mechanoelectrical-logic is a digital signal, it could potentially compete with the speed and information density of electronic logic. In addition, the ES^2 systems naturally possess the outstanding features of the TENGs, which have significantly high-volume power density (~490kW/m3) (Wang, 2013). This energy can be used to empower other miniaturized low-power consumption electronics. The ES^2 systems can be light in mass, low in density, low in cost, highly scalable, and they can be fabricated using inorganic and most of the organic materials. From a mechanical perspective, the ES^2 systems are composed of different materials that are organized in a periodic manner. Therefore, they do not only inherit all features of classical mechanical metamaterials but could also offer significantly boosted mechanical properties due to their composite structure.

5.2.2.3 Conclusion

The most important challenges in the application of multifunctional structures are scalability and the integration of advanced functionalities such as sensing, energy harvesting, and computing. Although mechanical performance of MFSs has been the subject of a number of studies, there is still an unmet need for more research with focus on tunning their mechanical response and adaptivity for designated smart city applications. This is the area where mechanical metamaterials can be considered as the most viable enabling technology. In this research, the ES^2 systems were being developed using energy harvesting and metamaterials integrated paradigms. A multifunctional beam with self-sensing and self-powering capabilities was demonstrated based

97

on the ES^2 concept. The experimental results revealed that the triboelectric signal generated by the beam can be used to monitor various damage states. Surprisingly, these damage states were not detectable by conventional electromechanical sensors. Based on the results, the ES^2 concept can be deployed to build scalable, self-diagnostic and nanogenerator MFSs for smart civil infrastructure systems. Enhancing these systems with digital computing, data storage and connectivity can potentially result in truly multifunctional and autonomous civil infrastructure that can operate similar to living systems.

5.2.3 Multifunctional Nanogenerator Concrete Material Systems

5.2.3.1 Introduction

Concrete is the most utilized material in the construction industry. Various type of reinforcement were implemented to improve the mechanical properties of concrete (Asprone et al., 2018; Scerrato et al., 2016; Sola et al., 2019; Wang et al., 2021). Using nanotechnology is reported to be a viable approach to reduce environment pollution and improve durability of concrete (Hanif et al., 2017; Saloma et al., 2015). Changing mixture properties has generally shown to be effective in increasing compressibility (Fu et al., 2020), whereas reinforcement bolsters flexural capacity (Salazar et al., 2020). Besides, the commonality between these studies is to fundamentally change concrete behavior to increase ductility. A ductile material can deform plasticly upon yielding and maintain functionality, whereas a brittle material such as concrete will fail immediately at yield. Ductility can increase the concrete materials capacity in any loading condition, most importantly bending, compression, and tension for structural applications. A next technological revolution in this arena is arguably creating a new generation of concrete materials

via a rational architectural design to explore properties significantly different from traditional concrete materials. This goal can be potentially achieved using the mechanical metamaterial concepts. Mechanical metamaterials are artificial material with engineered micro/nano-scale structures to provide unprecedented mechanical properties (Jiao and Alavi, 2020c). There has been a growing interest in exploring various aspects of metamaterials for engineering applications in recent years (Barri et al., 2021b; Zadpoor, 2016). While most of the studies in the area of metamaterial are focused on designing micro/nano-scale structures, a major challenge ahead of the metamaterial science is how to adopt them for large/mega scale applications, in particular in construction industry.

This research proposes the striking concept of nanogenerator mechanical metamaterial concrete. Nanogenerator concrete is created by incorporating mechanical metamaterials and nano energy harvesting techniques into the fabrication of concrete structures. The nanogenerator metamaterial concrete is composed of auxetic polymer lattices with triboelectric properties embedded inside a conductive concrete matrix. The entire composite concrete matrix is designed to have built-in contact-electrification when mechanical excitations occur. A series of experimental tests are conducted on the proof-of-concept metamaterial concrete prototypes to evaluate their energy harvesting functionality. Potential groundbreaking applications with this design are suggested to further accentuate the full capabilities of this material is commercial construction.

5.2.3.2 Principles of Metamaterial Concrete Systems

Metamaterials are defined by the geometrical arrangement of the subunits, which can bestow unthinkable properties such as zero or negative Poisson's ratio, negative stiffness, negative compressibility, and vanishing shear modulus (Liu et al., 2015; Yang and Ma, 2018). When

designing a metamaterial concrete, one can achieve desired mechanical properties by interfacing materials with different geometries. Figure 43 shows the vision for the proposed composite mechanical metamaterial concrete system with energy harvesting functionality. The nanogenerator concrete is modified version of "super compressible metamaterial concrete" systems recently invented by the authors (Alavi et al., 2021; Barri et al., 2022a). The proposed nanogenerator concrete naturally inherits the mechanical tunability and self-recovering features of super compressible metamaterial concrete. In a super compressible metamaterial concrete, the cement paste mixture provides the required strength and stiffness needed to complete the composite metamaterial. The remaining geometry of the metamaterial interlinks the auxetic arrangement, as shown in Figure 1a. Therefore, the concrete provides horizontal and vertical stability, and enhanced compressibility. An embedded auxetic polymeric structure serves both as concrete reinforcement and the main components of the built-in nanogenerator. By casting the concrete materials into an auxetic mechanical metamaterial polymeric structure, a snap-through, self-recovering behavior is observed. The auxetic polymeric lattice can be fabricated using a wide range of materials for the triboelectric series (Kim et al., 2020), e.g. TPU as Polymer a and PLA as Polymer 2 (see Figure 43a). In order to introduce the energy harvesting functionality, a triboelectric nanogenerator (TENG) mechanism is embedded within the structure. The TENG concept was first introduced by Wang et.al (Z. L. Wang et al., 2015). TENGs produce electrical output based on triboelectrification (contact-electrification) and electrostatic induction in response to external mechanical stimulations (Fan et al., 2012; Quan et al., 2016; Wang et al., 2017). TENGs have four fundamental working modes: vertical contact-separation mode, lateral sliding mode, single-electrode mode, and freestanding triboelectric-layer mode (Z. L. Wang et al., 2015). The vertical contact-separation mode is integrated into the design in this study.
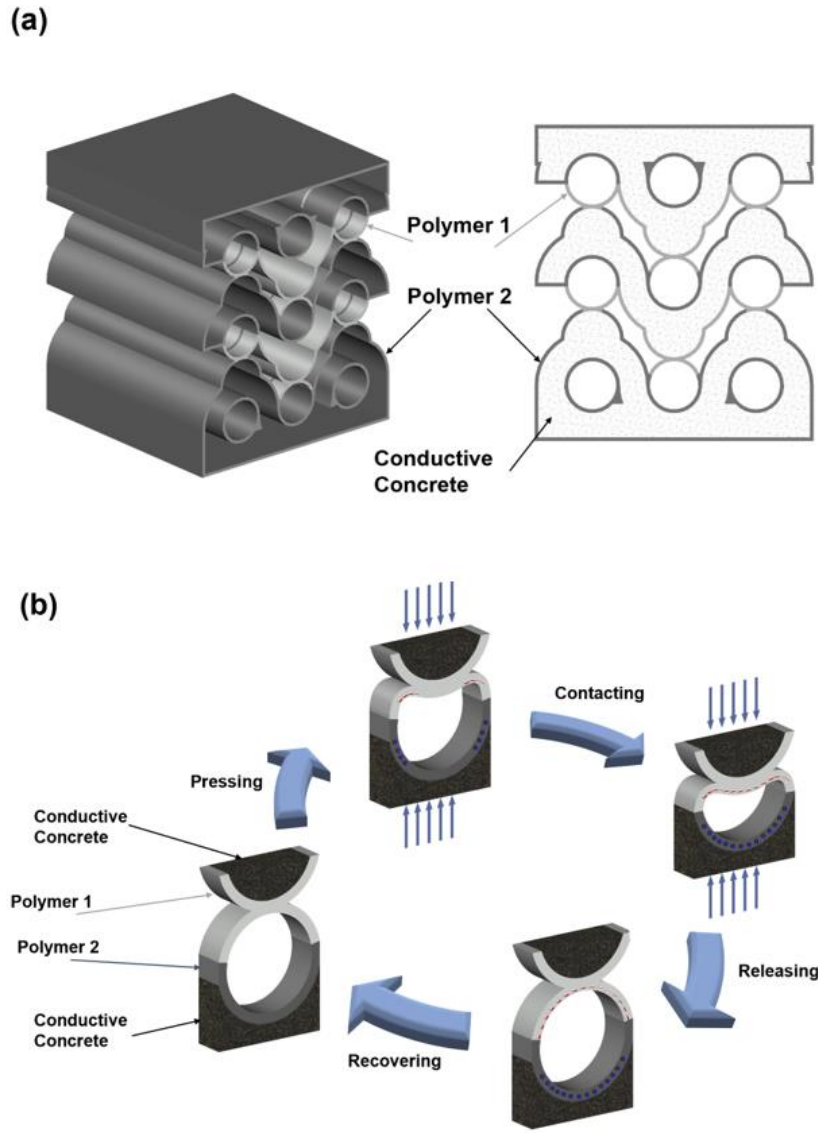
Figure 43 Vision for a nanogenerator metamaterial concrete system. (a) Composition of metamaterial matrix. (b) Working mechanism of the unit cells of a nanogenerator metamaterial concrete.

Figure 43b shows the unit cells of the metamaterial concrete with built-in contact-electrification mechanism. As seen, conductive concrete and non-conductive polymer matrix serve as the electrode, and the dielectric layers, respectively. As the metamaterial structure is loaded, contact-electrification occurs within the cells between the conductive and non-conductive layers. Due to the contact-electrification, the conductive and non-conductive layers accumulate positive and

negative charges, respectively. As the metamaterial structure is unloaded, the transferred charge remains on the dielectric surface. This forms a static electric field and a potential difference between the conductive layers. By increasing the loading amplitude, more conductive and dielectric layers of the matrix engage in the contact-separation process, which results in generating higher electrical output.

5.2.3.3 Results and Discussion

In order to validate the proposed metamaterial concrete concept, a proof-of-concept porotype was fabricated and tested under cyclic loadings. Regular concrete materials are not electrically conductive. In order to create a conductive mixture, the cement paste was enhanced by adding 2% of Graphite into the basic mixture of Type I Portland cement (Cemex Inc.). Graphite powder from Fasco Epoxies Inc. with 44-50 microns particle size were used in this study. Carbon graphite cannot be directly mixed in water due to agglomeration effects of van der Waals forces (Chauhan and Chawla, 2016). Therefore, it was dispersed with Ultrasonicator. Ultrasonic bath (42KHZ, 180 Watts, 6.5 Liter ultrasonic carburetor from Kaimashi Inc.) was used for graphite dispersion. ACI 318-14 Table 19.3.2.1 specifies a maximum water to cement ratio of 0.45 or 45% for plain concrete (ACI 318, 2014). After graphite was successfully mixed with water, the solution was finally mixed with cement following ASTM C 305 (ASTM-C305, 2014). Two inches by two inches (5.08× 5.08 cm) cement cubes was casted and aluminum and copper electrodes with different dimeters were embedded inside the specimen for electrical resistance measurement, as shown in Figure 44.

Figure 44 Two inches by two inches cement cubes added with Graphite powder and different electrodes for electrical resistance measurement.
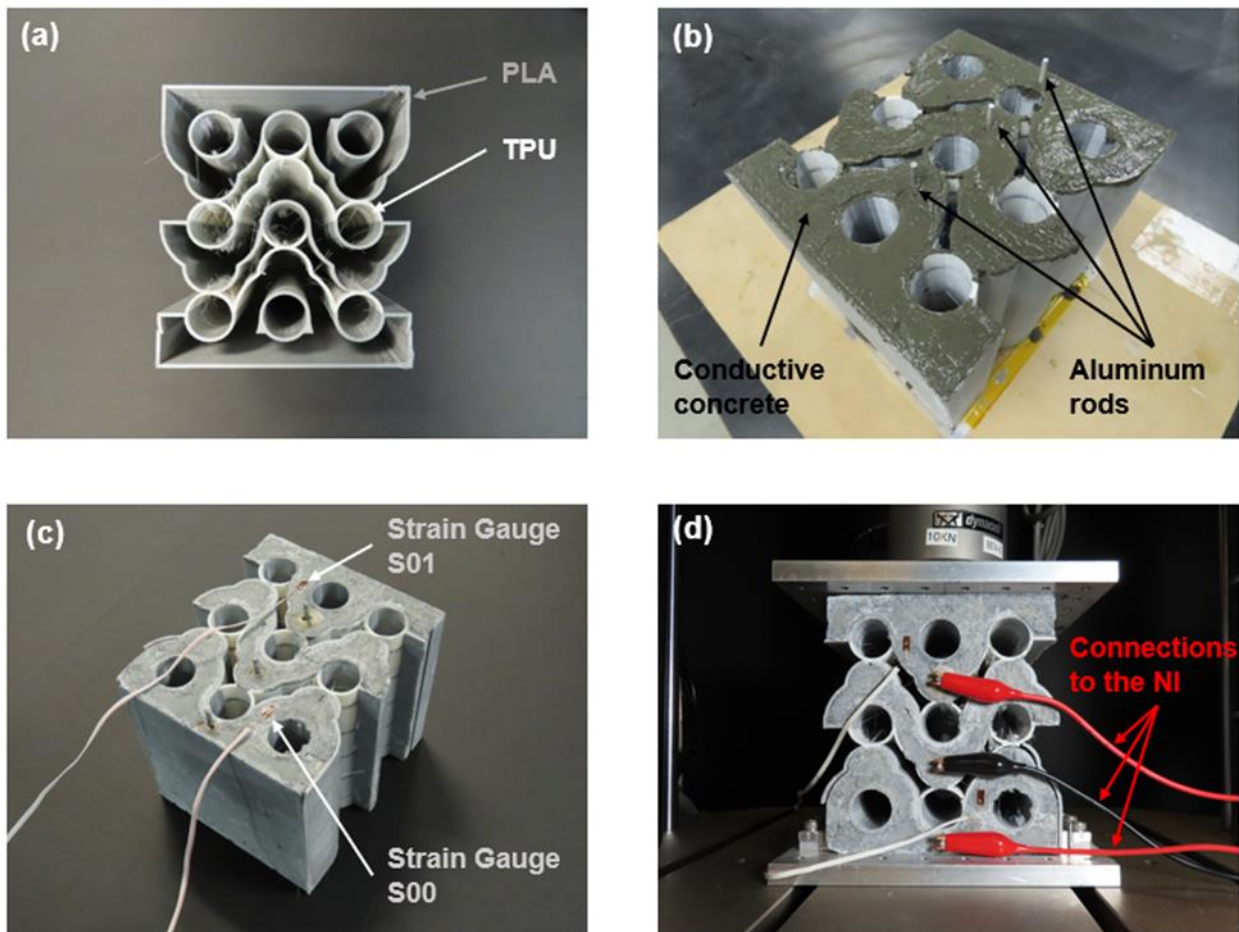
Figure 45 Fabricated nanogenerator metamaterial concrete sample with 3×3 unit cells. (a) 3D printed mold with PLA and TPU material to act as a TENG. (b) Freshly poured conductive concrete into the TENG mold. (c) Cured concrete TENG sample with three rods and two strain gauges. (d) Test setup.

The design for polymeric lattice with self-recovering snapping segments is shown in Figure 45a. The lattice has 3×3-unit cells and was 3D printed using an Ultimaker S3 printer. The material used for printing the lattice were PLA (E = 2.35 GPa, ν = 0.30), and TPU (E = 26 MPa, ν = 0.45). The proof-of-concept design may qualify as the "ideal" material ratio as an ideal design is dependent on the realistic application of the material. For the testing purpose, the standard cubic dimension was considered as a reference dimension, in order to provide empirical results regarding the longitudinal displacement and the subsequent recovery of the metamaterial when the compression is released. Therefore, the lattices were scaled to 6 in × 6 in× 6 in as a testing standard for future iterations of this design. The pours were executed carefully for each metamaterial design to avoid distorting the polymeric lattice geometry, which would conversely affect the composite's overall compressibility. Aluminum rods with diameter of 2 mm were inserted on the top and bottom cells for voltage measurements (Figure 45b). Each layer of concrete acts as electrodes, which conveys the induced electricity generated by PLA and TPU layers as the two parts of the TENG (Figure 45a,b). The top was covered, and the sample set aside to dry for 24 hours. Once the samples were drying, the modular molds and covers were gently removed, and the samples submerged in water to cure. The samples were cured for 4 weeks, and once finished they were removed from the water and prepared for the testing phase. Figure 45c and d show the fabricated nanogenerator metamaterial concrete sample with 3×3 unit cells. Static testing performance of each design was assessed via the Instron® 8874 Biaxial Servohydraulic Fatigue Testing System. There were two tests implemented to estimate the compressive properties of both metamaterial concrete designs. Both designs were initially tested in cyclic compression, consisting of multiple cycles of compression and subsequent release at a rate of 0.05 Hz. These trials were repeated to increase the vertical displacement of the metamaterial from the default at rest state. The vertical

displacement was deliberately capped to not exceed the space allocated by the auxetic cells. Following these tests, the samples were placed under ultimate compression. Ultimate compression featured a one-time vertical displacement exceeding the auxetic cell space to observe how the samples would recover under extreme loading conditions.

The designed 3×3 metamaterial concrete sample was tested under displacement-controlled (4 mm and 8 mm) cyclic tests. Two strain gauges were attached to the sample near the top and bottom cells (Figure 45c). The voltage generated by the nanogenerator metamaterial concrete was read using a National Instruments 9220 DAQ module with 1 GΩ impedance. An NI9220 module with 1 GΩ impedance was used to measure the generated voltage signals. An NI 9235 module was used to collect the strain gages outputs. A low-noise current amplifier (SR570, Stanford Research Systems) was used to measure the currents generated by the meta-tribomaterial prototypes. A LabVIEW program was developed to control and synchronize measurements from all modules and store readings in the host computer. Figure 46a and Figure 47a present the voltage generated after applying 4 mm and 8 mm displacement-controlled loading testing cycles, respectively. The peak-to-peak voltage value for 4 mm and 8 mm displacement were 3.5 V, and 14 V respectively. The applied cyclic loads and the generated current are shown in Figure 46(b), and Figure 47(b) . The maximum measured current for 4mm and 8mm displacement were 175 nA, and 236 nA respectively. The maximum generated power for 4 mm displacement was 6.13e-7 Watt, and for 8 mm displacement was 3.30e-6 Watt. As seen, the voltage and current are proportional to the applied displacement and accordingly to the strain induced in the concrete structure. Figure 46(d-f), and Figure 47(d-f) illustrate the charging characteristics of the metamaterial concrete under periodical mechanical motion. As seen in Figure 46d and Figure 47d, the low capacitance capacitors are charged rapidly and immediately reach saturation voltage. While for capacitors with

higher capacitance, saturation occurs more slowly. The saturation voltage for 4mm displacement was approximately 2.75 V, which is almost 78% of the maximum measured voltage. Similarly, for 8 mm displacement, the saturation voltage was about 12.6 V, comparing with the maximum measured voltage of 14 V. Figure 46f, and Figure 47f show the effect of capacitance on the voltage and charge stored in the capacitors after 90 seconds.
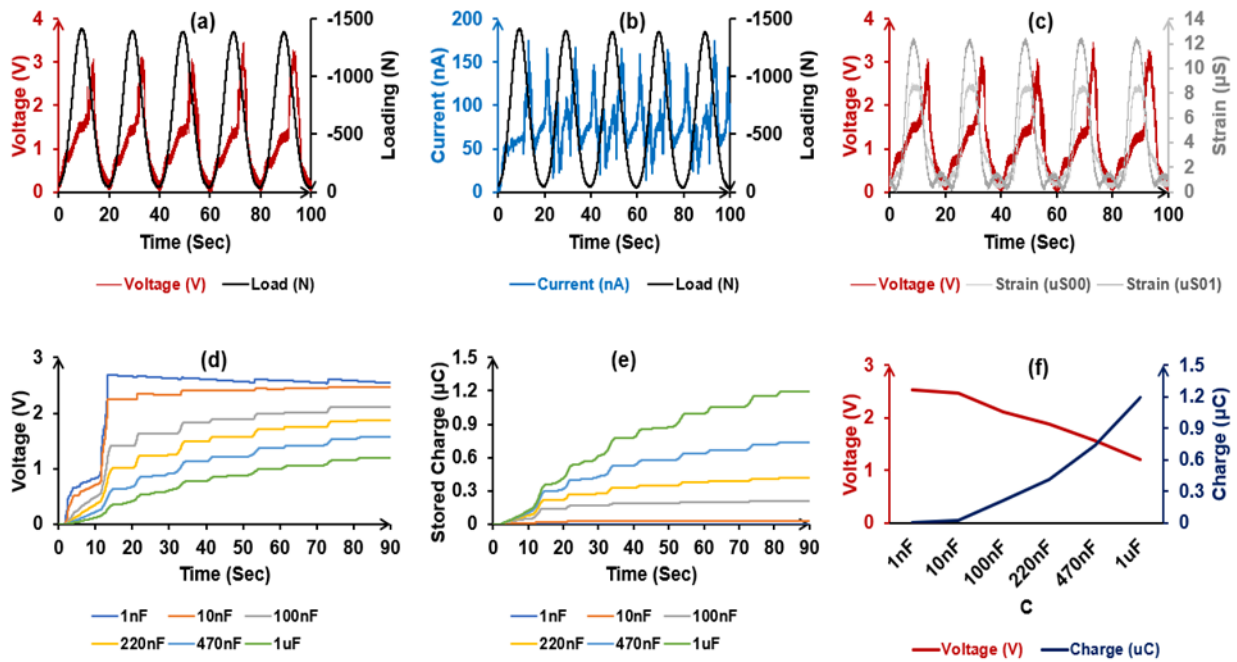
Figure 46 Stage 1) 4 mm displacement under the compressive load. Compressive loading and corresponding voltage (a), and current (b) generated by the concrete TENG. (c) Measured voltage and corresponding strains. (d) Voltage changes at different load capacitances. (e) Stored charge changes at different load capacitances. (f) Variations of the stored voltage and charge against capacitance at 90 s.
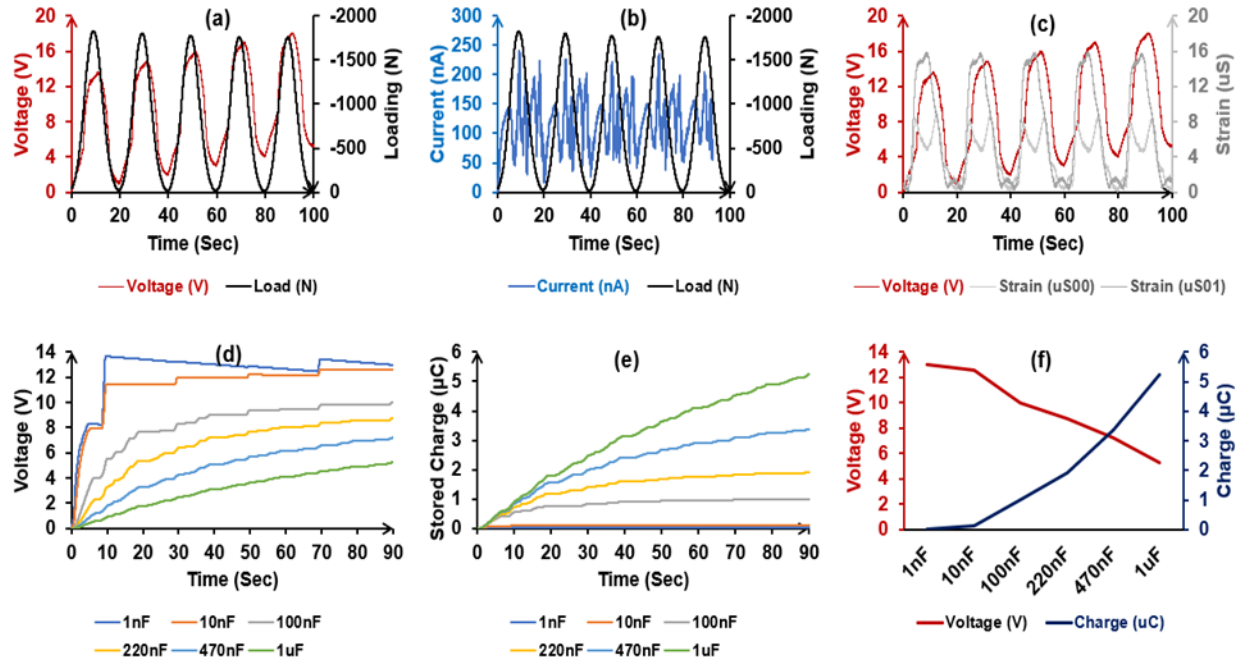
Figure 47 Stage 2) 8 mm displacement under the compressive load. Compressive loading and corresponding voltage (a), and current (b) generated by the concrete TENG. (c) Measured voltage and corresponding strains. (d) Voltage changes at different load capacitances. (e) Stored charge changes at different load capacitances. (f) Variations of the stored voltage and charge against capacitance at 90 s.

This study demonstrated the vision towards creating a concrete polymer composite constituency with an auxetic metamaterial design that can provide unusual/tunable mechanical and energy harvesting properties. This concept could open the door to the use of concrete in applications for which it is never considered and bolster concrete performance in applications for which it is already considered efficient. There is a growing interest in electric vehicles (EVs) as the future of environmentally friendly modes of transportation. Despite the significant interest in EVs, their diffusion has been slow mainly due to concerns regarding the required infrastructure and long charging times. A nanogenerator concrete structure can serve as a smart system that can communicate with EVs and poetically charge them. Note that the current volume power density of TENG-based systems has already reached 500 W/m2 (Wang, 2013; Z. L. Wang et al., 2015),

which is comparable with the power density of solar panels (Krac and Górecki, 2016). In addition, the proposed metamaterial concrete can be used to design a new generation of shock absorbing engineered materials arresting system (EMAS). EMASs are high energy absorbing strips of engineered materials with tailored strength designed at the end of runways to mitigate the severity of the consequences of aircraft landing overrun events (Ketabdari et al., 2020). A metamaterial concrete could be considered the very first concrete "beam-column" as it will have the ability to exhibit high resistance to compression and lateral forces. A base isolation system made of metamaterial concrete can be both retrofitted to any concrete column size in a superstructure or precast and delivered in different concrete forms, notably columns or girders. The compressibility and stiffness of the composite can be tuned based on the number of auxetic cells included in the design. With further research and testing, this design can be matched to any known building frequency. Endowing concrete girders with damping capabilities will further improve the structural resistance of concrete to ground acceleration and inter-story drift. Rather than merely focusing on the interface between the superstructure and the subgrade, this design will enable a holistic approach to damping in concrete structures.

5.2.3.4 Conclusion

In summary, this study demonstrated the vision toward developing a new generation of concrete materials with unprecedented mechanical and energy harvesting properties. The proposed metamaterial concrete is based on the fusion of snapping metamaterial, concrete design and TENG concepts. Integrating the concrete mixture with auxetic polymer structures with snap-through buckling behavior resulted in creating a concrete material system with new functionalities. The developed proof-of-concept prototype was experimentally tested to verify the efficiency of the proposed concept. The abilities of the metamaterial concrete could potentially revolutionize

108

concrete construction as it supplements the inherent weaknesses of concrete in fatigue applications. The composite constituency showed levels of compressibility, while maintaining a high level of stiffness. The compressibility of this material reveals the future for a ductile concrete, with a significantly higher flexural capacity and ability to absorb vibration without incurring any flaws. The novelty of the proposed concept demands further research on various mechanical and application aspects. More focus should be place on mechanical tunability of these metamaterials based on the number of auxetic cells, polymer material and concrete mixture. Yet, future work will focus on different empirical forms of this composite such as units beams and slabs, which are favored to be the most widely used application for this design.

6.0 Conclusion and Future Directions

In this dissertation, a new generation of multifunctional mechanical metamaterials called "meta-tribomaterials" has been introduced by combining the fields of mechanical metamaterials and nano energy harvesting. Advances in metamaterial design and energy harvesting was used to engineer new aspects of intelligence into the texture of materials for multifunctional applications. The so-called meta-tribomaterial systems were fabricated using finely tailored and topologically different triboelectric microstructures. Experiments and theoretical analyses were conducted to quantitatively investigate and maneuver the mechanical and electrical behaviors of the meta-tribomaterials. The wide application of the proposed meta-tribomaterial concept were highlighted for designing proof-of-concept multifunctional material systems such as self-sensing, self-monitoring and self-powering medical stents, smart medical implants, multifunctional structural elements, nanogenerator metamaterial concrete system, and shock absorbers. This study paves the way for the next stage of the technological revolution in material science in which "self-aware engineered materials and structures" can empower, sense and program themselves using their constituent components. Such meta-tribomaterials systems serve as a sensing medium to directly infer multiple types of hidden information relating to the structure. Although this dissertation presented proof-of-concepts meta-tribomaterials with snapping segments, the proposed concept can be applied to many other material types with different geometrical designs.

The main 2D design of the proposed meta-tribomaterial system were fabricated with two dielectric and conductive materials. TPU was used as a main part of the proposed meta-tribomaterial system, as well as one side of the embedded triboelectric system. Conductive PLA which had two main roles in the proposed meta-tribomaterial system, was used as the second

part of the embedded triboelectric system, and also formed a complex network of electrodes to convey the electrons in the proper paths. Uniaxial loading experiments were performed on the 3D printed metamaterial specimen. Different capacitors were used as storage system, in order to show the energy harvesting capability of the proposed meta-tribomaterial system.

Furthermore, the feasibility of integrating the developed 2D meta-tribomaterial mechanism to design multifunctional systems for real-life engineering applications, was demonstrated. In order to highlight the significantly broad applications of the proposed meta-tribomaterial concept, different areas of biomedical, automotive/aerospace, and civil/structural engineering were explored.

The first application was designing the patient specific medical implant, specifically a meta-tribomaterial spinal fusion cage. In this dissertation a first-of-its-kind multifunctional instrumentation with sensing and energy harvesting functionality was developed for post-operative biomechanical evaluation of lumbar spinal fusion. The proposed multifunctional interbody fusion cage is capable of detecting various levels of spinal fusion through continuous stability and load-sharing measurements directly at the intervertebral disc space level. This technology could provide physicians the ability to assess the progress of fusion without the need for radiographic imaging. The microscale meta-tribomaterial cage prototypes were 3D printed using conductive materials. There is a wide range of biocompatible and bioresorbable materials from the triboelectric series that can be used to fabricate the conductive and dielectric layers. The experimental studies performed on both synthetic spine and human cadaver spine models confirm the efficiency of the self-aware implants in assessing fusion process and harvesting energy from mechanical excitations. Under loading conditions similar to human lumbar spine, the fusion cage prototype could generate voltage and current values equal to 9.2 V and 4.9 nA, respectively. The saturation

voltage in order to charge the external capacitors was 8 V, which demonstrate the energy harvesting capability of the proposed smart implant.

The second application in the biomedical area was medical stents. In this dissertation, two types of medical stents were developed; a nano scale cardiovascular stent, and a micro scale esophageal stent. The cardiovascular and esophageal stents were first fabricated as auxetic meta-tribomaterial films and were then configured into tubular stent form. The cardiovascular stent prototype was fabricated using a 3D direct laser writer (Nanoscribe Photonic Professional, GT) with overall dimension of dimension of 7.5 mm x 7.5 mm x 300 um. The esophageal stent auxetic structure had a dimension of 72 mm x 52.6 mm x 4 mm, and was fabricated with TPU and conductive PLA using the Riase3D Pro2 dual extruder 3D printer. Experimental studies were performed for further evaluation of the electrical performance of the designed 3D configurations. The measured voltage and current for cardiovascular stent subjected to the cyclic loading at 1 Hz frequency were 0.6 mV and 172 nA, respectively, and for esophageal stent subjected to the cyclic loading at 0.05 Hz frequency were 3V and 7 nA, respectively.

The third application was designing self-sensing shock absorbers with energy harvesting capabilities. The proposed meta-tribomaterial shock absorber prototype was fabricated using the FDM 3D printing technique. Similar to the main 2D meta-tribomaterial system TPU and PLA were used as non-conductive and conductive layers, respectively. The maximum generated voltage and the corresponding measured current were 4 V and 5 nA respectively.

The other application was related to multifunctional structures and called engineered self-aware structures (ES^2s). In this part of the dissertation, the ES^2 concept is demonstrated through fabricating mechanically tunable multifunctional composite beam prototypes with sensing and energy harvesting functionalities. The entire system serves as an energy harvesting medium

as well as an active sensing system to directly collect information about its operating environment. The composite multifunctional ES^2 beam which is consist of two conductive network (Conductive PLA) and a non-conductive body (TPU) was fabricated using a Raise3D Pro2 dual extruder 3D printer. The overall dimension of the composite beam was 216.5 mm x 48.8 mm x 70 mm. Three-point bending test and uniaxial compression test were performed using an Instron 8874 universal testing machine at 0.5 Hz frequency. Different damage stages were introduced into the composite beam. The experimental results revealed that the triboelectric signal generated by the beam can be used to monitor various damage states. Surprisingly, these damage states were not detectable by conventional electromechanical sensors. Based on the results, the ES^2 concept can be deployed to build scalable, self-diagnostic and nanogenerator MFSs for smart civil infrastructure systems.

The last application which has been proposed in this dissertation is multifunctional nanogenerator concrete material system. The nanogenerator metamaterial concrete was composed of auxetic polymer lattices with triboelectric properties embedded inside a conductive concrete matrix. The entire composite concrete matrix was designed to have built-in contact-electrification when mechanical excitations occur. An embedded auxetic polymeric structure served both as concrete reinforcement and the main components of the built-in nanogenerator. The auxetic polymeric structure with 3x3 unit cells was fabricated with PLA and TPU material using a Rais3D Pro2 3D printer. The conductive concrete was made by adding 2% of Graphite into the basic mixture of Type I Portland cement. The overall dimension of the proposed nanogenerator metamaterial concrete was 150mm x 150mm x 150mm. Uniaxial compression tests at 0.05 Hz frequency were performed using an Instron 8874 universal testing machine. The maximum generated voltage and measured current for 8 mm displacement were 14 V, and 236 nA

respectively. The charging characteristics of the metamaterial concrete under a periodic mechanical motion were also obtained by using a simple bridge rectifier and different capacitors. The saturation voltage for 8mm displacement was approximately 12.6 V. The abilities of the proposed metamaterial concrete such as super compressibility, self-sensing, self-powering, and energy harvesting, could potentially revolutionize concrete construction.

As mentioned before, the meta-tribomaterial concept can address most of the challenges related to the traditional structural health monitoring approaches such as dense sensing systems, power supply problems, remote area and embedded sensors, cross-sectional or interlaminate failures, limited durability, as well as extensive maintenance requirements (Alavi et al., 2016a; Seifert et al., 2019). However, the novelty of the proposed concept makes it difficult to address all possible issues related to the robustness, durability or practicality of the meta-tribomaterials in actual implementation. For example, design optimization of the meta-tribomaterial-based systems, optimization of the triboelectric charge density, power management and storage, and effect of fatigue on the hierarchical structures should be taken into account. Besides, there are concerns about the long-term durability of TENG-based mechanisms. To cope with this issue, it is possible to deploy some of the successful fabrication solutions that have been previously proposed to improve the durability and output stability of the TENGs for continuous operation (Lin et al., 2020). The following research areas are particularly open to exploration in this regard:

6.1 Optimize the power density of the meta-tribomaterial systems

Future study should consider various rational designs for triboelectric layers, as well as physical and chemical surface modification approaches, to increase the power output in the order

of 100-500 µW. This range is extracted from the previous studies have shown the feasibility of achieving similar power levels using standard TENGs (Xu et al., 2021). Power optimization is critical for exploiting the energy harvesting functionality of the meta-tribomaterials. Practical examples include empowering wireless sensor nodes (~ 100 µW energy demand (Dziadak et al., 2016; Paul D. Mitcheson et al., 2008)), and implantable wireless data-loggers (e.g. piezoelectric floating-gate (FG) sensors: ~ 1 µW energy demand (Barri et al., 2022b)).

6.2 Digital computation and information storage functionalities using meta-tribomaterials

A crucial step to achieve cognitive metamaterials with full autonomy is to incorporate digital computing and information storage functionalities into their texture. The following studies can be done to build complex logic circuits for digital computation and data storage:

6.2.1 Meta-tribomaterial systems for mechanically-responsive data storage

There are very limited studies in the area of data storage using mechanical metamaterials (Chen et al., 2021; Mei et al., 2021). These studies present merely a "mechanical" information storage by leveraging the bistability of the mechanical metamaterial structures (Chen et al., 2021). Creating mechanical metamaterials with digital information storage is an outstanding challenge that has not yet been possible. In this regard, the capability of the meta-tribomaterial systems as a framework for self-powered digital information storage will be studied. The unique composition of the meta-tribomaterial structures enables us to explore a new class of information storage systems which are mechanically responsive data storage devices. In order to develop the

115

first-of-its-kind mechanically responsive data storage device, data will be incorporated into a set of self-recovering unit cell patterns that form the meta-tribomaterial matrix. A data storage can be viewed as a meta-tribomaterial structure in which only designated unit cells will have built-in contact-electrification mechanism.

Figure 48a shows a schematic of the envisioned data storage with three layers each with their specific stiffnesses. As the metamaterial structure is loaded, triboelectrification occurs only within the cells with embedded contact-electrification mechanism in the top and bottom layers (Figure 48b,d). Under axial loading, the unit cells in the second layer will buckle but will not generate a signal (Figure 48c). As these three layers with different snapping segment thicknesses (t) deform sequentially, the entire metamaterial structure will produce alternatively varying voltage signal in quasi-square wave (Figure 48e). The trough and crest of the quasi-square wave signal can be coded as binary bits of "0" and "1," respectively, while the time span of the trough and the crest is associated with the number of bits. In this schematic design, a string of codes "1001" is generated, which represents the decimal "9".

A proof-of-concept mechanically responsive device (Figure 48a) composed of 3×3 unit cells (radius = 7.6 mm) 3D printed using TPU and PLA materials. The dimensions of the porotype are 61 mm × 103 mm × 20 mm. The thicknesses of the layers are $t_1 = 1.5$ mm, $t_2 = 2.5$ mm, and $t_3 = 3.5$mm. The proposed data storage device can be considered as new class of sequential access memory (SAM) where stored data can be accessed in a deformation sequential order under mechanical stimulations. Its stiffness can be rationally designed to serve as either a flexible/soft or hard data storage system. Similar to advanced SAM technologies (e.g. IBM LTO 9 drives), the mechanically responsive data storage devices can potentially be low-cost, non-volatile, and long-term storage solutions (Mendell and Hogan, 2021; Starr et al., 2020).
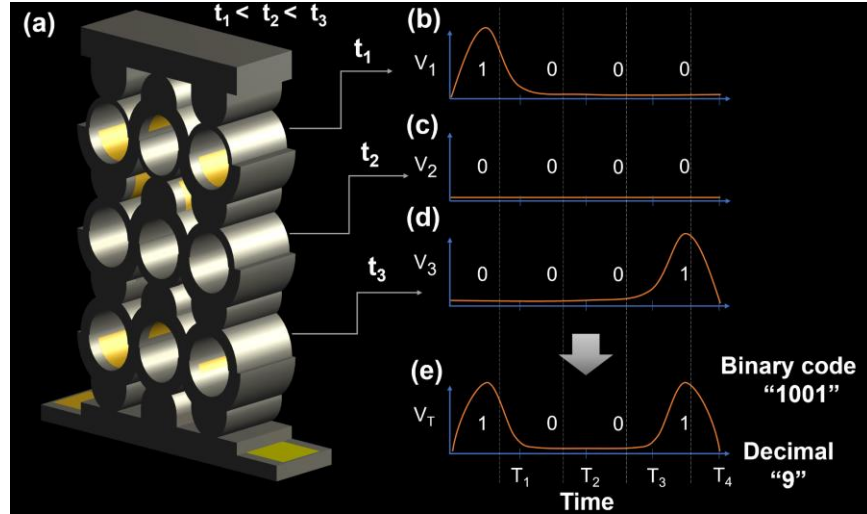
Figure 48 (a) Schematical representation of mechanically responsive data storage. (b)-(e) Using the built-in generated signal to process a string of codes "1001" and decimal "9" incorporated into the structure of the mechanically responsive data storage system.

6.2.2 Self-powering meta-tribomaterial logic gates for digital computation

In this preliminary study, self-powered mechanoelectrical-logic gates based on enhanced meta-tribomaterials have been developed capable of translating the mechanical deformation applied to their structural framework into digital bits without the use of an external power source. Mechanoelectrical-logic is a drastically different digital computing approach from the state-of-the-art embedded mechano-logic. The mechano-logic systems lack a digital electrical output (e.g. (Ion et al., 2017; Treml et al., 2018; Yasuda et al., 2021)), and can merely operate with an external power supply (e.g. (El Helou et al., 2021)). Figure 49 shows the first of a kind self-powered digital computations using a monostable origami-inspired meta-tribomaterial system. Compared to cellular metamaterials, origami-inspired mechanisms are more suitable options for digital

117

computation because they can be programed to deform locally on each crease. Figure 49a shows the 3D model of a proof-of-concept prototype designed with self-recovering unit cells and a two-layer structure to achieve various mechanical states. Under uniaxial and tortional loads applied to the top metamaterial surface, different deformation modes will be realized. Each deformation mode will activate the contact-electrification in a specific layer resulting in a distinct electrical signal, which will be used for digital computations. For instance, the prototype shown in Figure 49a is designed with contact-separation modes for the top and bottom layers. The layers will only generate a signal in a close-and-recover state. Under uniaxial compressive loading, both layers of the prototype are in a close-and-recover state and generate electrical signals (Figure 49b). When a clockwise rotation is applied, the top layer is in close-and-recover state, and the bottom layer is in open-and-recover state. Therefore, only one electric signal is generated for a clockwise rotation mechanical input. When counterclockwise rotation is applied, the top layer is in open-and-recover state, and the bottom layer is in close-and-recover state. Each of the mechanical inputs can be realized with the distinctive voltage patterns generated by the structural channels. The generated signals can then be translated into binary signals for digital computation. The meta-tribomaterial logic approach will simultaneously realize the triggering mechanical input type (e.g. compression, clockwise rotation), amplitude, and frequency.
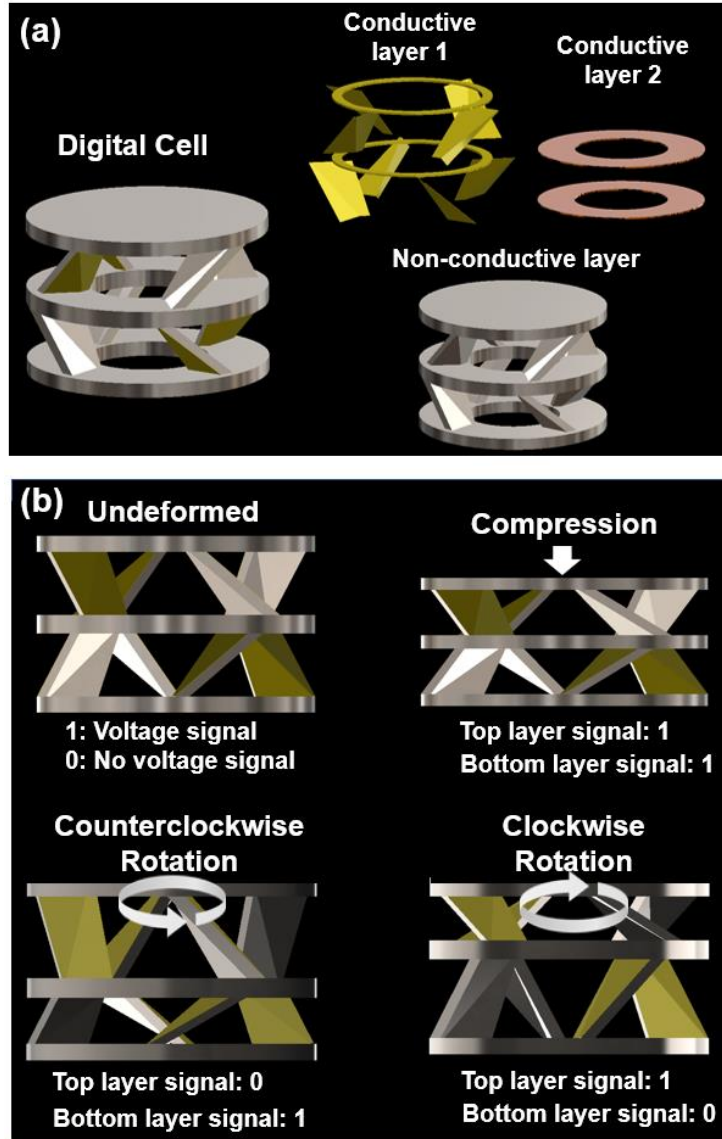
Figure 49 Self powered digital computations using a monostable origami-inspired meta-tribomaterial system. **(a) 3D model of a proof-of-concept origami-inspired prototype that can realize digital computations. (b) Motions of the self-recovering origami-inspired prototype. Compression, tension, and rotation mechanical inputs activate the built-in contact-electrification events in top and/or bottom layers. The activated layers generate voltage signals that represent "1" digital readout. A "0" digital readout implies the absence of the contact-electrification signal in the layer. For instance, with a counterclockwise rotation input (mode3), the bottom layer creates a voltage signal (1 digital readout). The top layer is not activated in this mode (0 digital readout). Thus, a counterclockwise rotation input registers 0 and 1 digital bits.**

The next step is to formulate a general logic method for cellular and origami-inspired designs to synthesize discrete mechanical configurations and to realize all digital logic gates and compute Boolean logic operations.
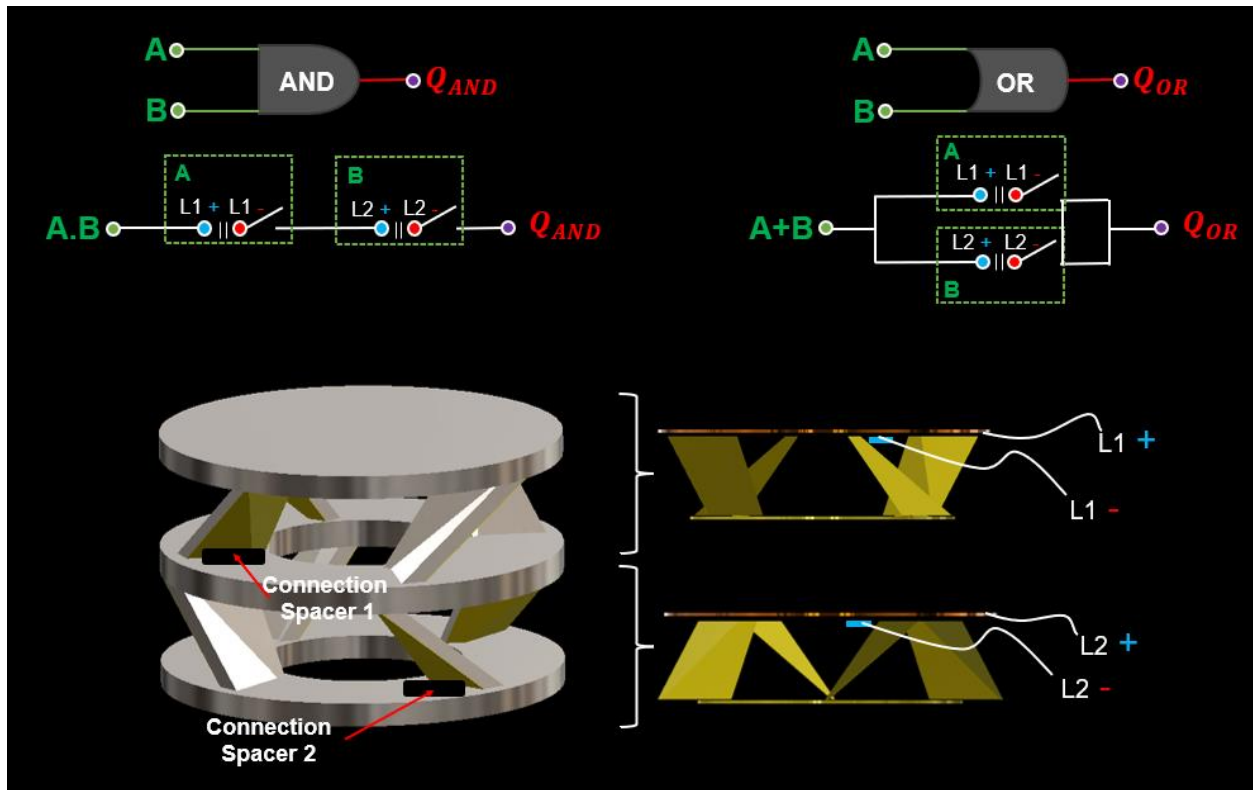
Figure 50 Model of unit cell to perform as "AND" and "OR" logical gates.

Figure 50 show the model of unit cell to perform as "AND" and "OR" logical gates. In this design, L1 and L2 are two sets of TENG system in layer 1 and layer 2 respectively. As a result, there are two sets of output connections. In each set of TENG, one output wire is connected to positive charge side of the TENG (L1+ and L2+), the other output wire is connected to the connection spacer. In initial condition, the connection spacer is disconnected from the negative charge side (L1- and L2-). When each layer in "close (1)" mode, the negative charge side will be connected to

the spacer to close the circuit. Two sets of TENG are connected in series to achieve "AND" logical gate. The circuit will be closed only when both layers are in "close (1)" mode, otherwise, it will be open circuit. Similarly, "OR" gate can be achieved by connecting two sets of TENG in parallel.

The proposed formulation of digital logic will intrinsically couple the mechanical buckling modes with the distinctive signatures and amplitudes of the electrical signals generated by the meta-tribomaterials. To validate the functioning of the mechanoelectrical logic gates, extensive numerical and experimental studies will be conducted to create a suite of meta-tribomaterial designs that can realize all eight standard digital logic gates, i.e., AND, OR, NAND, NOR, XOR, XNOR, NOT, and Buffer. Triggering mechanical signals with different amplitudes (10 to 3000 N) and frequencies (1-20 Hz) will be studied.

Bibliography

ACI 318, 2014. Building Code Requirements for Structural Concrete (ACI 318-14) Commentary on Building Code Requirements for Structural Concrete (ACI 318R-14) An ACI Standard and Report.

Ahn, Y.H., Chen, W.M., Lee, K.Y., Park, K.W., Lee, S.J., 2008. Comparison of the load-sharing characteristics between pedicle-based dynamic and rigid rod devices. Biomed. Mater. 3, 044101. https://doi.org/10.1088/1748-6041/3/4/044101

Al-Tabbaa Abir, Lark Bob, Paine Kevin, Jefferson Tony, Litina Chrysoula, Gardner Diane, Embley Tim, 2018. Biomimetic cementitious construction materials for next-generation infrastructure. https://doi.org/10.1680/jsmic.18.00005 171, 67–76. https://doi.org/10.1680/JSMIC.18.00005

Alavi, A., Barri, K., 2022. Self-aware composite mechanical metamaterials and method for making same. US Patent 2022/0011176 A1.

Alavi, A.H., Barri, K., Zhang, Q., Khazanovich, L., 2021. Super-Compressible Metamaterial Concrete and Method for Making Same, U.S. Provisional Pat. Ser. No. 63/245,300.

Alavi, A.H., Hasni, H., Lajnef, N., Chatti, K., Faridazar, F., 2016a. An intelligent structural damage detection approach based on self-powered wireless sensor data. Autom. Constr. 62, 24–44. https://doi.org/10.1016/J.AUTCON.2015.10.001

Alavi, A.H., Hasni, H., Lajnef, N., Chatti, K., Faridazar, F., 2016b. Damage detection using self-powered wireless sensor data: An evolutionary approach. Measurement 82, 254–283. https://doi.org/10.1016/J.MEASUREMENT.2015.12.020

Alavi, A.H., Zhang, Q., Barri, K., 2022. Advanced multifunctional structures for future smart cities. Rise Smart Cities 29–52. https://doi.org/10.1016/B978-0-12-817784-6.00004-7

Alazzawi, Y., Chakrabartty, S., 2016. Design of CMOS telemetry circuits for in-vivo wireless sonomicrometry. Proc. - IEEE Int. Symp. Circuits Syst. 2016-July, 2022–2025. https://doi.org/10.1109/ISCAS.2016.7538974

Albino, V., Berardi, U., Dangelico, R.M., 2015. Smart Cities: Definitions, Dimensions, Performance, and Initiatives. https://doi.org/10.1080/10630732.2014.942092 22, 3–21. https://doi.org/10.1080/10630732.2014.942092

Andrew Swartz, R., Lynch, J.P., Zerbst, S., Sweetman, B., Rolfes, R., 2010. Structural monitoring of wind turbines using wireless sensor networks. Smart Struct. Syst. 6, 183–196. https://doi.org/10.12989/SSS.2010.6.3.183

Argoubi, M., Shirazi-Adl, A., 1996. Poroelastic creep response analysis of a lumbar motion segment in compression. J. Biomech. 29, 1331–1339. https://doi.org/10.1016/0021-9290(96)00035-8

Ashby, M.F., Ash By, M.F., AUCKLAND BOSTON JOHANNESBURG MELBOURNE NEWDELHI Butterworth-Heinemann, O., 1992. MATERIALS SELECTION MECHANICAL DESIGN IN SECOND EDITION SECOND EDITION British Library Cataloguing in Publication Data Library of Congress Cataloguing in Publication Data.

Askari, H., Khajepour, A., Khamesee, M.B., Saadatnia, Z., Wang, Z.L., 2018. Piezoelectric and triboelectric nanogenerators: Trends and impacts. Nano Today 22, 10–13. https://doi.org/10.1016/j.nantod.2018.08.001

Asprone, D., Menna, C., Bos, F.P., Salet, T.A.M., Mata-Falcón, J., Kaufmann, W., 2018. Rethinking reinforcement for digital fabrication with concrete. Cem. Concr. Res. 112, 111–121. https://doi.org/10.1016/J.CEMCONRES.2018.05.020

ASTM-C305, 2014. Standard Practice for Mechanical Mixing of Hydraulic Cement Pastes and Mortars of Plastic Consistency.

Barri, K., Jiao, P., Zhang, Q., Chen, J., Wang, Z.L., Alavi, A.H., 2021a. Multifunctional meta-tribomaterial nanogenerators for energy harvesting and active sensing. Nano Energy 86, 106074. https://doi.org/10.1016/J.NANOEN.2021.106074

Barri, K., Zhang, Q., Jiao, P., Wang, Z.L., Alavi, A.H., 2021b. Multifunctional metamaterial sensor and nanogenerator, in: Proceedings of the American Professional Society of Photographic Instrumentation Engineers (SPIE), Smart Structures + Nondestructive Evaluation, Behavior and Mechanics of Multifunctional Materials. p. 1158907. https://doi.org/10.1117/12.2581050

Barri, K., Zhang, Q., Kline, J., Khazanovich, L., Alavi, A.H., 2022a. Super compressible multifunctional metamaterial concrete. https://doi.org/10.1117/12.2607689 12043, 382–389. https://doi.org/10.1117/12.2607689

Barri, K., Zhang, Q., Mehta, D., Chakrabartty, S., Debski, R., Alavi, A.H., 2022b. Studying the Feasibility of Postoperative Monitoring of Spinal Fusion Progress Using a Self-Powered Fowler-Nordheim Sensor-Data-Logger. IEEE Trans. Biomed. Eng. 69, 710–717. https://doi.org/10.1109/TBME.2021.3103776

Barri, K., Zhang, Q., Swink, I., Aucie, Y., Holmberg, K., Sauber, R., Altman, D.T., Cheng, B.C., Wang, Z.L., Alavi, A.H., 2022c. Patient-Specific Self-Powered Metamaterial Implants for Detecting Bone Healing Progress. Adv. Funct. Mater. 2203533. https://doi.org/10.1002/ADFM.202203533

Barri, K., Zhang, Q., Taylor, B.E., Sun, Z., Sachs, S., Khazanovich, L., Wang, Z.L., Alavi, A.H., 2022d. MULTIFUNCTIONAL NANOGENERATOR CONCRETE MATERIAL SYSTEMS, in: ASME 2022 Conference on Smart Materials, Adaptive Structures and Intelligent Systems SMASIS. Dearborn, Michigan.

Berglund, E.Z., Monroe, J.G., Ahmed, I., Noghabaei, M., Do, J., Pesantez, J.E., Fasaee, M.A.K., Bardaka, E., Han, K., Proestos, G.T., Levis, J., 2020. Smart Infrastructure: A Vision for the Role of the Civil Engineering Profession in Smart Cities. J. Infrastruct. Syst. 26, 03120001. https://doi.org/10.1061/(ASCE)IS.1943-555X.0000549

Bertoldi, K., Reis, P.M., Willshaw, S., Mullin, T., 2010. Negative Poisson's Ratio Behavior Induced by an Elastic Instability. Adv. Mater. 22, 361–366. https://doi.org/10.1002/ADMA.200901956

Bertoldi, K., Vitelli, V., Christensen, J., Van Hecke, M., 2017. Flexible mechanical metamaterials. Nat. Rev. Mater. 2017 211 2, 1–11. https://doi.org/10.1038/natrevmats.2017.66

Carrara, M., Cacan, M.R., Toussaint, J., Leamy, M.J., Ruzzene, M., Erturk, A., 2013. Metamaterial-inspired structures and concepts for elastoacoustic wave energy harvesting. Smart Mater. Struct. 22, 065004. https://doi.org/10.1088/0964-1726/22/6/065004

Carvalho, J.R.G., Conde, G., Antonioli, M.L., Dias, P.P., Vasconcelos, R.O., Taboga, S.R., Canola, P.A., Chinelatto, M.A., Pereira, G.T., Ferraz, G.C., 2020. Biocompatibility and biodegradation of poly(lactic acid) (PLA) and an immiscible PLA/poly(ε-caprolactone) (PCL) blend compatibilized by poly(ε-caprolactone-b-tetrahydrofuran) implanted in horses. Polym. J. 2020 526 52, 629–643. https://doi.org/10.1038/s41428-020-0308-y

Chaichana, K.L., Bydon, M., Santiago-Dieppa, D.R., Hwang, L., McLoughlin, G., Sciubba, D.M., Wolinsky, J.P., Bydon, A., Gokaslan, Z.L., Witham, T., 2014. Risk of infection following posterior instrumented lumbar fusion for degenerative spine disease in 817 consecutive cases: Clinical article. J. Neurosurg. Spine 20, 45–52. https://doi.org/10.3171/2013.10.SPINE1364

Chakrabartty, S., Lajnef, N., Elvin, N., Gore, A., 2006. Self-powered sensor, U.S. Patent US20080047355A1.

Chauhan, A.P.S., Chawla, K., 2016. Comparative studies on Graphite and Carbon Black powders, and their dispersions. J. Mol. Liq. 221, 292–297. https://doi.org/10.1016/J.MOLLIQ.2016.05.043

Che, K., Yuan, C., Wu, J., Qi, H.J., Meaud, J., 2017. Three-dimensional-printed multistable mechanical metamaterials with a deterministic deformation sequence. J. Appl. Mech. Trans. ASME 84. https://doi.org/10.1115/1.4034706/422427

Chen, G., Cui, Y., Chen, X., 2019. Proactively modulating mechanical behaviors of materials at multiscale for mechano-adaptable devices. Chem. Soc. Rev. 48, 1434–1447. https://doi.org/10.1039/C8CS00801A

Chen, H., Chan, C.T., Sheng, P., 2010. Transformation optics and metamaterials. Nat. Mater. 2010 95 9, 387–396. https://doi.org/10.1038/nmat2743

Chen, H.T., O'Hara, J.F., Azad, A.K., Taylor, A.J., Averitt, R.D., Shrekenhamer, D.B., Padilla, W.J., 2008. Experimental demonstration of frequency-agile terahertz metamaterials. Nat. Photonics 2008 25 2, 295–298. https://doi.org/10.1038/nphoton.2008.52

Chen, J., Wang, Z.L., 2017. Reviving Vibration Energy Harvesting and Self-Powered Sensing by a Triboelectric Nanogenerator. Joule 1, 480–521. https://doi.org/10.1016/j.joule.2017.09.004

Chen, T., Li, S., Sun, H., 2012. Metamaterials Application in Sensing. Sensors 2012, Vol. 12, Pages 2742-2765 12, 2742–2765. https://doi.org/10.3390/S120302742

Chen, T., Pauly, M., Reis, P.M., 2021. A reprogrammable mechanical metamaterial with stable memory. Nat. 2021 5897842 589, 386–390. https://doi.org/10.1038/s41586-020-03123-5

Chen, Xing, Assadsangabi, Babak, Hsiang, York, Takahata, Kenichi, Chen, X, Assadsangabi, B, Takahata, K, Hsiang, Y, 2018. Enabling Angioplasty-Ready "Smart" Stents to Detect In-Stent Restenosis and Occlusion. Adv. Sci. 5, 1700560. https://doi.org/10.1002/ADVS.201700560

Chen, Z., Guo, B., Yang, Y., Cheng, C., 2014. Metamaterials-based enhanced energy harvesting: A review. Phys. B Condens. Matter 438, 1–8. https://doi.org/10.1016/J.PHYSB.2013.12.040

Chen, Z., Yang, Y., Lu, Z., Luo, Y., 2013. Broadband characteristics of vibration energy harvesting using one-dimensional phononic piezoelectric cantilever beams. Phys. B Condens. Matter 410, 5–12. https://doi.org/10.1016/J.PHYSB.2012.10.029

Cook, B.W., Lanzisera, S., Pister, K.S.J., 2006. SoC issues for RF smart dust. Proc. IEEE 94, 1177–1195. https://doi.org/10.1109/JPROC.2006.873620

Cottone, F., Vocca, H., Gammaitoni, L., 2009. Nonlinear energy harvesting. Phys. Rev. Lett. 102, 080601. https://doi.org/10.1103/PHYSREVLETT.102.080601/FIGURES/4/MEDIUM

Davami, K., Zhao, L., Lu, E., Cortes, J., Lin, C., Lilley, D.E., Purohit, P.K., Bargatin, I., 2015. Ultralight shape-recovering plate mechanical metamaterials. Nat. Commun. 2015 61 6, 1–7. https://doi.org/10.1038/ncomms10019

Deng, B., Xu, R., Zhao, K., Lu, Y., Ganguli, S., Cheng, G.J., 2018. Composite bending-dominated hollow nanolattices: A stiff, cyclable mechanical metamaterial. Mater. Today 21, 467–474. https://doi.org/10.1016/J.MATTOD.2018.03.027

Dharmasena, R.D.I.G., Jayawardena, K.D.G.I., Mills, C.A., Deane, J.H.B., Anguita, J. V., Dorey, R.A., Silva, S.R.P., 2017. Triboelectric nanogenerators: Providing a fundamental framework. Energy Environ. Sci. 10, 1801–1811. https://doi.org/10.1039/c7ee01139c

Dimas, L.S., Buehler, M.J., 2013. Tough and stiff composites with simple building blocks. J. Mater. Res. 2013 2810 28, 1295–1303. https://doi.org/10.1557/JMR.2013.88

Dudek, K.K., Wolak, W., Gatt, R., Grima, J.N., 2019. Impact resistance of composite magnetic metamaterials. Sci. Reports 2019 91 9, 1–9. https://doi.org/10.1038/s41598-019-40610-w

Duoss, E.B., Weisgraber, T.H., Hearon, K., Zhu, C., Small IV, W., Metz, T.R., Vericella, J.J., Barth, H.D., Kuntz, J.D., Maxwell, R.S., Spadaccini, C.M., Wilson, T.S., 2014. Three-Dimensional Printing of Elastomeric, Cellular Architectures with Negative Stiffness. Adv. Funct. Mater. 24, 4905–4913. https://doi.org/10.1002/ADFM.201400451

Dziadak, B., Makowski, Ł., Michalski, A., 2016. Survey of energy harvesting systems for wireless sensor networks in environmental monitoring. Metrol. Meas. Syst. 23, 495–512. https://doi.org/10.1515/MMS-2016-0053

El Helou, C., Buskohl, P.R., Tabor, C.E., Harne, R.L., 2021. Digital logic gates in soft, conductive mechanical metamaterials. Nat. Commun. 2021 121 12, 1–8. https://doi.org/10.1038/s41467-021-21920-y

Elvin, N.G., Lajnef, N., Elvin, A.A., 2006. Feasibility of structural monitoring with vibration powered sensors. Smart Mater. Struct. 15, 977. https://doi.org/10.1088/0964-1726/15/4/011

Fan, F.R., Tang, W., Wang, Z.L., 2016. Flexible Nanogenerators for Energy Harvesting and Self-Powered Electronics. Adv. Mater. 28, 4283–4305. https://doi.org/10.1002/adma.201504299

Fan, F.R., Tian, Z.Q., Lin Wang, Z., 2012. Flexible triboelectric generator. Nano Energy 1, 328–334. https://doi.org/10.1016/j.nanoen.2012.01.004

Fan, R., Liu, Jie, Liu, Jun, 2020. Finite element investigation on the dynamic mechanical properties of low-frequency vibrations on human L2–L3 spinal motion segments with different degrees of degeneration. Med. Biol. Eng. Comput. 58, 3003–3016. https://doi.org/10.1007/S11517-020-02263-0/FIGURES/8

Ferrari, M., Baù, M., Guizzetti, M., Ferrari, V., 2011. A single-magnet nonlinear piezoelectric converter for enhanced energy harvesting from random vibrations. Sensors Actuators A Phys. 172, 287–292. https://doi.org/10.1016/J.SNA.2011.05.019

Fogel, Guy R, Toohey, J.S., Neidre, A., Brantigan, J.W., Fogel, GllY R, 2009. Outcomes of Posterior Lumbar Interbody Fusion With the 9-mm Width Lumbar IfF Cage and the Variable Screw Placement System. J. Surg. Orthop. Adv. 18, 77–82.

Formlabs, 2022. Stereolithography (SLA) 3D Printing Guide [WWW Document]. Online. URL https://formlabs.com/blog/ultimate-guide-to-stereolithography-sla-3d-printing/ (accessed 5.22.22).

Fowler, C., Zhou, J., 2017. A Metamaterial-inspired Approach to RF Energy Harvesting. https://doi.org/10.48550/arxiv.1705.07718

Fu, Y., Wang, X., Wang, L., Li, Y., 2020. Foam Concrete: A State-of-the-Art and State-of-the-Practice Review. Adv. Mater. Sci. Eng. 2020. https://doi.org/10.1155/2020/6153602

Gatt, R., Grima, J.N., 2008. Negative compressibility. Phys. status solidi – Rapid Res. Lett. 2, 236–238. https://doi.org/10.1002/PSSR.200802101

Gibson, R.F., 2010. A review of recent research on mechanics of multifunctional composite materials and structures. Compos. Struct. 92, 2793–2810. https://doi.org/10.1016/J.COMPSTRUCT.2010.05.003

Gonella, S., To, A.C., Liu, W.K., 2009. Interplay between phononic bandgaps and piezoelectric

microstructures for energy harvesting. J. Mech. Phys. Solids 57, 621–633. https://doi.org/10.1016/J.JMPS.2008.11.002

Griffin, M., Bayat, A., 2011. Electrical Stimulation in Bone Healing: Critical Analysis by Evaluating Levels of Evidence. Eplasty 11, e34.

Grima, J.N., Winczewski, S., Mizzi, L., Grech, M.C., Cauchi, R., Gatt, R., Attard, D., Wojciechowski, K.W., Rybicki, J., 2015. Tailoring graphene to achieve negative Poisson's ratio properties. Adv. Mater. 27, 1455–1459. https://doi.org/10.1002/ADMA.201404106

Grimberg, R., 2013. Electromagnetic metamaterials. Mater. Sci. Eng. B 178, 1285–1295. https://doi.org/10.1016/J.MSEB.2013.03.022

Haghpanah, B., Salari-Sharif, L., Pourrajab, P., Hopkins, J., Valdevit, L., 2016. Multistable Shape-Reconfigurable Architected Materials. Adv. Mater. 28, 7915–7920. https://doi.org/10.1002/ADMA.201601650

Haglin, J.M., Eltorai, A.E.M., Gil, J.A., Marcaccio, S.E., Botero-Hincapie, J., Daniels, A.H., 2016. Patient-Specific Orthopaedic Implants. Orthop. Surg. 8, 417–424. https://doi.org/10.1111/OS.12282

Hanif, A., Parthasarathy, P., Ma, H., Fan, T., Li, Z., 2017. Properties improvement of fly ash cenosphere modified cement pastes using nano silica. Cem. Concr. Compos. 81, 35–48. https://doi.org/10.1016/J.CEMCONCOMP.2017.04.008

Harrison, C., Eckman, B., Hamilton, R., Hartswick, P., Kalagnanam, J., Paraszczak, J., Williams, P., 2010. Foundations for Smarter Cities. IBM J. Res. Dev. 54. https://doi.org/10.1147/JRD.2010.2048257

Hewage, T.A.M., Alderson, K.L., Alderson, A., Scarpa, F., 2016. Double-Negative Mechanical Metamaterials Displaying Simultaneous Negative Stiffness and Negative Poisson's Ratio Properties. Adv. Mater. 28, 10116–10116. https://doi.org/10.1002/ADMA.201605935

Hinchet, R., Seung, W., Kim, S.W., 2015. Recent Progress on Flexible Triboelectric Nanogenerators for SelfPowered Electronics. ChemSusChem 8, 2327–2344. https://doi.org/10.1002/cssc.201403481

Hindy, P., Hong, J., Lam-Tsai, Y., Gress, F., 2012. A Comprehensive Review of Esophageal Stents. Gastroenterol. Hepatol. (N. Y). 8, 526.

Huang, C., Lajnef, N., Chakrabartty, S., 2010. Calibration and characterization of self-powered floating-gate usage monitor with single electron per second operational limit. IEEE Trans. Circuits Syst. I Regul. Pap. 57, 556–568. https://doi.org/10.1109/TCSI.2009.2024976

Indira, S.S., Vaithilingam, C.A., Oruganti, K.S.P., Mohd, F., Rahman, S., 2019. Nanogenerators as a Sustainable Power Source: State of Art, Applications, and Challenges. Nanomater. (Basel, Switzerland) 9. https://doi.org/10.3390/NANO9050773

Ion, A., Wall, L., Kovacs, R., Baudisch, P., 2017. Digital mechanical metamaterials. Conf. Hum. Factors Comput. Syst. - Proc. 2017-May, 977–988. https://doi.org/10.1145/3025453.3025624

Ip, H., Yang, G.-Z., 2015. Smart Implants for Surgery - IEEE Life Sciences [WWW Document]. URL https://lifesciences.ieee.org/lifesciences-newsletter/2014/march-2014/smart-implants-for-surgery/ (accessed 5.17.22).

Ivanova, O., Williams, C., Campbell, T., 2013. Additive manufacturing (AM) and nanotechnology: Promises and challenges. Rapid Prototyp. J. 19, 353–364. https://doi.org/10.1108/RPJ-12-2011-0127/FULL/XML

Jiang, Y., Liu, Zhiyuan, Matsuhisa, N., Qi, D., Leow, W.R., Yang, H., Yu, J., Chen, G., Liu, Y., Wan, C., Liu, Zhuangjian, Chen, X., 2018. Auxetic Mechanical Metamaterials to Enhance Sensitivity of Stretchable Strain Sensors. Adv. Mater. 30, 1706589. https://doi.org/10.1002/ADMA.201706589

Jiao, P., Alavi, A.H., 2020a. Artificial intelligence-enabled smart mechanical metamaterials: advent and future trends. https://doi.org/10.1080/09506608.2020.1815394

Jiao, P., Alavi, A.H., 2020b. Evolutionary computation for design and characterization of nanoscale metastructures. Appl. Mater. Today 21, 100816. https://doi.org/10.1016/J.APMT.2020.100816

Jiao, P., Alavi, A.H., 2020c. Artificial intelligence-enabled smart mechanical metamaterials: advent and future trends. Int. Mater. Rev. 0, 1–29. https://doi.org/10.1080/09506608.2020.1815394

Jiao, P., Alavi, A.H., 2019. Size-dependent buckling instability and recovery of beam-like, architected microstructures. Mater. Des. 162, 405–417. https://doi.org/10.1016/J.MATDES.2018.12.003

Jiao, P., Nicaise, S.M., Lin, C., Purohit, P.K., Bargatin, I., 2019. Extremely Sharp Bending and Recoverability of Nanoscale Plates with Honeycomb Corrugation. Phys. Rev. Appl. 11, 034055. https://doi.org/10.1103/PHYSREVAPPLIED.11.034055/FIGURES/14/MEDIUM

Kadic, M., Bückmann, T., Stenger, N., Thiel, M., Wegener, M., 2012. On the practicability of pentamode mechanical metamaterials. Appl. Phys. Lett. 100, 191901. https://doi.org/10.1063/1.4709436

Kamel, H.M., 2018. SIMULATING AN INTERVERTEBRAL LUMBAR SPINE DISC. Int. Conf. Appl. Mech. Mech. Eng. 18, 1–11. https://doi.org/10.21608/AMME.2018.35023

Kanayama, M., Cunningham, B.W., Weis, J.C., Parker, L.M., Kaneda, K., McAfee, P.C., 1997. Maturation of the posterolateral spinal fusion and its effect on load-sharing of spinal instrumentation. An in vivo sheep model. J. Bone Joint Surg. Am. 79, 1710–1720. https://doi.org/10.2106/00004623-199711000-00013

Ketabdari, M., Toraldo, E., Crispino, M., Lunkar, V., 2020. Evaluating the interaction between

engineered materials and aircraft tyres as arresting systems in landing overrun events. Case Stud. Constr. Mater. 13, e00446. https://doi.org/10.1016/J.CSCM.2020.E00446

Kettler, A., Wilke, H.J., Dietl, R., Krammer, M., Lumenta, C., Claes, L., 2000. Stabilizing effect of posterior lumbar interbody fusion cages before and after cyclic loading. J. Neurosurg. Spine 92, 87–92. https://doi.org/10.3171/SPI.2000.92.1.0087

Kim, D.W., Lee, J.H., Kim, J.K., Jeong, U., 2020. Material aspects of triboelectric energy generation and sensors. NPG Asia Mater. 2020 121 12, 1–17. https://doi.org/10.1038/s41427-019-0176-0

Kim, K.Y., Tsauo, J., Song, H.Y., Park, J.H., Jun, E.J., Zhou, W.Z., Kim, M.T., 2017. Evaluation of a New Esophageal Stent for the Treatment of Malignant and Benign Esophageal Strictures. Cardiovasc. Intervent. Radiol. 40, 1576–1585. https://doi.org/10.1007/S00270-017-1677-2/FIGURES/5

Kolken, H.M.A., Janbaz, S., Leeflang, S.M.A., Lietaert, K., Weinans, H.H., Zadpoor, A.A., 2018. Rationally designed meta-implants: a combination of auxetic and conventional meta-biomaterials. Mater. Horizons 5, 28–35. https://doi.org/10.1039/C7MH00699C

Kondapalli, S.H., Alazzawi, Y., Malinowski, M., Timek, T., Chakrabartty, S., 2018. Multiaccess in vivo biotelemetry using sonomicrometry and M-scan ultrasound imaging. IEEE Trans. Biomed. Eng. 65, 149–158. https://doi.org/10.1109/TBME.2017.2697998

Kondapalli, S.H., Chakrabartty, S., 2021. Sub-nanowatt ultrasonic bio-telemetry using B-scan imaging. IEEE Open J. Eng. Med. Biol. 2, 17–25. https://doi.org/10.1109/OJEMB.2021.3053174

Krac, E., Górecki, K., 2016. Modelling characteristics of photovoltaic panels with thermal phenomena taken into account. IOP Conf. Ser. Mater. Sci. Eng. 104, 012013. https://doi.org/10.1088/1757-899X/104/1/012013

Krammer, M., Dietl, R., Lumenta, C.B., Kettler, A., Wilke, H.J., Büttner, A., Claes, L., 2001. Resistance of the Lumbar Spine Against Axial Compression Forces after Implantation of Three Different Posterior Lumbar Interbody Cages. Acta Neurochir. 2001 14312 143, 1217–1222. https://doi.org/10.1007/S007010100017

Kubosch, D., Kubosch, E.J., Gueorguiev, B., Zderic, I., Windolf, M., Izadpanah, K., Südkamp, N.P., Strohm, P.C., 2016. Biomechanical investigation of a minimally invasive posterior spine stabilization system in comparison to the Universal Spinal System (USS). BMC Musculoskelet. Disord. 17, 1–8. https://doi.org/10.1186/S12891-016-0983-1/FIGURES/7

Leary, M., 2017. Surface roughness optimisation for selective laser melting (SLM): Accommodating relevant and irrelevant surfaces. Laser Addit. Manuf. Mater. Des. Technol. Appl. 99–118. https://doi.org/10.1016/B978-0-08-100433-3.00004-X

Li, Y., Baker, E., Reissman, T., Sun, C., Liu, W.K., 2017. Design of mechanical metamaterials for simultaneous vibration isolation and energy harvesting. Appl. Phys. Lett. 111, 251903.

https://doi.org/10.1063/1.5008674

Lin, J.-T., Jackson, D., Aebersold, J., Walsh, K., Naber, J., Hnat, W., 2011. Inductively Coupled Telemetry in Spinal Fusion Application Using Capacitive Strain Sensors. Mod. Telem. https://doi.org/10.5772/22984

Lin, J.T., Walsh, K.W., Jackson, D., Aebersold, J., Crain, M., Naber, J.F., Hnat, W.P., 2007. Development of capacitive pure bending strain sensor for wireless spinal fusion monitoring. Sensors Actuators, A Phys. 138, 276–287. https://doi.org/10.1016/j.sna.2007.04.069

Lin, Z., Zhang, B., Zou, H., Wu, Z., Guo, H., Zhang, Y., Yang, J., Wang, Z.L., 2020. Rationally designed rotation triboelectric nanogenerators with much extended lifetime and durability. Nano Energy 68, 104378. https://doi.org/10.1016/J.NANOEN.2019.104378

Lincoln, R.L., Scarpa, F., Ting, V.P., Trask, R.S., 2019. Multifunctional composites: a metamaterial perspective. Multifunct. Mater. 2, 043001. https://doi.org/10.1088/2399-7532/AB5242

Liu, J., Yang, S., Zhou, F., Lu, J., Xia, C., Wang, H., Chen, C., 2020. The feasibility of short-segment Schanz screw implanted in an oblique downward direction for the treatment of lumbar 1 burst fracture: a finite element analysis. J. Orthop. Surg. Res. 15, 1–11. https://doi.org/10.1186/S13018-020-02024-7/FIGURES/8

Liu, R., Ji, C., Zhao, Z., Zhou, T., 2015. Metamaterials: Reshape and Rethink. Engineering 1, 179–184. https://doi.org/10.15302/J-ENG-2015036

Lynch, J.P., Loh, K.J., 2006. A Summary Review of Wireless Sensors and Sensor Networks for Structural Health Monitoring. Shock Vib. Dig. 38, 91–128. https://doi.org/10.1177/0583102406061499

Matlack, K.H., Serra-Garcia, M., Palermo, A., Huber, S.D., Daraio, C., 2018. Designing perturbative metamaterials from discrete models. Nat. Mater. 2018 174 17, 323–328. https://doi.org/10.1038/s41563-017-0003-3

Mehta, D., Aono, K., Chakrabartty, S., 2020. A self-powered analog sensor-data-logging device based on Fowler-Nordheim dynamical systems. Nat. Commun. 2020 111 11, 1–9. https://doi.org/10.1038/s41467-020-19292-w

Mei, T., Meng, Z., Zhao, K., Chen, C.Q., 2021. A mechanical metamaterial with reprogrammable logical functions. Nat. Commun. 2021 121 12, 1–11. https://doi.org/10.1038/s41467-021-27608-7

Mendell, M.C., Hogan, M., 2021. DNA in the Archive Material and Metaphor of a New Data Storage Format. Dr. Diss. New York Univ.

Meza, L.R., Das, S., Greer, J.R., 2014. Strong, lightweight, and recoverable three-dimensional ceramic nanolattices. Science (80-.). 345, 1322–1326. https://doi.org/10.1126/SCIENCE.1255908/SUPPL_FILE/MEZA.SM.PDF

Meza, L.R., Zelhofer, A.J., Clarke, N., Mateos, A.J., Kochmann, D.M., Greer, J.R., 2015. Resilient 3D hierarchical architected metamaterials. Proc. Natl. Acad. Sci. U. S. A. 112, 11502–11507. https://doi.org/10.1073/PNAS.1509120112/SUPPL_FILE/PNAS.1509120112.SM06.MP4

Mi, H.Y., Jing, X., Napiwocki, B.N., Hagerty, B.S., Chen, G., Turng, L.S., 2017. Biocompatible, degradable thermoplastic polyurethane based on polycaprolactone-block-polytetrahydrofuran-block-polycaprolactone copolymers for soft tissue engineering. J. Mater. Chem. B 5, 4137–4151. https://doi.org/10.1039/C7TB00419B

Milton, G.W., Cherkaev, A. V., 1995. Which Elasticity Tensors are Realizable? J. Eng. Mater. Technol. 117, 483–493. https://doi.org/10.1115/1.2804743

Mitcheson, Paul D, Yeatman, E.M., Kondala Rao, G., Holmes, A.S., Green, T.C., 2008. Energy Harvesting From Human and Machine Motion for Wireless Electronic Devices Practical miniature devices are becoming available for harnessing kinetic energy as a substitute for batteries in medical, and many other, low power applications. Proc. IEEE. https://doi.org/10.1109/JPROC.2008.927494

Mitcheson, Paul D., Yeatman, E.M., Rao, G.K., Holmes, A.S., Green, T.C., 2008. Energy harvesting from human and machine motion for wireless electronic devices. Proc. IEEE 96, 1457–1486. https://doi.org/10.1109/JPROC.2008.927494

MOMODA, L.A., 2004. The Future of Engineering Materials: Multifunction for Performance-Tailored Structures, in: Frontiers of Engineering. pp. 18–21.

Munch, E., Launey, M.E., Alsem, D.H., Saiz, E., Tomsia, A.P., Ritchie, R.O., 2008. Tough, bio-inspired hybrid materials. Science 322, 1516–1520. https://doi.org/10.1126/SCIENCE.1164865

Najafi, K., Galchev, T., Aktakka, E.E., Peterson, R.L., McCullagh, J., 2011. Microsystems for energy harvesting. 2011 16th Int. Solid-State Sensors, Actuators Microsystems Conf. TRANSDUCERS'11 1845–1850. https://doi.org/10.1109/TRANSDUCERS.2011.5969888

Nicolaou, Z.G., Motter, A.E., 2012. Mechanical metamaterials with negative compressibility transitions. Nat. Mater. 2012 117 11, 608–613. https://doi.org/10.1038/nmat3331

Nikkhoo, M., Hsu, Y.C., Haghpanahi, M., Parnianpour, M., Wang, J.L., 2013. A meta-model analysis of a finite element simulation for defining poroelastic properties of intervertebral discs. Proc. Inst. Mech. Eng. Part H J. Eng. Med. 227, 672–682. https://doi.org/10.1177/0954411913480668

Nikkhoo, M., Khalaf, K., Kuo, Y.W., Hsu, Y.C., Haghpanahi, M., Parnianpour, M., Wang, J.L., 2015. Effect of degeneration on fluid-solid interaction within intervertebral disk under cyclic loading - A meta-model analysis of finite element simulations. Front. Bioeng. Biotechnol. 3, 4. https://doi.org/10.3389/FBIOE.2015.00004/BIBTEX

Niu, S., Liu, Y., Chen, X., Wang, S., Zhou, Y.S., Lin, L., Xie, Y., Wang, Z.L., 2015. Theory of freestanding triboelectric-layer-based nanogenerators. Nano Energy 12, 760–774.

https://doi.org/10.1016/j.nanoen.2015.01.013

Niu, S., Liu, Y., Wang, S., Lin, L., Zhou, Y.S., Hu, Y., Wang, Z.L., 2014. Theoretical investigation and structural optimization of single-electrode triboelectric nanogenerators. Adv. Funct. Mater. 24, 3332–3340. https://doi.org/10.1002/adfm.201303799

Niu, S., Liu, Y., Wang, S., Lin, L., Zhou, Y.S., Hu, Y., Wang, Z.L., 2013. Theory of sliding-mode triboelectric nanogenerators. Adv. Mater. 25, 6184–6193. https://doi.org/10.1002/adma.201302808

Niu, S., Wang, Z.L., 2014. Theoretical systems of triboelectric nanogenerators. Nano Energy 14, 161–192. https://doi.org/10.1016/j.nanoen.2014.11.034

Pan, S., Zhang, Z., 2019. Fundamental theories and basic principles of triboelectric effect: A review. Friction 7, 2–17. https://doi.org/10.1007/s40544-018-0217-7

Park, G., Farrar, C.R., Rosing, T., Todd, M.D., Hodgkiss, W., 2008. Energy Harvesting for Structural Health Monitoring Sensor Networks. J. Infrastruct. Syst. 14, 64–79. https://doi.org/10.1061/(ASCE)1076-0342(2008)14:1(64)

Patterson, F., Miralami, R., Tansey, K.E., Prabhu, R.K., Priddy, L.B., 2021. Deleterious effects of whole-body vibration on the spine: A review of in vivo, ex vivo, and in vitro models. Anim. Model. Exp. Med. 4, 77–86. https://doi.org/10.1002/AME2.12163

Pishvar, M., Harne, R.L., 2020. Foundations for Soft, Smart Matter by Active Mechanical Metamaterials. Adv. Sci. 7, 2001384. https://doi.org/10.1002/ADVS.202001384

Qi, S., Oudich, M., Li, Y., Assouar, B., 2016. Acoustic energy harvesting based on a planar acoustic metamaterial. Appl. Phys. Lett. 108, 263501. https://doi.org/10.1063/1.4954987

Qu, J., Kadic, M., Naber, A., Wegener, M., 2017. Micro-Structured Two-Component 3D Metamaterials with Negative Thermal-Expansion Coefficient from Positive Constituents. Sci. Reports 2017 71 7, 1–8. https://doi.org/10.1038/srep40643

Quan, T., Wang, Z.L., Yang, Y., 2016. A Shared-Electrode-Based Hybridized Electromagnetic-Triboelectric Nanogenerator. ACS Appl. Mater. Interfaces 8, 19573–19578. https://doi.org/10.1021/ACSAMI.6B07162/ASSET/IMAGES/MEDIUM/AM-2016-07162Y_0008.GIF

Queheillalt, D.T., Carbajal, G., Peterson, G.P., Wadley, H.N.G., 2008. A multifunctional heat pipe sandwich panel structure. Int. J. Heat Mass Transf. 51, 312–326. https://doi.org/10.1016/J.IJHEATMASSTRANSFER.2007.03.051

Rafsanjani, A., Akbarzadeh, A., Pasini, D., 2015. Snapping Mechanical Metamaterials under Tension. Adv. Mater. 27, 5931–5935. https://doi.org/10.1002/ADMA.201502809

Salazar, B., Aghdasi, P., Williams, I.D., Ostertag, C.P., Taylor, H.K., 2020. Polymer lattice-reinforcement for enhancing ductility of concrete. Mater. Des. 196, 109184.

https://doi.org/10.1016/J.MATDES.2020.109184

Saloma, Nasution, A., Imran, I., Abdullah, M., 2015. Improvement of Concrete Durability by Nanomaterials. Procedia Eng. 125, 608–612. https://doi.org/10.1016/J.PROENG.2015.11.078

Scerrato, D., Giorgio, I., Della Corte, A., Madeo, A., Dowling, N.E., Darve, F., 2016. Towards the design of an enriched concrete with enhanced dissipation performances. Cem. Concr. Res. 84, 48–61. https://doi.org/10.1016/J.CEMCONRES.2016.03.002

Schaedler, T.A., Carter, W.B., 2016. Architected Cellular Materials. http://dx.doi.org/10.1146/annurev-matsci-070115-031624 46, 187–210. https://doi.org/10.1146/ANNUREV-MATSCI-070115-031624

Schaedler, T.A., Jacobsen, A.J., Torrents, A., Sorensen, A.E., Lian, J., Greer, J.R., Valdevit, L., Carter, W.B., 2011. Ultralight metallic microlattices. Science (80-.). 334, 962–965. https://doi.org/10.1126/SCIENCE.1211649/SUPPL_FILE/SCHAEDLER.SOM.PDF

Schueler, M., Mandel, C., Puentes, M., Jakoby, R., 2012. Metamaterial inspired microwave sensors. IEEE Microw. Mag. 13, 57–68. https://doi.org/10.1109/MMM.2011.2181448

Seifert, R., Patil, M., Seidel, G., 2019. Topology optimization of self-sensing nanocomposite structures with designed boundary conditions. Smart Mater. Struct. 28, 074006. https://doi.org/10.1088/1361-665X/AB1179

Singh, G., Singh, G., Marwaha, A., 2015. A Review of Metamaterials and its Applications. Int. J. Eng. Trends Technol. 19, 305–310.

Sola, E., Ožbolt, J., Balabanić, G., Mir, Z.M., 2019. Experimental and numerical study of accelerated corrosion of steel reinforcement in concrete: Transport of corrosion products. Cem. Concr. Res. 120, 119–131. https://doi.org/10.1016/J.CEMCONRES.2019.03.018

Starr, M., Ninesling, M., Polet, E., 2020. Comparing tape and cloud storage for long-term data preservation, in: IEEE 36th Symposium on Mass Storage Systems and Technologies. Santa Clara, CA.

Surjadi, J.U., Gao, L., Du, H., Li, X., Xiong, X., Fang, N.X., Lu, Y., 2019. Mechanical Metamaterials and Their Engineering Applications. Adv. Eng. Mater. 21, 1–37. https://doi.org/10.1002/adem.201800864

Szivek, J.A., Roberta, R.F., Margolis, D.S., 2005. In vivo strain measurements from hardware and lamina during spine fusion. J. Biomed. Mater. Res. Part B Appl. Biomater. 75B, 243–250. https://doi.org/10.1002/JBM.B.30262

Szivek, J.A., Roberto, R.F., Slack, J.M., Majeed, B.S., 2002. An implantable strain measurement system designed to detect spine fusion: preliminary results from a biomechanical in vivo study. Spine (Phila. Pa. 1976). 27, 487–497. https://doi.org/10.1097/00007632-200203010-00009

Talreja, R., Singh, C.V., 2012. Damage and failure of composite materials.

Tao, H., Gibert, J., 2020. Multifunctional Mechanical Metamaterials with Embedded Triboelectric Nanogenerators. Adv. Funct. Mater. 30, 2001720. https://doi.org/10.1002/ADFM.202001720

Treml, B., Gillman, A., Buskohl, P., Vaia, R., 2018. Origami mechanologic. Proc. Natl. Acad. Sci. U. S. A. 115, 6916–6921. https://doi.org/10.1073/PNAS.1805122115

Wang, B., Teo, K.H., Nishino, T., Yerazunis, W., Barnwell, J., Zhang, J., 2011. Experiments on wireless power transfer with metamaterials. Appl. Phys. Lett. 98, 254101. https://doi.org/10.1063/1.3601927

Wang, L., Ma, G., Liu, T., Buswell, R., Li, Z., 2021. Interlayer reinforcement of 3D printed concrete by the in-process deposition of U-nails. Cem. Concr. Res. 148, 106535. https://doi.org/10.1016/J.CEMCONRES.2021.106535

Wang, S., Lin, L., Wang, Z.L., 2015. Triboelectric nanogenerators as self-powered active sensors. Nano Energy 11, 436–462. https://doi.org/10.1016/j.nanoen.2014.10.034

Wang, S., Lin, L., Wang, Z.L., 2012. Nanoscale triboelectric-effect-enabled energy conversion for sustainably powering portable electronics. Nano Lett. 12, 6339–6346. https://doi.org/10.1021/NL303573D/SUPPL_FILE/NL303573D_SI_005.AVI

Wang, Y., Peng, C., Zhang, W., 2014. Mechanical and electrical behavior of a novel satellite multifunctional structural battery. J. Sci. Ind. Res. 73, 163–167.

Wang, Y., Yang, Y., Wang, Z.L., 2017. Triboelectric nanogenerators as flexible power sources. npj Flex. Electron. 1, 1–9. https://doi.org/10.1038/s41528-017-0007-8

Wang, Z.L., 2013. Triboelectric nanogenerators as new energy technology for self-powered systems and as active mechanical and chemical sensors. ACS Nano 7, 9533–9557. https://doi.org/10.1021/NN404614Z/ASSET/IMAGES/MEDIUM/NN-2013-04614Z_0020.GIF

Wang, Z.L., Chen, J., Lin, L., 2015. Progress in triboelectric nanogenerators as a new energy technology and self-powered sensors. Energy Environ. Sci. 8, 2250–2282. https://doi.org/10.1039/C5EE01532D

Wang, Z.L., Lin, L., Chen, J., Niu, S., Zi, Y., 2018. Triboelectric Nanogenerators. https://doi.org/10.1007/978-981-10-5945-2_38

Wang, Z.L., Song, J., 2006. Piezoelectric nanogenerators based on zinc oxide nanowire arrays. Science (80-.). 312, 242–246. https://doi.org/10.1126/science.1124005

Wen, Z., Fu, J., Han, L., Liu, Y., Peng, M., Zheng, L., Zhu, Y., Sun, X., Zi, Y., 2018. Toward self-powered photodetection enabled by triboelectric nanogenerators. J. Mater. Chem. C 6, 11893–11902. https://doi.org/10.1039/c8tc02964d

Wilson, S.A., Jourdain, R.P.J., Zhang, Q., Dorey, R.A., Bowen, C.R., Willander, M., Wahab, Q.U., Willander, M., Al-hilli, S.M., Nur, O., Quandt, E., Johansson, C., Pagounis, E., Kohl, M., Matovic, J., Samel, B., van der Wijngaart, W., Jager, E.W.H., Carlsson, D., Djinovic, Z., Wegener, M., Moldovan, C., Abad, E., Wendlandt, M., Rusu, C., Persson, K., 2007. New materials for micro-scale sensors and actuators: An engineering review. Mater. Sci. Eng. R Reports 56, 1–129. https://doi.org/10.1016/J.MSER.2007.03.001

Xu, C., Quinn, B., Lebel, L.L., Therriault, D., L'espérance, G., 2019. Multi-Material Direct Ink Writing (DIW) for Complex 3D Metallic Structures with Removable Supports. ACS Appl. Mater. Interfaces 11, 8499–8506. https://doi.org/10.1021/ACSAMI.8B19986/SUPPL_FILE/AM8B19986_SI_004.AVI

Xu, L., Hasan, M.A.M., Wu, H., Yang, Y., 2021. Electromagnetic–Triboelectric Hybridized Nanogenerators. Energies 2021, Vol. 14, Page 6219 14, 6219. https://doi.org/10.3390/EN14196219

Yang, H., Ma, L., 2019. Multi-stable mechanical metamaterials by elastic buckling instability. J. Mater. Sci. 54, 3509–3526. https://doi.org/10.1007/S10853-018-3065-Y/FIGURES/10

Yang, H., Ma, L., 2018. Multi-stable mechanical metamaterials with shape-reconfiguration and zero Poisson's ratio. Mater. Des. 152, 181–190. https://doi.org/10.1016/J.MATDES.2018.04.064

Yang, J.H., Kim, Y.K., Lee, J.Y., 2015. Simplified process for manufacturing macroscale patterns to enhance voltage generation by a triboelectric generator. Energies 8, 12729–12740. https://doi.org/10.3390/en81112340

Yang, J.J., Huang, M., Tang, H., Zeng, J., Dong, L., 2013. Metamaterial sensors. Int. J. Antennas Propag. 2013. https://doi.org/10.1155/2013/637270

Yasuda, H., Buskohl, P.R., Gillman, A., Murphey, T.D., Stepney, S., Vaia, R.A., Raney, J.R., 2021. Mechanical computing. Nat. 2021 5987879 598, 39–48. https://doi.org/10.1038/s41586-021-03623-y

Yu, H., He, X., Ding, W., Hu, Y., Yang, D., Lu, S., Wu, C., Zou, H., Liu, R., Lu, C., Wang, Z.L., 2017. A Self-Powered Dynamic Displacement Monitoring System Based on Triboelectric Accelerometer. Adv. Energy Mater. 7, 1700565. https://doi.org/10.1002/AENM.201700565

Yu, X., Zhou, J., Liang, H., Jiang, Z., Wu, L., 2018. Mechanical metamaterials associated with stiffness, rigidity and compressibility: A brief review. Prog. Mater. Sci. 94, 114–173. https://doi.org/10.1016/J.PMATSCI.2017.12.003

Zadpoor, A.A., 2020. Meta-biomaterials. Biomater. Sci. 8, 18–38. https://doi.org/10.1039/C9BM01247H

Zadpoor, A.A., 2016. Mechanical meta-materials. Mater. Horizons 3, 371–381. https://doi.org/10.1039/C6MH00065G

Zhang, H., Quan, L., 2019. Theoretical Prediction and Optimization Approach to Triboelectric Nanogenerator. Electrost. Disch. - From Electr. Break. Micro-gaps to Nano-generators. https://doi.org/10.5772/INTECHOPEN.86992

Zheludev, N.I., 2015. Obtaining optical properties on demand. Science (80-.). 348, 973–974. https://doi.org/10.1126/SCIENCE.AAC4360/ASSET/218DBED4-31E2-4D83-B1CB-4AB1D5580E9C/ASSETS/GRAPHIC/348_973_F1.JPEG

Zheludev, N.I., 2010. The Road Ahead for Metamaterials. Science (80-.). 328, 582–583. https://doi.org/10.1126/SCIENCE.1186756

Zheludev, N.I., Kivshar, Y.S., 2012. From metamaterials to metadevices. Nat. Mater. 2012 1111 11, 917–924. https://doi.org/10.1038/nmat3431

Zheng, X., Lee, H., Weisgraber, T.H., Shusteff, M., DeOtte, J., Duoss, E.B., Kuntz, J.D., Biener, M.M., Ge, Q., Jackson, J.A., Kucheyev, S.O., Fang, N.X., Spadaccini, C.M., 2014. Ultralight, ultrastiff mechanical metamaterials. Science (80-.). 344, 1373–1377. https://doi.org/10.1126/SCIENCE.1252291/SUPPL_FILE/ZHENG.SM.PDF

Zhu, G., Pan, C., Guo, W., Chen, C.Y., Zhou, Y., Yu, R., Wang, Z.L., 2012. Triboelectric-generator-driven pulse electrodeposition for micropatterning. Nano Lett. 12, 4960–4965. https://doi.org/10.1021/NL302560K/SUPPL_FILE/NL302560K_SI_001.PDF

Zi, Y., Wang, Z.L., 2017. Nanogenerators: An emerging technology towards nanoenergy. APL Mater. 5. https://doi.org/10.1063/1.4977208